Manipulation of short pulses

by

Raphael Okoye

Thesis presented in partial fulfilment of the requirements for the degree of ***Master of Science*** *at the University of Stellenbosch*

Departement of Physics,
University of Stellenbosch,
Private Bag X1, Matieland 7602, South Africa.

Supervisors:

Supervisor: Prof. Erich G. Rohwer
Co-supervisors: Prof. Heinrich Schwoerer and Dr. Pieter H. Neethling

December 2013

Declaration

By submitting this thesis electronically, I declare that the entirety of the work contained therein is my own, original work, that I am the sole author thereof (save to the extent explicitly otherwise stated), that reproduction and publication thereof by Stellenbosch University will not infringe any third party rights and that I have not previously in its entirety or in part submitted it for obtaining any qualification.

Date: December, 2013 .....

Abstract

Manipulation of short pulses

R. Okoye

Departement of Physics,
University of Stellenbosch,
Private Bag X1, Matieland 7602, South Africa.

Thesis: MSc

December 2013

An ultra-fast laser pulse can be described in the time or frequency domain. If the time-bandwidth product of an ultra-fast pulse is not satisfied, then the pulse is stretched. Stretching can be described in the time or frequency domain. In the time domain, it is called a chirp and in the frequency domain, it is known as the group delay dispersion GDD. Various techniques can be used to stretch and compress laser pulses. In this project, a prism pulse compressor used for compressing stretched pulses was built. A 200nm supercontinnum generated in an all normal dispersion photonic crystal fibre (ANDi-PCF) was compressed using the prism pulse compressor from 2ps to 140fs. The experiment and physical interpretation presented in this project suggest that a shorter pulse duration less than the measured 140fs of the compressed supercontinnum can be obtained.

Opsomming

n Ultra-vinnige laser puls kan beskryf word in tyd of frekwensie. As die tyd-bandwydte produk van ‘n ultra-vinnige puls nie bevredig is nie, dan is die puls uitgerek. Hierdie uitrekking kan beskryf word in tyd of frekwensie. In tyd word dit tjirp genoem en in frekwensie groep vertraging dispersie. Verskeie tegnieke kan gebruik word om ‘n laser puls te rek of saam te pers. In hierdie projek is ‘n prisma puls kompressor gebou om uitgerekte pulse saam te pers. ‘n 200nm breë bandwydte puls (“supercontinuum”) is gegenereer in ‘n fotoniese kristal optiese vesel wat uitsluitlik normale dispersie toon (ANDI-PCF) en die puls is toe saamgepers met behulp van die prisma puls kompressor van‘n oorspronklike 2ps na 140fs. Die eksperiment en fisiese interpretasie wat in hierdie projek aangebied word dui daarop dat ‘n nog korter puls, minder as die gemete 140 fs, verkry kan word deur die breë bandwydte puls verder saam te pers.

Acknowledgements

My gratitude to my supervisors Prof Eric.G.Rohwer and Dr Pieter.H.Neethling for their supervision, support and encouragements. A big thank you to Prof Heinrich Schwoerer for all his support and suggestions.Special thanks to Dirk Spangenberg, Dr Gurthwin Bosman for their help with the experimental set up. Thanks to the entire LRI group for their useful discussions and suggestions.

Thanks to all my friends, especially Tommiwa Ajabonna of the Perimeter Institute Canada, Rahim Soliu of the Cape Peninsula University of Technology, Adams Duniya of the University of Western Cape, Damilola Mommodu of the University of Pretoria, Cynthia Adaeze of Nnamdi Azikiwe University Awka and Frances Ogodumdu of the University of Bordaeux Talence, Obiageli Umeogochukwu of Stellenbosch University, Mrs Chika Yinka Banjo and Mrs Ukomadu Uzonnah of the University of Cape Town. Hannatu Bala and all lectors of Our Lady Queen of Peace Parish, Ahamdu Bello University Zaria. Thanks to the Chukwuma's family, Mr and Mrs Innocent Akaogu and all members of the Redeemed Christian church of God, desire of nations parish especially to pastor Funlola Olojede, Olufemi Opeyemi Olaoye, Akinlotan Morenikeji Deborah, Adewumi John Babafemi and Ugochukwu Ihekoronye.

Thanks to my lecturers in Nigeria, especially Dr Gani Balogun, Dr Collins Chiemeke now lecturer at the Federal University of Otuoke Bayelsa, Prof Marius.N.Umego now the HOD department of physics Nnamdi Azikiwe University Awka, Prof T.C.Akpan and Prof I.G.Ibeanu. Thanks to Prof Bernd Schroers of Heriot-Watt University UK and Prof Robert De Mello Koch University of the Witwatersrand.

Special thanks to my lovely parents Mr and Mrs Raphael.N.Okoye and my brother Kenneth Okoye for their prayers, support and love.

Above all, thanks to God almighty, for bringing me thus far.

Dedication

This work is dedicated to God Almighty, giver of all wisdom, knowledge and understanding.

Contents

Declaration i

Abstract ii

Opsomming iii

Acknowledgements iv

Dedication v

Contents vi

List of Figures viii

1 Introduction 1
- 1.1 Aim . . . 1
- 1.2 Fourier transform . . . 1
- 1.3 Dispersion . . . 2
- 1.4 Optical fibre . . . 3
  - 1.4.1 Non-linear photonic crystal fibres . . . 6
  - 1.4.2 Supercontinuum (SC) generation . . . 7
- 1.5 Spatial light liquid modulator (SLM) as a pulse compressor . . . 8

2 Polarization of light 10
- 2.1 Electromagnetic waves . . . 10
  - 2.1.1 The wave equation and plane waves . . . 11
- 2.2 Polarization of light . . . 13
  - 2.2.1 The Jones vector . . . 14
  - 2.2.2 Orthogonal polarizations. . . . 16
    - 2.2.2.1 Expansion of arbitrary polarization as a superposition of two orthogonal polarizations . . . 17
- 2.3 Polarisation optics . . . 18
  - 2.3.1 Retarders . . . 19
  - 2.3.2 Quarter-wave plate . . . 20
  - 2.3.3 Half-wave plate . . . 21
- 2.4 Malus's law . . . 21

2.4.1 Jones matrix of a polarizer . . . 22
2.4.2 Validation of Malus's law using the Jones formalism . . . 23
2.5 Optical isolator . . . 25
2.6 Liquid crystals . . . 29
2.6.1 Optical properties of twisted nematic liquid crystals . . . 30
2.6.2 Liquid crystal as a spatial light modulator . . . 33
2.6.2.1 Components of the pulse shaper . . . 33

3 Dispersion in optics **36**
3.1 Definition . . . 36
3.1.1 Mathematical description . . . 36
3.1.2 Group velocity dispersion . . . 38
3.1.3 The effect of dispersion on a Gaussian pulse. . . . 42
3.1.4 Self-phase modulation . . . 44
3.1.5 Chirped pulses . . . 46

4 Prism pulse compressor **52**
4.1 Pulse re-compression . . . 52
4.2 Geometry of a prism used in a pulse compressor . . . 53
4.2.1 Model considering one optical path by Fork et al [35] . . . 57
4.2.2 Model considering all optical paths . . . 60
4.2.3 Spatial light modulator (SLM) as a pulse compressor . . . 65

5 Experimental set up and results **68**
5.1 Characterization of PCF output . . . 68
5.1.1 Prism pulse compressor set up . . . 69
5.1.2 Optimizing prism compressor set up . . . 72
5.2 Pulse duration measurement using background free autocorrelation technique . . . 72
5.2.1 Background free autocorrelation set up . . . 73

6 Discussions **78**

Bibliography **82**

List of Figures

1.1 Optic fibre . . . 3
1.2 Types of waves in a fibre . . . 4
1.3 Construction of an optical fibre . . . 4
1.4 Propagation of light in an optical fibre . . . 4
1.5 Refraction of light in an optic fibre . . . 5
1.6 Critical angle in an optic fibre . . . 5
1.7 Schematic of the classical triangular cladding single-core photonic crystal fibre. Hole size d and the hole pitch Λ determines the fibre structure . . . 7
1.8 **A** SEM picture of a multimode fibre with zero dispersion at visible wavelengths. **B** Optical microscope picture of a single-mode fibre with zero dispersion at wavelengths around 800 nm. The relative hole-sizes are ≈ 0.9 and 0.5 respectively. . . . 7
1.9 Scanning electron microscope image of fiber cross-section with scale bar 5μm(inset), and measured dispersion, D, of the all-normal dispersion PCF . . . 8

2.1 Propagation of a transverse wave . . . 13
2.2 Propagation of **E** and **B** field . . . 13
2.3 Schematic of a vertically polarized light . . . 15
2.4 Schematic of a horizontally polarized light . . . 16
2.5 Transmission through a linear polarizer . . . 19
2.6 Experimental plot of polarization of a quarter wave plate (qwp) . . . 21
2.7 Experimental plot of polarization of a half wave plate (hwp) . . . 22
2.8 Propagation of light via polarizers A and B . . . 23
2.9 Optical Isolator . . . 25
2.10 Faraday Rotation . . . 26
2.11 Forward mode . . . 26
2.12 Reverse mode . . . 27
2.13 Molecular organization of different types of liquid . . . 30
2.14 Propagation of light in a twisted nematic liquid crystal with angle of twist of 90° . . . 30
2.15 4-f pulse shaper set-up . . . 33

3.1 Typical refractive index variation for transparent optical materials . . . 38
3.2 Simulation showing pulse with $GDD = 0$ . . . 44
3.3 Simulation showing pulse with $GDD = 400\text{fs}^2$ . . . 45

3.4 Simulation comparing intensities of both pulses. Pluse with $GDD = 0$ has a pulse duration of 20fs while pulse with $GDD = 400\text{fs}^2$ has a pulse duration of 60fs. 45
3.5 The blue pulse represents $I(t)$ while the red pulse represents $\omega(t)$. The front of the plot is shifted to lower frequencies, and the back to higher frequencies. In the center, the frequency shift is approximately linear 47
3.6 Simulated result of a temporal profile of a Gaussian pulse with chirp parameter $b = 0$ 50
3.7 Simulated result of a temporal profile of a Gaussian pulse with chirp parameter $b = 0.0175\ \text{fs}^{-2}$ 50
3.8 Simulated result comparing intensities of chirped and unchirped pulses 51

4.1 GDD from a dispersing prism 53
4.2 Ray diagram of light passing through a prism 53
4.3 Ray diagram of light passing through a prism at Brewster's angle, $\phi_1 = \phi_2$ and angle of minimum deviation $\phi' = \phi'_2$. ε_{min} = angle of minimum deviation 56
4.4 Model of prism pulse compressor by Fork et al 58
4.5 Simulation comparing GDD from the two models of the prism pulse compressor . . . 59
4.6 Light path in a pair of dispersing prisms 60
4.7 Light path in a pair of prisms 64
4.8 4-f set up 67

5.1 Normalized measured super continuum(SC) of PCF for various input power 69
5.2 Measured super continuum(SC) of PCF for various input power on logarithmic scale 69
5.3 Experimental set up 70
5.4 Prism support 70
5.5 Some components of experimental set up 71
5.6 Some components of experimental set up 71
5.7 Spectral range of BG39 filter 72
5.8 Optimization graph of prism pulse compressor set up 73
5.9 BFA set up 74
5.10 Compressed pulse in oscilloscope time 75
5.11 Compressed pulse in real time 75
5.12 Compressed and uncompressed pulse in real time 76
5.13 Pulse spectrum from ANDi-PCF before compression 76
5.14 Fit of compressed pulse 77

6.1 Dependence of beam size on prism with bandwidth for LAkL21 Glass 78
6.2 Light course in a pair of dispersing prisms 79
6.3 Limit of prism size to pulse duration of compressed pulse 80

Chapter 1

Introduction

1.1 Aim

The main aim of this project is to compress the spectrally broadened light generated by an all normal dispersion photonic crystal fibre (ANDi-PCF). Nonlinear processes inside the fibre spectrally broaden the femtosecond laser pulse and due to dispersion of the fibre material, the pulse is also chirped. In chapter one, basic concepts in ultrafast optics are introduced. This work entails the study of polarization which is extensively discussed in chapter two. In chapter three, the concept of dispersion and the effects it has on a pulse is theoretically considered. In chapter four, we present two models of a prism pulse compressor used for pulse compression and also compare both models. To compress a pulse, the apex to apex separation distance between both prisms which will compress the stretched pulse from the photonic crystal fibre is calculated and is presented in chapter four. The experimental setup developed for this work is presented in chapter five alongside results obtained. Background free autocorrelation (BFA) is used to measure the pulse duration of the compressed pulse.

1.2 Fourier transform

In optics, when dealing with phenomena that are frequency dependent such as dispersion discussed in section 3.1, theoretical calculations of such phenomena is done in the frequency domain and the tool employed is the Fourier transform. Given an arbitrary complex-valued function $g(\alpha)$, we can compose the integral [1],

$$F(\xi) = \int_{-\infty}^{\infty} g(\alpha) e^{-i2\pi\xi\alpha} d\alpha \tag{1.2.1}$$

where ξ is any real variable. $F(\xi)$ is called the Fourier transform of $g(\alpha)$. Conditions for $F(\xi)$ to exist are [1]:

- $g(\alpha)$ is single valued.
- $g(\alpha)$ has a finite number of turning points in any finite interval.
- $g(\alpha)$ is everywhere integrable on $(-\infty, \infty)$.
- $g(\alpha)$ has, at most, a finite number of turning points in any finite interval.

The above conditions are automatically satisfied if $g(\alpha)$ accurately describes a real physical quantity. However, it is obvious that many functions used for practical purposes do not satisfy them e.g. constant functions and all periodic functions. But they are found to be a good approximation and their simple form useful. Equation (1.2.1) can be inverted to get [1]

$$g(\alpha) = \int_{-\infty}^{\infty} F(\beta) e^{i2\pi\beta\alpha} d\beta. \tag{1.2.2}$$

Assuming that $F(\beta)$ exists, equation (1.2.2) is called the inverse Fourier transform. In equation (1.2.2), $F(\beta)$ is a complex-valued weighting factor, prescribing the correct magnitude and phase shift for all exponential components or Fourier components of which $f(\alpha)$ consists [1]. Similarly, in equation (1.2.1), $f(\alpha)$ describes the magnitude and phase shift for all of the Fourier components of $F(\xi)$. Equation (1.2.1) and equation (1.2.2) together, are known as the inverse Fourier integrals [1]. Note that the only distinction between equation (1.2.1) and equation (1.2.2) is the sign of the exponent.

We now find the Fourier transform, as an example, of a Gaussian pulse. The Gaussian pulse is of significance since our laser pulses have a typical Gaussian temporal distribution. Consider [2],

$$g(t) = \frac{\alpha}{\sqrt{2\pi}\sigma} \exp -(\frac{1}{2}(\frac{t}{\sigma})^2) \tag{1.2.3}$$

$$\mathcal{F}\{g(t)\} = \int_{-\infty}^{\infty} \frac{\alpha}{\sqrt{2\pi}\sigma} \exp -(\frac{1}{2}(\frac{t}{\sigma})^2) \exp -(i2\pi f t) dt \tag{1.2.4}$$

$$= \frac{\alpha}{\sqrt{2\pi}\sigma} \exp -\frac{1}{2\sigma^2}(2\sigma^2\pi f)^2 \int_{-\infty}^{\infty} \exp -\frac{1}{2\sigma^2}(t + 2i\sigma^2\pi f)^2 dt. \tag{1.2.5}$$

Let

$$s = \frac{t + 2i\sigma^2\pi f}{\sqrt{2}\sigma} \tag{1.2.6}$$

$$s^2 = \frac{(t + 2i\sigma^2\pi f)^2}{2\sigma^2} \tag{1.2.7}$$

$$dt = \sqrt{2}\sigma ds$$

$\therefore$

$$\mathcal{F}\{g(t)\} = \frac{\alpha}{\sqrt{2\pi}\sigma} \exp -\frac{1}{2\sigma^2}(2\sigma^2\pi f)^2 \int_{-\infty}^{\infty} \exp -(s^2) ds \sqrt{2}\sigma ds \tag{1.2.8}$$

$$= \alpha \exp -(\frac{1}{2\sigma^2}(2\sigma^2\pi f)^2). \tag{1.2.9}$$

Clearly, comparing equations (1.2.3) and (1.2.9), we see that the Fourier transform of a Gaussian is also a Gaussian which is a very important property of Gaussian pulses.

1.3 Dispersion

When a dielectric is subjected to an applied electric field, the internal charge distribution is distorted. This corresponds to the generation of electric dipole moments, which in turn contribute

to the total internal electric field. The resultant dipole moment per unit volume is called the electric polarization $\vec{\mathbf{P}}$. For most materials, the electric field $\vec{\mathbf{E}}$ and $\vec{\mathbf{P}}$ are proportional and are related by [3]

$$(\epsilon - \epsilon_0)\,\vec{\mathbf{E}} = \vec{\mathbf{P}}. \tag{1.3.1}$$

In equation (1.3.1), ϵ_0 is the permittivity of free space and ϵ is the permittivity of the material. Light is dispersed when it propagates through optics. The amount of dispersion in a medium through which light propagates, depends on the refractive index n of the medium which will be shown in equation (2.1.12) to be related to ε. Examples of such media are glass and optical fibre. Due to the large distance travelled by light in an optical fibre, dispersion which leads to the temporal broadening of an ultrafast pulse is more pronounced when compared to that obtained in an optic e.g a thin piece of glass.

The dependence of refractive index on wavelength has two effects on a pulse. These effects are observed in space and time. Dispersion in space is known as angular dispersion. If observed in time, we call it a chirp. A chirped pulse is a pulse in which the frequency content of the pulse increases or decreases as the pulse travels in time. A detailed discussion will be given in section 5.10. For example, if white light is incident on a prism, the white light is dispersed into it's constituent colours, which we call the spectrum. The angular dispersion due to the blue component is more compared to the red component. A thorough discussion of dispersion will be given in section 3.1.

1.4 Optical fibre

Optical fibres are thin transparent glass or plastic fibres which can guide light. They work by the principle of total internal reflection from diametrically opposite walls. See figure 1.1. As a result, light can be taken anywhere because fibres have enough flexibility. This property

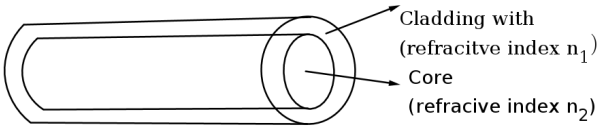

Figure 1.1: Optical fibre [4].

makes them suitable for data communication, design of fine endoscopes, micro sized microscopes amongst others. An optic fibre consists of a core that is surrounded by a cladding which are normally made of silica glass or plastic [4]. In fibres, three types of waves are distinguished. They are the core waves, cladding waves and space waves [5], see figure 1.2. Light propagation over large distances occurs only with the waves in the core. Excitation of the other waves leads to losses. Hence, every effort is geared towards coupling light into the core. To this end, the angle of incidence should not be made too large, otherwise part of the light induces cladding and space waves. The basic construction of an optic fibre is shown in figure 1.3. To understand the propagation of light through an optical fibre, consider figure 1.4. Consider a ray of light labelled (i) entering the core at a point A, travelling through the core until it reaches the core-cladding

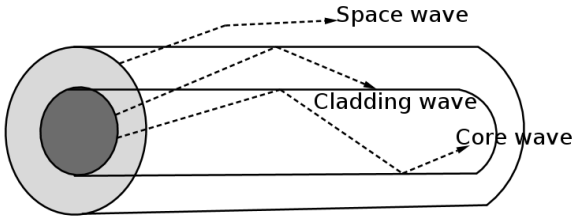

Figure 1.2: Types of waves in a fibre [5].

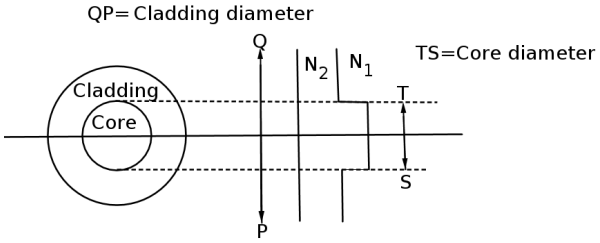

Figure 1.3: Construction of an optical fibre [4].

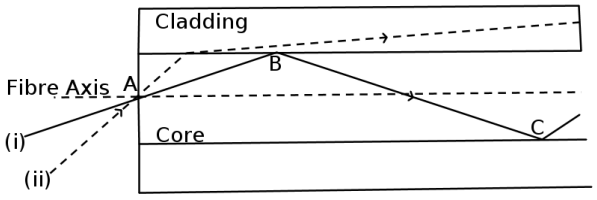

Figure 1.4: Propagation of light in an optical fibre [4].

boundary at a point B. As long as the light ray intersects the core-cladding boundary at small angles, the ray will be reflected back into the core to travel to point C where the process of reflection is repeated that is, total internal reflection takes place. Total internal reflection occurs only when the angle of incidence is greater than the critical angle. If a ray enters an optical fibre at a steep angle labelled (ii), reflection back into the core does not take place and the light ray is lost in the cladding. So, reflection back into the core does not take place and the light ray is lost in the cladding. This means that to be guided through an optical fibre, a light ray must enter the core with an angle less than a particular angle called the acceptance angle of the fibre. A ray which enters the fibre with an angle greater than the acceptance angle will be lost in the cladding.

Consider an optical fibre having a core of refractive index n_1 and cladding of refractive index n_2. Let the incident light make an angle i with the core axis as shown in the figures 1.5 and 1.6. The light gets refracted at an angle θ, and falls on the core-cladding interface at an angle θ' given by, [4]

$$\theta' = 90 - \theta. \tag{1.4.1}$$

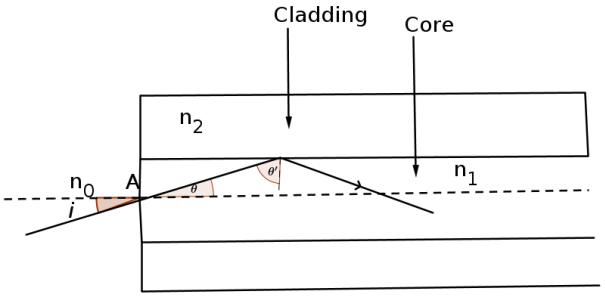

Figure 1.5: Refraction of light in an optic fibre [4].

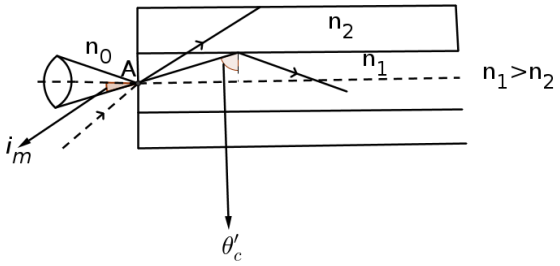

Figure 1.6: Critical angle in an optic fibre [4].

Applying Snell's law at the point of entrance of light into the optical fibre we get [4]

$$n_0 \sin i = n_1 \sin \theta \tag{1.4.2}$$

where n_0 is the refractive index of the medium outside the fibre. Since the refractive index in air is 1, $n_0 = 1$. When light travels from core to cladding it moves from a denser to a less dense medium hence, it may be totally reflected back to the core medium if θ' exceeds the critical angle θ'_c. The critical angle is that angle of incidence in the denser medium n_1 for which the angle of refraction becomes 90°. Snell's law at the core cladding interface gives [4]

$$n_1 \sin \theta'_c = n_2 \sin 90 \tag{1.4.3}$$

or

$$\sin \theta'_c = \frac{n_2}{n_1}. \tag{1.4.4}$$

Hence, for light to be propagated within the core of optical fibre, the angle of incidence at core-cladding interface should be greater than θ'_c. From equations (1.4.1) and (1.4.2), we see that as i increases, θ increases and so θ' decreases. Therefore, there is a maximum value of angle of incidence beyond which, it does not propagate rather it is refracted into the cladding medium, see figure 1.6. This maximum value of i say i_m is called the maximum angle of acceptance and $n_0 \sin i_m$ is called the numerical aperture (NA). From equation (1.4.2)

$$\text{NA} = n_0 \sin i_m = n_1 \sin \theta \tag{1.4.5}$$

$$= n_1 \sin(90 - \theta'_c) \tag{1.4.6}$$

or

$$\text{NA} = n_1 \cos\theta_c' \tag{1.4.7}$$

$$= n_1\sqrt{1-\sin^2\theta_c'}. \tag{1.4.8}$$

From equation (1.4.4)

$$\sin\theta_c' = \frac{n_2}{n_1}. \tag{1.4.9}$$

Substitute equation (1.4.9) into equation (1.4.8) and get,[4]

$$\text{NA} = n_1\sqrt{1-\frac{n_2^2}{n_1^2}} \tag{1.4.10}$$

$$= \sqrt{n_1^2-n_2^2} \tag{1.4.11}$$

from equation (1.4.11), we see that NA is always positive since for a fibre design, $n_1 > n_2$. In a dispersive medium such as the optical fibre, the refractive index depends on the wavelength. Thus, dispersion can alter the NA of a fibre since the refractive index changes with wavelength.

In reality, light is propagated inside an optical fibre through modes. Modes are the possible solutions of the Helmholtz equation for waves [6]. These modes define the way the wave travels through space, that is, how the wave is distributed in space [6]. In single mode fibres (fibres designed to carry only a single mode) such as the ANDi-PCF used in this project, we have waves of different frequencies but of the same mode. This means that the waves are distributed in space in the same way and that gives a single ray of light [6].

1.4.1 Non-linear photonic crystal fibres

The term photonic crystal fibre is inspired by the unique cladding structure of this fibre class. Standard fibres guide light by total internal reflection between a core with a high refractive index, embedded in a cladding with a lower refractive index. The index differences in photonic crystal fibres are obtained by forming a matrix of different material with high and low refractive index. With this method, a hybrid material is created with properties not obtainable in solid materials. The hybrid material cladding can be constructed with a structure similar to that found in certain crystals, which is where the term photonic crystal fibre originates [7]. Two fundamental classes of photonic crystal fibres (PCFs) exist. They are the index guiding PCFs and fibres that confine light through a photonic band gap (PBG) [7]. An index guiding PCF comprises of a solid glass high-index core, embedded in an air-filled cladding structure where a number of air holes are arranged in a pattern that runs along the length of the fibre. This creates a hybrid air-silica material with a refractive index lower than the core.

Figure 1.7 shows the principle of the classical triangular cladding single-core photonic crystal fibre, which has one of the most efficient and flexible designs, forming the basis of most PCFs today [7]. The fibre in figure 1.7 is a large mode area-type fibre. The outer diameter of the fibres is typically 125 μm and the pitch which is the distance between the centres of two air holes of

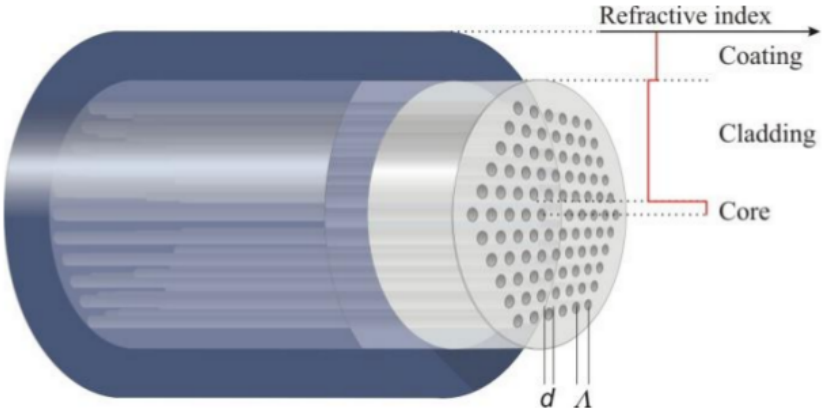

Figure 1.7: Schematic of the classical triangular cladding single-core photonic crystal fibre. Hole size d and the hole pitch Λ determines the fibre structure [7].

the fibre is consequently 10-15μm [7]. Non-linear fibres are typically designed with a pitch of approximately 1-3μm. Therefore, the microstructred region of a non-linear PCF only takes up the inner 20-50% of the fibre cross section [7].

Non-linear PCFs are of two basic types, there are the multimode fibres with extremely small core and cobweb like structure, and single-mode fibres with slightly larger cores, smaller holes and engineered zero dispersion wavelength. Figure 1.8 shows the difference in microstructure for the two types of non-linear PCFs

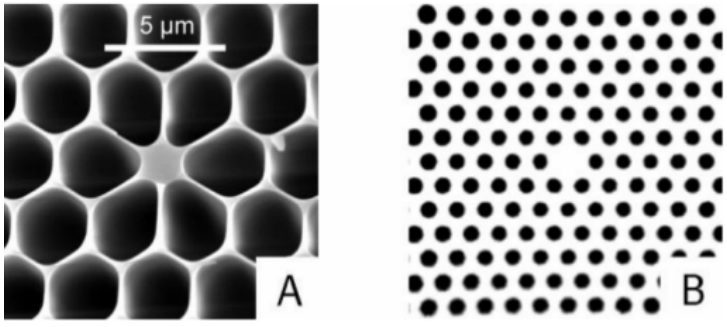

Figure 1.8: **A** SEM picture of a multimode fibre with zero dispersion at visible wavelengths. **B** Optical microscope picture of a single-mode fibre with zero dispersion at wavelengths around 800 nm. The relative hole-sizes are $\approx$ 0.9 and 0.5 respectively. The pictures are shown on the same scale [7].

1.4.2 Supercontinuum (SC) generation

Supercontinuum is the conversion of a narrow bandwidth (10nm -15nm), in this case the output from our Tsunami laser operating at 800nm, into a broadband spectrum, through a complex combination of high non-linear effects in an optically non-linear medium. Supercontinuum sources such as the all normal dispersion photonic crystal fibre used in this work, are a new type of light source that provide a combination of high output power, a broad flat spectrum and a high degree

of spatial coherence that allows tight focusing. Spatial coherence is a measure of the correlation of the phase difference between the electric fields at different locations across the beam profile [8]. A high spatial coherence means that the phase difference is constant at any location across the beam profile. The dispersion curve of the all normal dispersion photonic crystal fibre is shown in figure 1.9.

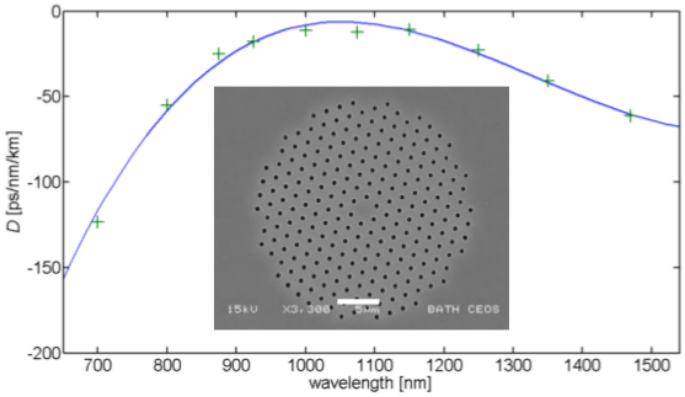

Figure 1.9: Scanning electron microscope image of fiber cross-section with scale bar 5μm(inset), and measured dispersion, D, of the all-normal dispersion PCF [9].

A supercontinuum source typically consists of a laser pulse and a non-linear element in which a combination of non-linear effects broaden the narrow-band laser radiation into a continuous spectrum without destroying the spatial coherence of the laser light [7]. ANDi-PCF is good because the non-linear effects does not destroy the spatial coherence of the laser hence, forms a stable supercontinumm. Photonic crystal fibres are uniquely suited as the non-linear medium for such sources, thus offering high non-linearity and suitable dispersion. By suitable dispersion, we mean dispersion in the all normal dispersion regime. The broadband supercontinuum generated by a non-linear medium such as the photonic crystal fibre also has a chirp. The pulse is stretched in time due to the dispersion and since in the all normal dispersion regime, a constant phase relation exists in the pulse [10], it can be compressed to give very short pulses using the standard known pulse compression techniques such as the one discussed in section 4.2.2.

1.5 Spatial light liquid modulator (SLM) as a pulse compressor

Optical pulses in the 5-fs region have been generated using chirped mirrors for chirp compensation [11]. The SLM as a pulse shaper is further discussed in section 2.6.2. This pulse shaping technique using the liquid crystal spatial light modulator (SLM) for pulse compression has an advantage over the prism pulse compressor discussed in section 4.2.2 because of it's ability to accommodate large bandwidth(300nm-1500nm). This is essential because as explained in equation (6.0.2), the larger the bandwidth, the shorter pulses can be compressed. Also, the SLM can be used to compensate for higher order chirps which the prism pulse compressor cannot compensate for since it only compensates for linear chirp. Compensating for higher order chirp by the SLM simply bring to the fore the ability of the SLM to accommodate light of large bandwidths. Details of the SLM as a pulse compressor will be discussed in section 4.2.3

The main objective of this work was to develop and build a prism pulse compressor in order to compress white light from an ANDi-PCF. To aid in carrying out the main objective of this project, a brief knowledge of optical fibres was discussed in sections 1.4 and 1.4.1 . In addition, the use of an SLM as a pulse compressor using the 4-f set up was theoretically investigated using the Fourier transform discussed in section 1.2 as a tool.

Chapter 2

Polarization of light

Spatial light modulators (SLM) can be used to compress a pulse as will be discussed in section 4.2.3. In order to compress a pulse, the SLM effects polarization changes on the beam. How it effects polarization changes on the beam will be studied in this chapter.

2.1 Electromagnetic waves

Since an ultrashort laser pulse is made up of light which is a form of electromagnetic radiation, Maxwell's equations are employed to describe it. Maxwell's equations are a set of relationships between the electric field **E** measured in Vm^{-1} and the magnetic field **H** measured in Am^{-1}. If an electromagnetic radiation travels inside a medium, charge density ρ measured in Cm^{-3}, polarization **P** measured in Cm^{-2}, magnetization density **M** measured in Am^{-1} and current density **J** measured in Am^{-2} are considered in order to include the effect of the fields on the matter [12]. The electric and magnetic flux densities **D** measured in Cm^{-2} and **B** measured in T are also included. Maxwell's equations are given as [12]

$$\nabla \cdot \mathbf{D} = \rho \tag{2.1.1}$$

$$\nabla \cdot \mathbf{B} = 0 \tag{2.1.2}$$

$$\nabla \times \mathbf{E} = -\frac{\partial \mathbf{B}}{\partial t} \tag{2.1.3}$$

$$\nabla \times \mathbf{H} = \mathbf{J} + \frac{\partial \mathrm{D}}{\partial t}. \tag{2.1.4}$$

The relations defining **D** and **B** are [12]

$$\mathrm{D} = \varepsilon_0 \mathrm{E} + \mathbf{P} \tag{2.1.5}$$

$$\mathrm{B} = \mu_0(\mathbf{H} + \mathbf{M}) \tag{2.1.6}$$

ε_0 and μ_0 are respectively the permittivity and permeability of free space with values $8.85 \times 10^{-12}\mathrm{Fm}^{-1}$ and $4\pi \times 10^{-7}\mathrm{Hm}^{-1}$.

In a source-free medium, $\rho = 0$ and $\mathbf{J} = 0$ hence, in free space, [12]

$$\rho = \mathbf{J} = \mathbf{P} = \mathbf{M} = 0 \tag{2.1.7}$$

In a linear medium, the medium response that is, polarization and magnetization, is linear in the applied fields. For the case of the electric field we have [12]

$$\mathbf{P} = \varepsilon_0 \chi_e \mathbf{E} \tag{2.1.8}$$

where χ_e is a dimensionless quantity known as the electric susceptibility. Substituting equation (2.1.5) into equation (2.1.8) we have [12]

$$\mathbf{D} = \varepsilon_0(1 + \chi_e)\mathbf{E} \tag{2.1.9}$$

$$= \varepsilon \mathrm{E}. \tag{2.1.10}$$

The proportionality constant ϵ is called the dielectric constant [12]

$$\varepsilon = (1 + \chi_e)\varepsilon_0. \tag{2.1.11}$$

Other forms of ε include the relative dielectric constant $\frac{\varepsilon}{\varepsilon_0}$ and the refractive index n where [12]

$$n^2 = \frac{\varepsilon}{\varepsilon_0}. \tag{2.1.12}$$

For the case of the magnetic field, we have [12]

$$\mathrm{M} = \chi_m \mathbf{H} \tag{2.1.13}$$

where χ_m is the magnetic polarizability. Substituting equation (2.1.6) into equation (2.1.13) we get [12]

$$\mathbf{B} = \mu_0(1 + \chi_m)\mathbf{H} \tag{2.1.14}$$

$$= \mu \mathbf{H}. \tag{2.1.15}$$

In ultrafast optics, one is generally interested in nonmagnetic materials for which $\mathbf{M}= 0$ for which equation (2.1.14) becomes [12]

$$\mathbf{B} = \mu_0 \mathbf{H}. \tag{2.1.16}$$

Equations (2.1.8) and (2.1.13) specify the response of a material to fields. The forms of equations (2.1.8) and (2.1.13) are true because a linear medium and isotropic media have been assumed. For example, nonlinear optical effects require by definition that $\mathbf{P}$ be a non-linear function of $\mathbf{E}$ [12].

2.1.1 The wave equation and plane waves

We now consider the propagation of electromagnetic waves in a linear and source free medium. Taking the curl of equation (2.1.2) and inserting in equation (2.1.3) using the vector identity [12]

$$\nabla \times \nabla \times \mathbf{A} = \nabla(\nabla \cdot \mathbf{A}) - \nabla^2 \mathbf{A} \tag{2.1.17}$$

we get [12]

$$\nabla \times \nabla \times \mathbf{E} = \nabla(\nabla \cdot \mathbf{E}) - \nabla^2 \mathbf{E} = -\mu\varepsilon \frac{\partial^2 \mathbf{E}}{\partial t^2} \tag{2.1.18}$$

Substituting $\nabla \cdot \mathbf{E} = 0$ into equation (2.1.18), we get the wave equation [12],

$$\nabla^2 \mathbf{E} = \mu\varepsilon \frac{\partial^2 \mathbf{E}}{\partial t^2}. \tag{2.1.19}$$

Of special interest is the case where the field varies only one direction, say in the x direction. Then equation (2.1.19) becomes [12]

$$\frac{\partial^2 \mathbf{E}}{\partial z^2} = \mu\varepsilon \frac{\partial^2 \mathbf{E}}{\partial t^2}. \tag{2.1.20}$$

The general solution of equation (2.1.20) takes the form [12]

$$\mathbf{E}(z,t) = \mathrm{E}_0(t - \frac{z}{v}) \tag{2.1.21}$$

where $\mathbf{E}_0$ is a vector in the x-y plane and $v = \frac{1}{\sqrt{\mu\varepsilon}}$. Equation (2.1.21) is called a plane-wave solution since the field does not vary in the transverse plane that is, the x-y plane. It also represents a travelling wave, since the field propagates in the z direction without changing it's form. In the case of a pulsed field, $\mathbf{E}_0(t)$ represents the pulse shape [12]. The propagation velocity in free space c, is given as [12]

$$c = \frac{1}{\sqrt{\mu_0 \varepsilon_0}} \approx 2.99 \times 10^8 \mathrm{ms}^{-1}. \tag{2.1.22}$$

For dielectric media, $\mu \approx \mu_0$, hence making ϵ_0 subject in equation (2.1.12) and substituting into equation (2.1.22) we derive the velocity of propagation within a medium as [12]

$$v = \frac{c}{n} \tag{2.1.23}$$

where n is the refractive index. In deriving equations (2.1.12) and (2.1.18), we have assumed that the refractive index n, is independent of frequency. In section 3.1, we will see that in a dispersive media, n is frequency dependent.

In the case of a sinusoidal solution to the wave equation, equation (2.1.21) is written as [12]

$$\mathbf{E}(z,t) = \mathbf{E}_0 \cos(\omega t - \beta z + \phi) \tag{2.1.24}$$

where $\mathbf{E}_0$ is now a constant vector, ω is the angular frequency, ϕ the phase and the propagation constant β is given by [12]

$$\beta = \frac{\omega n}{c} = n k_0. \tag{2.1.25}$$

Where $k_0 = \frac{2\pi}{\lambda_0}$. The wave has a temporal oscillation period of $\frac{2\pi}{\omega}$ and a spatial period or wavelength in the medium given by $\lambda = \frac{2\pi}{\beta}$. The wavelength in free space denoted by λ_0 is given by [12]

$$\lambda_0 = \frac{2\pi c}{\omega}. \tag{2.1.26}$$

Equation (2.1.24)can also written in the equivalent form [12]

$$\mathbf{E}(z,t) = Re\{\tilde{\mathbf{E}}_0 e^{i(\omega t - \beta z)}\} \tag{2.1.27}$$

where Re $\{\cdots\}$ denotes the real part and the phase ϕ has been incorporated into the complex vector $\tilde{\mathbf{E}}_0$. Equation (2.1.27) is the complex notation of equation (2.1.24). Equation (2.1.27) is preferred when working with waves because analytically, it is simpler to work with.

2.2 Polarization of light

Light is a transverse electromagnetic wave, therefore it's propagation can be explained using the properties of transverse waves. A transverse wave, see figure 2.1, can be pictured as traced by a point that oscillates sinusoidally in a plane, in such a manner that the direction of oscillation is perpendicular to the direction of propagation of the wave. The oscillating point depicts the oscillation of the electric field **E** of the light wave. In figure 2.2, **B** is the magnetic field which oscillates in a direction perpendicular to **E**. The magnetic field is ignored when studying polarization because it is weak hence, only the electric field is calculated. In figures 2.1 and 2.2, only one electric field vector is shown. In reality, light emitted from a source e.g an incandescent light bulb consists of many such electric field vectors, hence the light is said to be unpolarized.

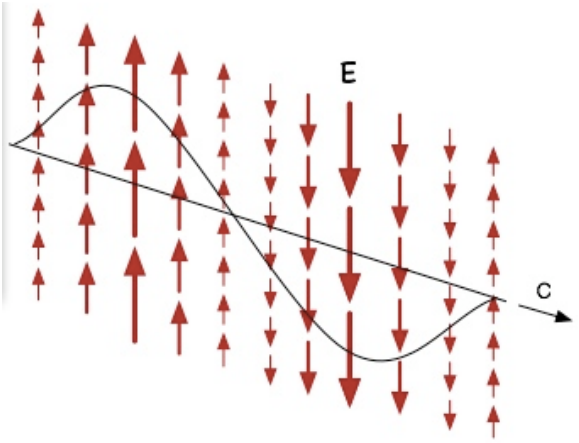

Figure 2.1: Propagation of a transverse wave [13].

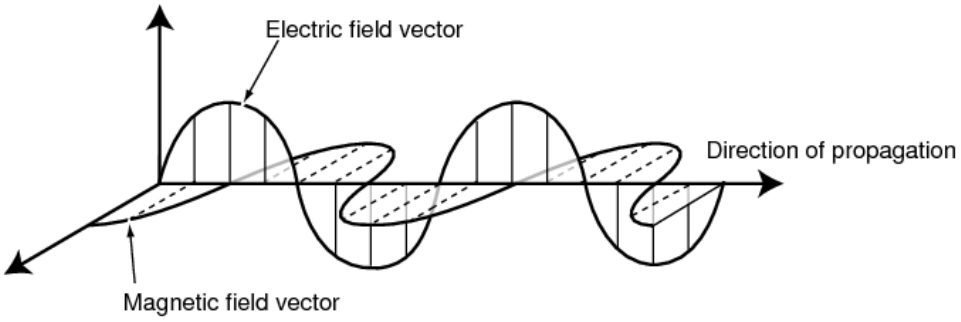

Figure 2.2: Propagation of **E** and **B** field [13].

Partially polarized light occurs if the **E** vectors have a preferred direction of oscillation. If all the electric field vectors oscillate in the same plane, parallel to a fixed direction referred to as a polarization plane, then the light is totally linearly polarized or plane polarized. The special case of vertically polarized light is represented by a vertical arrow, a dot is used to represent a horizontally polarized light indicating that **E** oscillates into and out of the page. For a linearly polarized light, the plane of polarization is a plane parallel both to the direction of oscillation of the electric field vector and the direction of propagation of the wave. The behaviour of electromagnetic waves is studied by considering two orthogonal components of the electric field vector, the phase between these two components explain the different states of polarization. If the phase difference is random, then the light is unpolarized, if the phase difference is random but more of one component is present, then the light is partially polarized. But, if the phase difference is a constant, then the light is totally polarized. Specifically, a phase difference of $0°$ or $180°$ implies a linearly polarized light, a phase difference of $90°$ or $270°$ and both components have equal amplitude the light is circularly polarized. Also, if a constant phase difference other than $0°, 90°, 180°$ or $270°$ exist and/or the amplitudes of the components are not equal, then the light is elliptically polarized. In contrast to linear polarization where the plane of polarization remains constant, in circular and elliptical polarizations, the plane of polarization rotates. Two directions of linearly polarized light exist. Right-hand circularly polarized light is defined such that the electric field is rotating clock-wise as seen by an observer as the wave travels towards the observer. Left- handed circularly polarized light is defined such that the electric field is rotating anti-clockwise as seen by an observer as the wave travels towards the observer.

2.2.1 The Jones vector

The Jones vector is employed when dealing with coherent light sources such as lasers because it deals with the instantaneous electric field $\mathbf{E}_0$ [14]. But the Stokes and Muller vectors describe a time-averaged optical signal, hence they are preferred for use with light of rapidly and randomly changing polarization state such as natural sunlight [14]

In section 2.1.1, the complex form of equation (2.1.24), which is a solution to the wave equation given by equation (2.1.20) can be written as [12]

$$\tilde{E}(z,t) = E_{ox}e^{i\psi}. \tag{2.2.1}$$

Consider another orthogonal solution to the wave equation given by [12]

$$\tilde{E}'(z,t) = E_{oy}e^{i\phi}. \tag{2.2.2}$$

Where $\psi = \omega_1 t$ and $\phi = \omega_2 t$. The state of polarization of light is determined by the relative amplitudes of E_{ox} and E_{oy} and relative phases δ between the two components $\tilde{E}(z,t)$ and $\tilde{E}'(z,t)$ where $\delta = \phi - \psi$. The independent complex amplitude is written as a two element matrix called the Jones matrix given as [14]

$$J = \begin{bmatrix} \tilde{E}_{ox} \\ \tilde{E}_{oy} \end{bmatrix} \tag{2.2.3}$$

$$= \begin{bmatrix} E_{ox}e^{i\psi} \\ E_{oy}e^{i\phi} \end{bmatrix} \tag{2.2.4}$$

$$= e^{i\psi} \begin{bmatrix} E_{ox} \\ E_{oy}e^{i\delta} \end{bmatrix}. \tag{2.2.5}$$

Let equations (2.2.1) and(2.2.2) represent the oscillations of the electric field along the x and y axis respectively with phases ψ and ϕ.

The basis for the Jones vector is chosen to be $\vec{E_h}$, the horizontal and $\vec{E_v}$, the vertical polarization states. For vertically polarized light, see figure 2.3, we set in equation 2.2.4 $\phi = 0$ and $E_{ox} = 0$ (since the electric field has no component in the x-direction) and get [14]

$$\vec{E_v} = \begin{bmatrix} 0 \\ E_{oy} \end{bmatrix}. \tag{2.2.6}$$

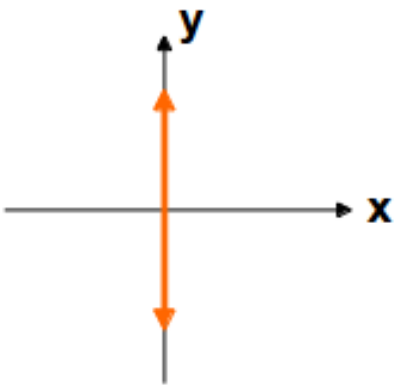

Figure 2.3: Schematic of a vertically polarized light [5].

Similarly, for horizontal polarized light, see figure 2.4, we set $\psi = 0$ in equation (2.2.4) and get [14]

$$\vec{E_h} = \begin{bmatrix} E_{ox} \\ 0 \end{bmatrix}. \tag{2.2.7}$$

In their normalized forms, equations (2.2.6) and (2.2.7) are given by [14]

$$\vec{E_h} = \begin{bmatrix} 1 \\ 0 \end{bmatrix}. \tag{2.2.8}$$

and

$$\vec{E_v} = \begin{bmatrix} 0 \\ 1 \end{bmatrix}. \tag{2.2.9}$$

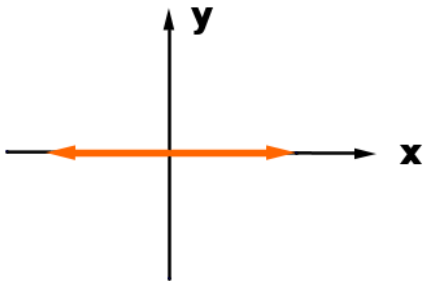

Figure 2.4: Schematic of a horizontally polarized light [5].

We also have the right-circular and left-circular polarizations. In the right circular, the phase of the y-component leads the x-component by $\frac{\pi}{2}$ while for the left circular, it is the x component that leads by $\frac{\pi}{2}$. Thus for right circular polarization $\vec{E_R}$, the Jones vector is [14]

$$\vec{E_R} = \begin{bmatrix} E_o e^{i\phi} \\ E_o e^{i(\phi - \frac{\pi}{2})} \end{bmatrix}. \tag{2.2.10}$$

Normalizing equation (2.2.10) yields, [14]

$$\vec{E_R} = \frac{1}{\sqrt{2}} \begin{bmatrix} 1 \\ e^{i\frac{\pi}{2}} \end{bmatrix} = \frac{1}{\sqrt{2}} \begin{bmatrix} 1 \\ -i \end{bmatrix}. \tag{2.2.11}$$

Similarly, the normalized representation for left circular light $\vec{E_L}$ is given by [14]

$$\vec{E_L} = \frac{1}{\sqrt{2}} \begin{bmatrix} 1 \\ i \end{bmatrix}. \tag{2.2.12}$$

2.2.2 Orthogonal polarizations.

Two polarization states given by two Jones vectors J_1 and J_2 are orthogonal if their inner product is zero. Suppose J_1 and J_2 are defined as

$$J_1 = \begin{bmatrix} A_{1x} \\ A_{1y} \end{bmatrix} \tag{2.2.13}$$

and

$$J_2 = \begin{bmatrix} A_{2x} \\ A_{2y} \end{bmatrix}. \tag{2.2.14}$$

Then, their inner product is given by [15]

$$(J_1, J_2) = A_{1x} {A^*}_{2x} + A_{1y} {A^*}_{2y} \tag{2.2.15}$$

where A_{1x} and A_{1y} are elements of J_1 and ${A^*}_{2x} {A^*}_{2y}$ are elements of J_2.

2.2.2.1 Expansion of arbitrary polarization as a superposition of two orthogonal polarizations

A Jones vector J can be visualized as a superposition of two orthogonal Jones vectors J_1 and J_2. J_1 and J_2 are called the expansion basis. That is, [15]

$$J = \alpha_1 J_1 + \alpha_2 J_2. \tag{2.2.16}$$

Normalizing J_1 and J_2 we have [15]

$$(J_1, J_1) = (J_2, J_2) = 1 \tag{2.2.17}$$

with expansion coefficients given by [15]

$$\alpha_1 = (J, J_1) \tag{2.2.18}$$

and

$$\alpha_2 = (J, J_2)\,. \tag{2.2.19}$$

As an example we show that the linearly polarized wave with plane of polarization making an angle θ with the x-axis is equivalent to a superposition of right and left circularly polarized waves with weights $\frac{1}{\sqrt{2}}\left(e^{-i\theta}\right)$ and $\frac{1}{\sqrt{2}}\left(e^{i\theta}\right)$.

Right circularly polarized waves have a Jones vector given by

$$J_1 = \frac{1}{\sqrt{2}}\begin{bmatrix}1\\ i\end{bmatrix}. \tag{2.2.20}$$

A left circularly polarized wave has a Jones vector given by

$$J_1 = \frac{1}{\sqrt{2}}\begin{bmatrix}1\\ -i\end{bmatrix}. \tag{2.2.21}$$

The weight α_1 attached to J_1 is

$$\alpha_1 = \frac{1}{\sqrt{2}}\left(e^{-i\theta}\right) \tag{2.2.22}$$

and α_2, the weight attached to J_2 is

$$\alpha_2 = \frac{1}{\sqrt{2}}\left(e^{i\theta}\right). \tag{2.2.23}$$

Using equation (2.2.16) we get,

$$J = \frac{1}{2}\begin{pmatrix} e^{-i\theta} \\ ie^{ie^{-i\theta}} \end{pmatrix} + \frac{1}{2}\begin{pmatrix} e^{i\theta} \\ -ie^{i\theta} \end{pmatrix} \tag{2.2.24}$$

$$J = \frac{1}{2}\begin{pmatrix} e^{-i\theta} + e^{i\theta} \\ ie^{-i\theta} - ie^{i\theta} \end{pmatrix}. \tag{2.2.25}$$

Using,

$$\cos\theta = \frac{e^{-i\theta} + e^{i\theta}}{2} \tag{2.2.26}$$

and

$$\sin\theta = \frac{e^{i\theta} - e^{-i\theta}}{2i} \tag{2.2.27}$$

$\therefore$

$$J = \begin{pmatrix} \cos\theta \\ \sin\theta \end{pmatrix}. \tag{2.2.28}$$

Equation (2.2.28) shows that a linearly polarized wave with plane of polarization making an angle θ with the x-axis is equivalent, in fact same as the superposition of right and left circularly polarized waves with weights $\frac{1}{\sqrt{2}}\left(e^{-i\theta}\right)$ and $\frac{1}{\sqrt{2}}\left(e^{i\theta}\right)$

2.3 Polarisation optics

Certain materials have the property of transmitting an incident unpolarized light in one polarization direction only. Such materials are termed dichroic materials. Dichroic polarizing sheets are manufactured by stretching long-chained polymer molecules after which they are saturated with dichroic materials such as iodine. The direction perpendicular to the orientated molecular chains is called the transmission axis of the polariser. A polarising sheet has a characteristic polarizing direction along it's transmission axis. All components perpendicular to the transmission axis are completely absorbed by the dichroic material making up the polariser. This is called selective absorption. Therefore, light emerging from a polariser is linearly polarized in a direction parallel to the transmission axis of the polariser. Figure 2.5 illustrates the idea. The linear polariser is orientated such that it's transmission axis is horizontal. Light incident on the polariser is unpolarized, since the **E** vectors of the unpolarized light can be resolved into two orthogonal components, one parallel to the transmission axis of the polariser and the other perpendicular to it, the resulting light emerging from the linear polariser is now linearly polarized in the horizontal direction.

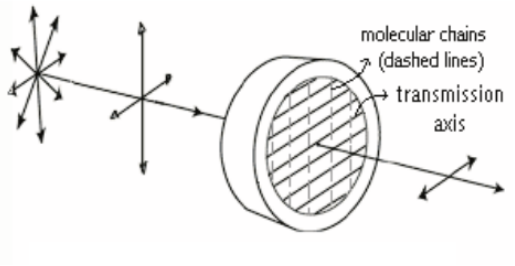

Figure 2.5: Transmission through a linear polarizer [16].

2.3.1 Retarders

Retarders are optics which delay one polarization component with respect to the other. Examples of retarders include the half and quarter wave plates which will be discussed in sections 2.3.3 and 2.3.2 respectively. As an example, we wish to find the matrix for a retarder M, which will transform E_1 and E_2 given by [17]

$$E_1 = E_{ox}e^{i\psi} \tag{2.3.1}$$
$$E_2 = E_{oy}e^{i\phi} \tag{2.3.2}$$

into E_1' and E_2' given by [17]

$$E_1' = E_{ox}e^{i(\psi+\varepsilon_x)} \tag{2.3.3}$$
$$E_2' = E_{oy}e^{i(\phi+\varepsilon_y)}. \tag{2.3.4}$$

By inspection, the matrix which will transform equations (2.3.1) and (2.3.2) to equations (2.3.3) and (2.3.4) is [17]

$$M = \begin{bmatrix} e^{i\varepsilon_x} & 0 \\ 0 & e^{i\varepsilon_y} \end{bmatrix}. \tag{2.3.5}$$

Equation (2.3.5) can also be written as [17]

$$M = e^{i\varepsilon_x}\begin{bmatrix} 1 & 0 \\ 0 & e^{i(\varepsilon_y-\varepsilon_x)} \end{bmatrix} = e^{i\varepsilon_x}\begin{bmatrix} 1 & 0 \\ 0 & e^{\delta} \end{bmatrix} \tag{2.3.6}$$

where

$$\delta = \varepsilon_y - \varepsilon_x. \tag{2.3.7}$$

For a birefringent material of thickness d, the phase delay acquired by light after travelling through it is given by [17]

$$\delta = kn_y d - kn_x d = \frac{2\pi}{\lambda}\Delta n d \tag{2.3.8}$$

where Δn is the difference in refractive index. Thus, it's Jones matrix is, [17]

$$\begin{bmatrix} 1 & 0 \\ 0 & e^{\Delta\phi}. \end{bmatrix} \tag{2.3.9}$$

Employing the analysis yielding equation (2.3.9), the Jones matrix of any retarder can easily be calculated if $\Delta\phi$ is known.

2.3.2 Quarter-wave plate

A quarter wave plate is a retarder such that [17]

$$\Delta\phi = \frac{\pi}{2}. \tag{2.3.10}$$

Equation (2.3.10) simply tells us that the quarter wave plate offers a delay of $\frac{\pi}{2}$ between the two components of light incident on it. Substituting equation 2.3.10 into equation 2.3.9 gives the Jones matrix M_{qwp}, for a quarter wave plate as [17]

$$M_{qwp} = \begin{bmatrix} 1 & 0 \\ 0 & i \end{bmatrix}. \tag{2.3.11}$$

When light with linear polarization at $+45°$ passes through the quarter wave plate, it gets converted to right circular polarization. In the Jones matrix formalism already established in section 2.2.1, the new polarization state can be written as [17]

$$\frac{1}{\sqrt{2}}\begin{bmatrix} 1 \\ i \end{bmatrix} = \frac{1}{\sqrt{2}}\begin{bmatrix} 1 & 0 \\ 0 & i \end{bmatrix}\begin{bmatrix} 1 \\ 1 \end{bmatrix}. \tag{2.3.12}$$

Similarly, if the wave incident on the quarter wave plate is linearly polarized at $-45°$, it gets converted to left circular polarization. In the Jones matrix formalism, it is written as [17]

$$\frac{1}{\sqrt{2}}\begin{bmatrix} 1 \\ -i \end{bmatrix} = \frac{1}{\sqrt{2}}\begin{bmatrix} 1 & 0 \\ 0 & i \end{bmatrix}\begin{bmatrix} 1 \\ -1 \end{bmatrix} \tag{2.3.13}$$

where the left hand of equations (2.3.12) and (2.3.13) represent right and left circularly polarized light and the factor $\frac{1}{\sqrt{2}}$ is a normalization factor. Figure 2.6 clearly demonstrates the effect of a quarter wave plate on light incident on it. In figure 2.6, various positions α, of the quarter wave plate with respect to the input polarization is shown. At $\alpha = \frac{\pi}{4} = 45°$, we see that the transmitted intensity shown by the yellow legend is independent of β, which is the angle rotated by the second polarizer, hence, we have circularly polarized light as shown in equation 2.3.12.

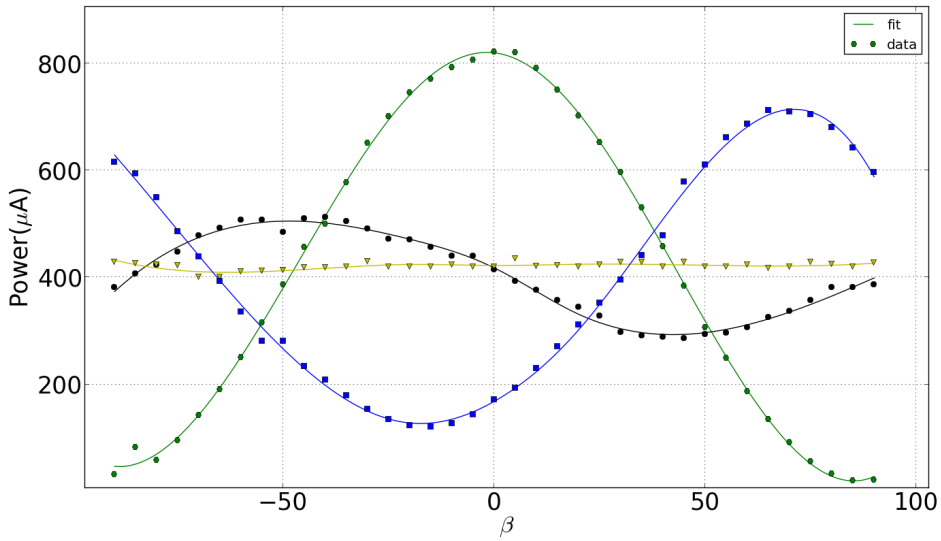

Figure 2.6: Experimental plot of polarization of a quarter wave plate (qwp) for various positions α, of it's axis with respect to the input polarization . Green legend: qwp at 0°, black legend: qwp at 30°, yellow legend: qwp at 45°, blue legend: qwp at 60°.

2.3.3 Half-wave plate

A half wave plate is a retarder such that [17]

$$\Delta\phi = \pi. \tag{2.3.14}$$

Equation (2.3.14) in equation (2.3.9) gives the Jones matrix M_{hwp} for a half wave plate as [17]

$$M_{hwp} = \begin{bmatrix} 1 & 0 \\ 0 & -1 \end{bmatrix}. \tag{2.3.15}$$

When light polarized linearly at an angle θ passes through a half wave plate, it gets converted to linear polarized light at a new angle $-\theta$. In the Jones matrix formalism, we have [17]

$$\begin{bmatrix} 1 & 0 \\ 0 & -1 \end{bmatrix} \begin{bmatrix} \cos\theta \\ \sin\theta \end{bmatrix} = \begin{bmatrix} \cos\theta \\ -\sin\theta \end{bmatrix} = \begin{bmatrix} \cos(-\theta) \\ \sin(-\theta) \end{bmatrix}. \tag{2.3.16}$$

From equation (2.3.16), we see that basically, the half wave plate flips the polarization of the light incident on it. See figure 2.7. In figure 2.7, various positions α, of the quarter wave plate with respect to the input polarization are shown. We see that the polarization at $\alpha = 0$ and the polarization at $\alpha = 45° = \frac{\pi}{4}$ are exactly opposite. In figure 2.7, β is the angle rotated by the second polarizer. This clearly show that a half wave plate flips the polarization of the light incident on it by 90° as shown in equation (2.3.16).

2.4 Malus's law

A polarizer selectively attenuates one polarization. Malus discovered that an analyzer oriented at an angle θ with respect to a polarizer would have a transmission $I(\theta)$ given by [17]

$$I(\theta) = I_0 \cos^2\theta. \tag{2.4.1}$$

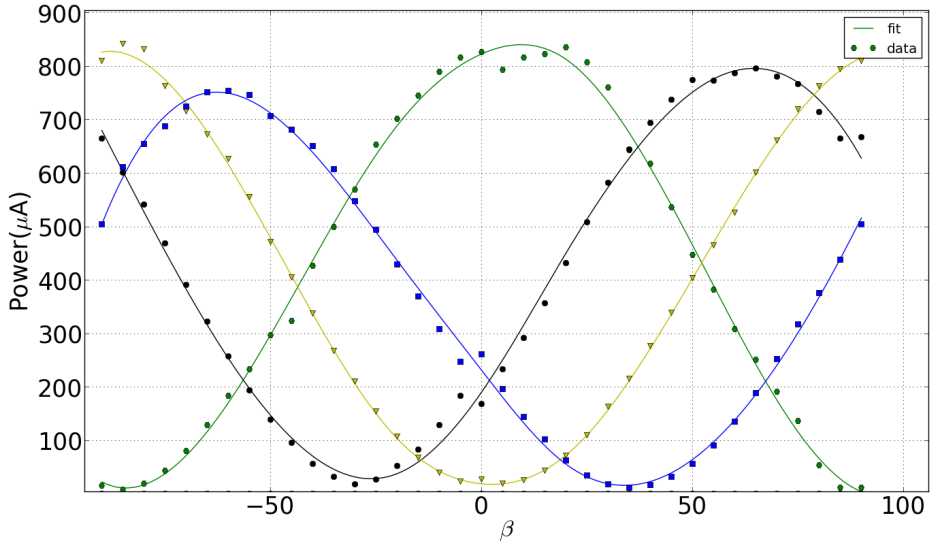

Figure 2.7: Experimental plot of polarization of a half wave plate (hwp). Green legend: hwp at 0°, black legend: hwp at 30°, yellow legend: hwp at 45°, blue legend: hwp at 60°

Equation (2.4.1) is known as Malus's law. It is very useful for theoretical determination of the intensity of light after propagating through a polarizer without making any experimental measurements.

2.4.1 Jones matrix of a polarizer

We wish to find the Jones matrix for a polarizer that transmits horizontally polarized light. Using the already established Jones matrix formalism in section 2.2.1, this can be written as [17]

$$\begin{bmatrix} 1 \\ 0 \end{bmatrix} = \begin{bmatrix} x_1 & x_2 \\ x_3 & x_4 \end{bmatrix} \begin{bmatrix} 1 \\ 1 \end{bmatrix}. \tag{2.4.2}$$

By inspection,

$$\begin{bmatrix} x_1 & x_2 \\ x_3 & x_4 \end{bmatrix} = \begin{bmatrix} 1 & 0 \\ 0 & 0 \end{bmatrix}. \tag{2.4.3}$$

Equation (2.4.3) is the Jones matrix for a polarizer which when acted upon by a Jones vector of a linearly polarized light, produces horizontally polarized light.

A rotation matrix can be written as [17]

$$R(\theta) = \begin{bmatrix} \cos\theta & \sin\theta \\ -\sin\theta & \cos\theta \end{bmatrix}. \tag{2.4.4}$$

$R(\theta)$ is used to change a polarization state and also to calculate the matrix of a rotated optical element. For example, if a polarizer P which only transmits horizontal polarization P_x(such as that in equation (2.4.3)) is rotated by an angle θ, the rotated polarizer has a matrix $P(\theta)$, given by [17]

$$P(\theta) = R(\theta)P_xR(-\theta) \tag{2.4.5}$$

Now, suppose the polarizer given in equation (2.4.3) is rotated by an angle θ, using equation (2.4.5), we can calculate the new polarization Jones matrix as [17]

$$\begin{bmatrix} E_{x,2} \\ E_{y,2} \end{bmatrix} = \begin{bmatrix} \cos\theta & \sin\theta \\ -\sin\theta & \cos\theta \end{bmatrix} \begin{bmatrix} 1 & 0 \\ 0 & 0 \end{bmatrix} \begin{bmatrix} \cos\theta & -\sin\theta \\ \sin\theta & \cos\theta \end{bmatrix} \tag{2.4.6}$$

where the left hand side of equation (2.4.6) is the Jones vector of the new polarization state and $E_{x,2}$ and $E_{y,2}$ are the x and y components of the electric field making up the Jones vector.

2.4.2 Validation of Malus's law using the Jones formalism

Now, the Jones matrix will be used to validate Malus's law given in equation (2.4.1) in section 2.4. Consider light travelling from point E_0 to E_2 having two polarizers A and B placed in the path of the light, see figure 2.8.

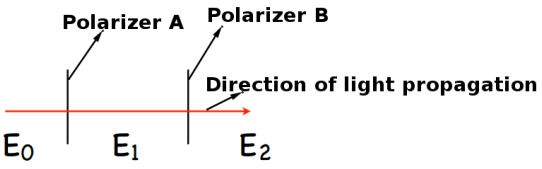

Figure 2.8: Propagation of light via polarizers A and B [17].

Suppose the Jones matrix for polarizer A is that given in equation (2.4.3) in section 2.4.1, then the polarization state of a linearly polarized light after polarizer A is given by [17]

$$\begin{bmatrix} E_{x,1} \\ E_{y,1} \end{bmatrix} = \begin{bmatrix} 1 & 0 \\ 0 & 0 \end{bmatrix} \begin{bmatrix} 1 \\ 1 \end{bmatrix} \tag{2.4.7}$$

$$= \begin{bmatrix} 1 \\ 0 \end{bmatrix} \tag{2.4.8}$$

were $E_{x,1}$ and $E_{x,2}$ are components of the Jones vector of the new polarization state after the light has travelled through polarizer A.

Now, if the light is allowed to propagate through polarizer B, rotated by an angle θ, the new polarization state is given as [17]

$$\begin{bmatrix} E_{x,2} \\ E_{y,2} \end{bmatrix} = \begin{bmatrix} \cos\theta & \sin\theta \\ -\sin\theta & \cos\theta \end{bmatrix} \begin{bmatrix} 1 & 0 \\ 0 & 0 \end{bmatrix} \begin{bmatrix} \cos\theta & -\sin\theta \\ \sin\theta & \cos\theta \end{bmatrix} \begin{bmatrix} E_{x,1} \\ E_{y,1} \end{bmatrix} \tag{2.4.9}$$

were $E_{x,2}$ and $E_{y,2}$ are components of the Jones vector of the new polarization state after the light has travelled through polarizer B. Substituting equation (2.4.8) into equation (2.4.9), we have [17]

$$\begin{bmatrix} E_{x,2} \\ E_{y,2} \end{bmatrix} = \begin{bmatrix} \cos\theta & \sin\theta \\ -\sin\theta & \cos\theta \end{bmatrix} \begin{bmatrix} 1 & 0 \\ 0 & 0 \end{bmatrix} \begin{bmatrix} \cos\theta & -\sin\theta \\ \sin\theta & \cos\theta \end{bmatrix} \begin{bmatrix} 1 \\ 0 \end{bmatrix}. \tag{2.4.10}$$

Multiplying the last two matrices in equation (2.4.10) gives [17]

$$\begin{bmatrix} E_{x,2} \\ E_{y,2} \end{bmatrix} = \begin{bmatrix} \cos\theta & \sin\theta \\ -\sin\theta & \cos\theta \end{bmatrix} \begin{bmatrix} 1 & 0 \\ 0 & 0 \end{bmatrix} \begin{bmatrix} \cos\theta E_{x,0} \\ \sin\theta E_{x,0} \end{bmatrix} \tag{2.4.11}$$

$$= \begin{bmatrix} \cos\theta & \sin\theta \\ -\sin\theta & \cos\theta \end{bmatrix} \begin{bmatrix} \cos\theta E_{x,0} \\ 0 \end{bmatrix} \tag{2.4.12}$$

$$= \begin{bmatrix} \cos^2\theta E_{x,0} \\ -\sin\theta\cos\theta E_{x,0} \end{bmatrix}. \tag{2.4.13}$$

Squaring equation (2.4.13), we have [17]

$$\begin{bmatrix} E_{x,2}^2 \\ E_{y,2}^2 \end{bmatrix} = \begin{bmatrix} \cos^4\theta E_{x,0}^2 \\ -\sin^2\theta\cos^2\theta E_{x,0}^2 \end{bmatrix}. \tag{2.4.14}$$

Equation (2.4.14) can be written as [17]

$$E_{x,2}^2 = \cos^4\theta E_{x,0}^2 \tag{2.4.15}$$

$$E_{y,2}^2 = \sin^2\theta\cos^2 E_{x,0}^2. \tag{2.4.16}$$

Summing equations (2.4.15) and (2.4.16) yields,

$$E_{x,2}^2 + E_{y,2}^2 = \cos^2\theta E_{x,0}^2(\cos^2\theta + \sin^2\theta) \tag{2.4.17}$$

$$= \cos^2\theta E_{x,0}^2. \tag{2.4.18}$$

As stated in equation (2.4.9), $E_{x,2}$ and $E_{y,2}$ are the components of the electric field of the new polarization state after propagating through polarizer B, their sum $E_{x,2} + E_{y,2}$, gives the total electric field E_T. Thus, we can write [17]

$$E_{x,2}^2 + E_{y,2}^2 = E_T^2 \tag{2.4.19}$$

substituting equation (2.4.19) in equation (2.4.18) noting that intensity is proportional to the square of the electric field, equation (2.4.18) becomes [17]

$$I_T = \cos^2\theta I_0 \tag{2.4.20}$$

or

$$I_T = I_0\cos^2\theta. \tag{2.4.21}$$

Clearly, the analysis yielding equation (2.4.21) indeed shows that the Jones matrix formalism can be used to prove Malus's law earlier stated in section 2.4.

Figure 2.9: Optical Isolator [18].

2.5 Optical isolator

An optical isolator is a passive magneto-optic device that only allows light to travel in one direction. See figure 2.9. The optical isolator must be mounted such that the incident light travels in the direction of the arrow. They are used to protect a source from back reflections that may occur after the isolator. Back reflections can damage a laser source or cause it to mode hop, amplitude modulate or frequency shift [18]. An isolator's function is based on the Faraday effect [18]. Michael Faraday discovered that the plane of polarized light rotates while transmitting through glass or any other material that is exposed to a magnetic field. The direction of rotation is dependent on the direction of the magnetic field and not on the direction of propagation of light.

The amount of rotation Q is given by [18]

$$Q = V \times L \times H \tag{2.5.1}$$

where V is the Verdet constant measured in radians per Telsa per meter. It describes the strength of the Faraday effect for a particular material. L is the length through the optical material in meters and H is the magnetic field in Telsa. An optical isolator consists of an input polariser, a Faraday rotator with magnet and an output polariser [18] see figure 2.10. The input polariser works as a filter to allow only linearly polarized light into the Faraday rotator. In the forward mode, see figure 2.11, laser light whether or not polarized, enters the input polariser of the polariser and becomes linearly polarized, say in the vertical plane. It then travels through the rotator rod which rotates the plane of polarization (POP) of the light incident on it by 45°. Finally, light exits through the half wave plate whose axis is at $-22.5°$ with respect to the input polarizer. Hence, the light leaving the optical isolator has the same polarization as the light incident on it. In the reverse mode, see figure 2.12, light travelling backwards through the optical isolator first enters the half wave plate whose axis is set at $-22.5°$ with respect to the input polarizer. It then passes through the Faraday rotator, and the plane of polarization is again rotated by $-45°$. The net result is a rotation of $-90°$ with respect to the input polarizer, thus, the plane of polarisation is now perpendicular to the transmission axis of the input polarizer. Hence, for the reason given in section 2.2, the light will be absorbed and will not propagate through.

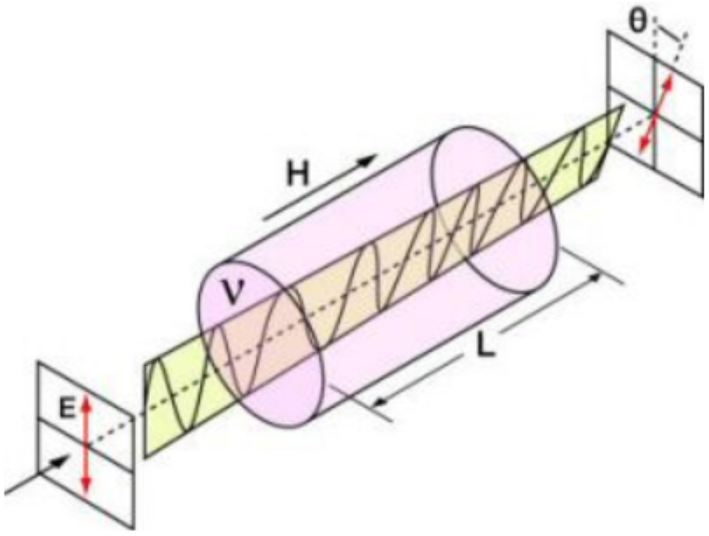

Figure 2.10: Faraday Rotation [18].

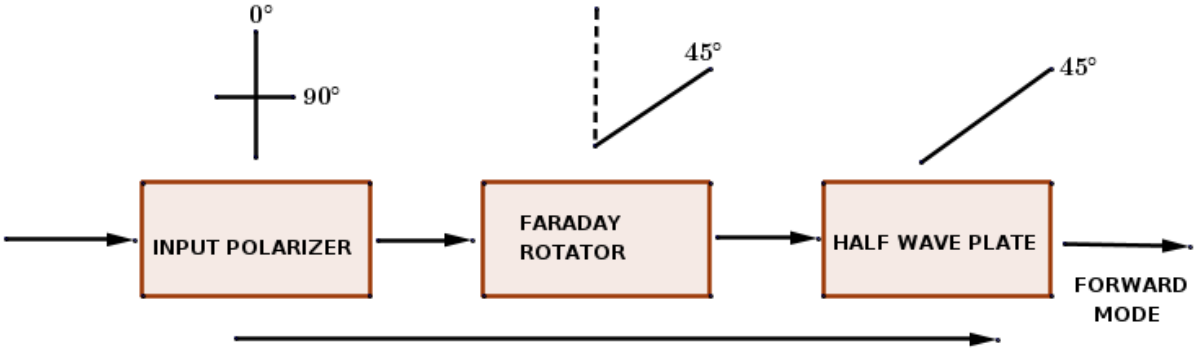

Figure 2.11: Forward mode [18].

The Jones vector could be used to understand the changes that the light undergoes inside the optical isolator system. Let the Jones vector, $\vec{P}_{in}$ of the light at the input of the polarizer be given as [14]

$$\vec{P}_{in} = \begin{bmatrix} 1 \\ 0 \end{bmatrix}. \tag{2.5.2}$$

The light with Jones vector given in equation (2.5.2) now travels though the Faraday rotator inside the optical isolator. The Jones matrix M, for the rotator in the Faraday isolator is given as[17]

$$M = \begin{bmatrix} \cos\theta & \sin\theta \\ -\sin\theta & \cos\theta. \end{bmatrix} \tag{2.5.3}$$

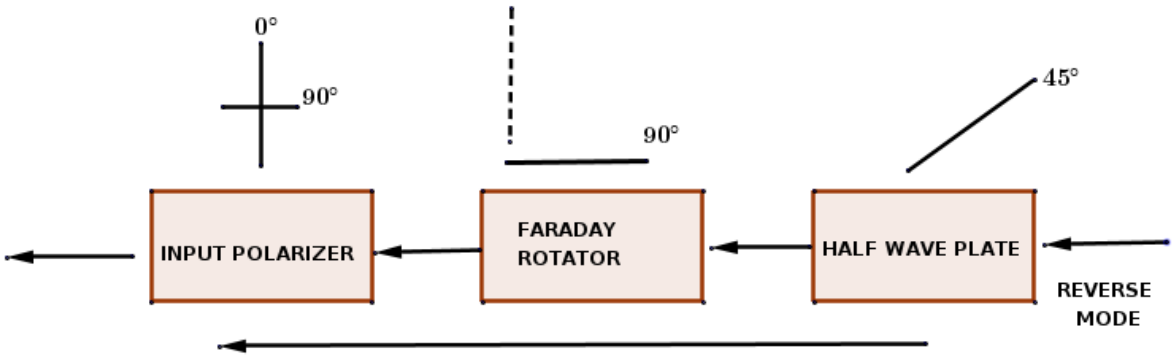

Figure 2.12: Reverse mode [18].

The Jones matrix M_p, of the input polarizer is given by equation (2.4.3) in section 2.4. It is given by [17]

$$M_p = \begin{bmatrix} 1 & 0 \\ 0 & 0. \end{bmatrix} \tag{2.5.4}$$

In the forward mode see figure 2.11, the Faraday rotator rotates the plane of polarization by $\theta = 45°$. Substituting $\theta = 45°$ into equation (2.5.3), we get the Jones matrix F_r of the Faraday rotator as [17]

$$F_r = \frac{1}{\sqrt{2}} \begin{bmatrix} 1 & 1 \\ -1 & 1 \end{bmatrix}. \tag{2.5.5}$$

After passing through the Faraday isolator, the light travels through a half wave plate see figure 2.11. Because a half wave plate rotates polarization by 2θ, the axis of the half wave plate is set at $-22.5°$ with respect to the input polarizer so that it reverses the effect of the Faraday rotator on the light. Hence, if the Faraday rotator rotates the plane of polarization by θ, the half wave plate will rotate the plane of polarization, by $-\theta$. Thus, replacing θ in equation (2.5.3) by $-\theta$, we get the Jones matrix the half wave plate M_{hp} as [17]

$$M_{hp} = \begin{bmatrix} \cos\theta & -\sin\theta \\ \sin\theta & \cos\theta \end{bmatrix}. \tag{2.5.6}$$

Substituting $\theta = 45°$ into equation (2.5.6) we get

$$M_{hp} = \frac{1}{\sqrt{2}} \begin{bmatrix} 1 & -1 \\ 1 & 1 \end{bmatrix}. \tag{2.5.7}$$

Hence, in the forward mode, the Jones vector $\vec{P}_f$ of the output light from the optical isolator will be [17]

$$\vec{P}_f = M_{hp} \cdot F_r \cdot M_p \cdot \vec{P}_{in}. \tag{2.5.8}$$

Substituting equations (2.5.4), (2.5.5), (2.5.7) and (2.5.2), into equation (2.5.8), we get [17]

$$\vec{P}_f = \frac{1}{\sqrt{2}} \begin{bmatrix} 1 & -1 \\ 1 & 1 \end{bmatrix} \frac{1}{\sqrt{2}} \begin{bmatrix} 1 & 1 \\ -1 & 1 \end{bmatrix} \begin{bmatrix} 1 & 0 \\ 0 & 0 \end{bmatrix} \begin{bmatrix} 1 \\ 0 \end{bmatrix}. \tag{2.5.9}$$

Multiplying the matrices in equation (2.5.9) gives [17]

$$\vec{P}_f = \begin{bmatrix} 1 \\ 0 \end{bmatrix}. \tag{2.5.10}$$

Equation (2.5.10) is the Jones vector of the light as it exists the half wave plate in the optical isolator. Comparing equations (2.5.2) and (2.5.10), we see that the optical isolator does not change the polarization of light incident on it.

In the reverse mode, light first travels through the half wave plate, then through the Faraday rotator. Since the direction of the magnetic field with respect to the propagation direction has been reversed, the Faraday rotator will rotate the polarization by $-45°$ in the backward direction. Substituting $\theta = -45°$ into equation (2.5.3), we get the Jones matrix of the Faraday rotator F_r' in the reverse mode as [17]

$$F_r' = \frac{1}{\sqrt{2}} \begin{bmatrix} 1 & -1 \\ 1 & 1 \end{bmatrix}. \tag{2.5.11}$$

This $-45°$ adds to the $-45°$ induced by the half wave plate, resulting in a total polarization change of $-90°$. The Jones matrix $\vec{P}_f'$, of the light after propagating inside the optical isolator in the reverse mode is given by [17]

$$\vec{P}_f = M_p \cdot F_r' \cdot M_{hp} \cdot \vec{P}_{in}. \tag{2.5.12}$$

Substituting equations (2.5.2), (2.5.4), (2.5.7) and (2.5.11) into equation (2.5.12), we have [17]

$$\vec{P}_f' = \begin{bmatrix} 1 & 0 \\ 0 & 0 \end{bmatrix} \frac{1}{\sqrt{2}} \begin{bmatrix} 1 & -1 \\ 1 & 1 \end{bmatrix} \frac{1}{\sqrt{2}} \begin{bmatrix} 1 & -1 \\ 1 & 1 \end{bmatrix} \begin{bmatrix} 1 \\ 0 \end{bmatrix}. \tag{2.5.13}$$

Multiplying the matrices in equation (2.5.13) we get [17]

$$\vec{P}_f' = \begin{bmatrix} 0 \\ 0 \end{bmatrix}. \tag{2.5.14}$$

Equation (2.5.14) is the Jones vector of the light at the input polarizer of the optical isolator in the reverse mode. Comparing equations (2.5.10) and (2.5.14), we see that in the forward

mode, light is allowed to exist the optical isolator but in the reverse mode no light is allowed to go through. This means that no light is allowed to return to the optical isolator source in our case the femtosecond laser. That is why the optical isolator is used to prevent back reflections back to the femtosecond laser which cause damage to the laser.

2.6 Liquid crystals

The liquid-crystal state is a state of matter in which the molecules which are cigar shaped have orientational order, like crystals, but lack positional order, like liquids [15]. Orientational order means that the constituent atoms or molecules in a crystal are aligned in a unique or particular pattern whereas a lack of positional order means the location of molecules, say for example in a liquid, can be anywhere at any time.

Three phases of liquid crystals are known, they are

- **Nematic liquid crystals**: In Nematic liquid crystals, the molecules of the crystal are parallel but their positions are random.
- **Semectic liquid crystals**: In semectic liquid crystals, the molecules of the crystal are parallel but their centres are stacked in parallel layers within which they have random positions. This ensures they have positional order only in one dimension.
- **Cholestric phase**: The cholestric phase is a distorted form of the nematic phase in which the orientation undergoes helical rotation about an axis.

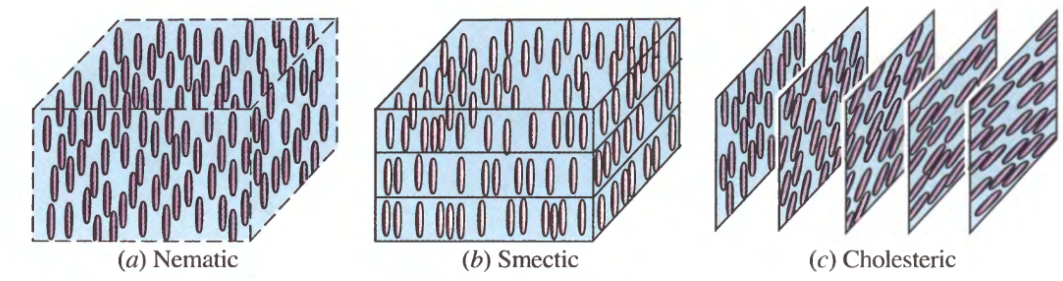

Figure 2.13: Molecular organization of different types of liquid [15].

Figure 2.13 show various phases of optics liquid crystals. Basically, liquid crystallinity is a fluid state of matter. The molecules in the liquid crystal change their orientation when subjected to a force, which most often is in the form of an electric field. Twisted nematic liquid crystals are nematic liquid crystals on which a twist similar to the twist that naturally occurs in the cholesteric phase, is imposed by external forces [15]. Twisted nematic crystals are widely used in the manufacture of liquid crystal displays and also for the manufacture of the spatial light modulator (SLM) discussed in section 2.6.2.

2.6.1 Optical properties of twisted nematic liquid crystals

The twisted nematic liquid crystal introduced in section 2.6 is an optically inhomogeneous anisotropic medium whose optic axis is parallel to the molecular direction. See figure 2.14.

The twisted nematic liquid crystal is divided into thin layers perpendicular to the axis of twist, each of which acts as a uni-axial crystal with the optic axis slowly rotating in a helical manner. See figure 2.14. Consider the propagation of light along the axis of twist, the z-axis of

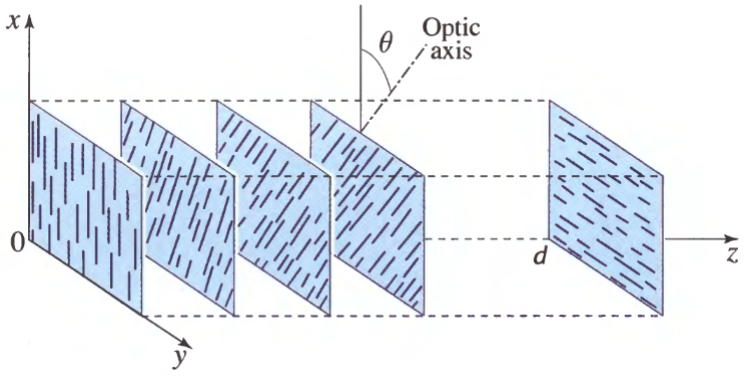

Figure 2.14: Propagation of light in a twisted nematic liquid crystal with angle of twist of 90° [15].

a twisted nematic liquid crystal. Assume that the twist angle varies linearly with z,

$$\theta = \alpha z \tag{2.6.1}$$

In equation (2.6.1), α is known as the twist coefficient in degrees per unit length. The optic axis is therefore parallel to the x-y plane and makes an angle θ with the x direction [15]. The ordinary and extra ordinary indices n_0 and n_e usually ($n_e > n_0$) and the phase retardation coefficient measured in retardation per unit length is [15]

$$\beta = (n_e - n_0)k_0 \tag{2.6.2}$$

where α and β are the twist and retardation coefficients respectively [15]. These coefficients describe completely the liquid crystal cell.

In practice, β is far greater than α ($\beta >> \alpha$) which implies that many cycles of phase retardation are introduced before the optic axis rotates appreciably. If an incident wave at $z = 0$ is linearly polarized in the x-direction then when $\beta >> \alpha$, the wave maintains it's linearly polarized state but the plane of polarization rotates in alignment with the molecular twist so that the angle of rotation is $\theta = \alpha z$ and the rotation in a crystal of length d is the angle of twist αd [15]. Divide the width d of the cell into N incremental layers of equal widths [15]

$$\Delta z = \frac{d}{N}. \tag{2.6.3}$$

The mth layer located at a distance given by[15]

$$z = z_m \tag{2.6.4}$$

$$= m\Delta_m \quad m = 1, 2, 3, 4 \cdots N \tag{2.6.5}$$

The mth layer is a wave retarder whose slow axis which is the optic axis makes an angle with the x-axis given by [15]

$$\theta_m = m\Delta\theta \tag{2.6.6}$$

where

$$\Delta\theta = \alpha\Delta z. \tag{2.6.7}$$

It's Jones Matrix is therefore given by [15]

$$T_m = R(-\theta_m)T_r(\theta_m) \tag{2.6.8}$$

where [15]

$$T_r = \begin{bmatrix} \exp(in_e k_0 \Delta z) & 0 \\ 0 & \exp(-in_0 k_0 \Delta z) \end{bmatrix}. \tag{2.6.9}$$

Equation (2.6.9) is the Jones matrix of a retarder with axis in the x-direction and $R(\theta_m)$ is the co-ordinate rotation matrix given by

$$R(\theta) = \begin{bmatrix} \cos\theta & \sin\theta \\ -\sin\theta & \cos\theta \end{bmatrix}. \tag{2.6.10}$$

Substituting β given in equation (2.6.2) into equation (2.6.9) gives [15]

$$T_r = \exp(i\psi\Delta z) \begin{bmatrix} \exp(-i\beta\frac{\Delta z}{z}) & 0 \\ 0 & \exp(i\beta\frac{\Delta z}{z}) \end{bmatrix}. \tag{2.6.11}$$

In equation (2.6.11),

$$\psi = \frac{(n_0 + n_e)k_0}{2}. \tag{2.6.12}$$

Multiplying equation (2.6.11) by equation (2.6.12) which is a constant phase factor has no effect on the state of polarization. Hence equation (2.6.12) is ignored in equation (2.6.11). The overall Jones matrix of the device is [15]

$$T = \prod_{m=1}^{N} T_m \tag{2.6.13}$$

$$= \prod_{m=1}^{N} R(-\theta_m)T_r R(\theta_m)). \tag{2.6.14}$$

Using equation (2.6.8) and noting that [15]

$$R(\theta_m)R(-\theta_{m-1}) = R(\theta_m - \theta_{m-1}) \tag{2.6.15}$$

$$= R(\Delta\theta) \tag{2.6.16}$$

we get,

$$T = R(-\theta_N)\big[T_r R(\Delta\theta)\big]^{N-1} T_r R(\theta_1). \tag{2.6.17}$$

Multiplying equations (2.6.11) and (2.6.10) gives

$$T_r R(\Delta\theta) = \begin{bmatrix} \exp(-i\beta\frac{\Delta z}{z}) & 0 \\ 0 & \exp(i\beta\frac{\Delta z}{z}) \end{bmatrix} . \begin{bmatrix} \cos\alpha\Delta z & \sin\alpha\Delta z \\ -\sin\alpha\Delta z & \cos\alpha\Delta z \end{bmatrix} \tag{2.6.18}$$

Using equations (2.6.17) and (2.6.18), the Jones matrix T of the device can in principle be determined in terms of α, β and $d = N\Delta z$.

When $\alpha << \beta$ we assume that the incremental rotation matrix $R(\Delta\theta)$ is approximately an identity matrix and obtain from equation (2.6.17) [15]

$$T_r \approx R(-\theta_N)\big[T_r\big]^N R(\theta_1) \tag{2.6.19}$$

$$\tag{2.6.20}$$

$$R(-\alpha N\Delta z) \begin{bmatrix} \exp(-i\beta\frac{\Delta z}{z}) & 0 \\ 0 & \exp(i\beta\frac{\Delta z}{z}). \end{bmatrix}^N \tag{2.6.21}$$

As $N \longrightarrow \infty$, $\Delta \longrightarrow 0$ and $N\Delta z \longrightarrow d$, equation (2.6.21) becomes

$$R(-\alpha d) \begin{bmatrix} \exp(-i\beta\frac{d}{2}) & 0 \\ 0 & \exp(i\beta\frac{d}{2}) \end{bmatrix} . \tag{2.6.22}$$

Equation (2.6.22) is the Jones matrix representation of a wave retarder of retardation βd whose slow axis is along the x-direction, followed by a polarization rotator with rotation angle αd [15]. If the incident wave on the wave retarder is linearly polarised along the x-direction, then the wave retarder provides a phase shift, that is, it shifts the phase of the linearly polarised light. The wave retarder simply rotates the polarization by an angle αd equal to the twist angle [15].

Spatial light modulators (SLM) modulates light by effecting polarization changes to a beam and these polarization changes are effected as the value of β given by equation (2.6.2) is varied. In the laboratory, this is achieved by connecting the SLM to a computer control via a computer software called Labview. The Labview software is used to write various voltages which are sent to the SLM. These voltages, produce electric fields in the crystals of the SLM which change the orientation of the crystals. This provides a very efficient method of altering the polarization of any light beam incident on it the SLM.

2.6.2 Liquid crystal as a spatial light modulator

Basically, spatial light modulator (SLM) arrays are configured for either phase-only or phase-and -amplitude operation in pulse shaping applications [19]. Figure 2.15 shows a pulse shaper set-up. The liquid crystal array allows for a continuous variable phase control of each separate pixel [20] and allows on a millisecond time scale, programmable control of the pulse shape.

The distance between each lens from each grating equal one focal length of the lens and the distance between each lens and the modulation element is also one focal length of the lens. Hence,

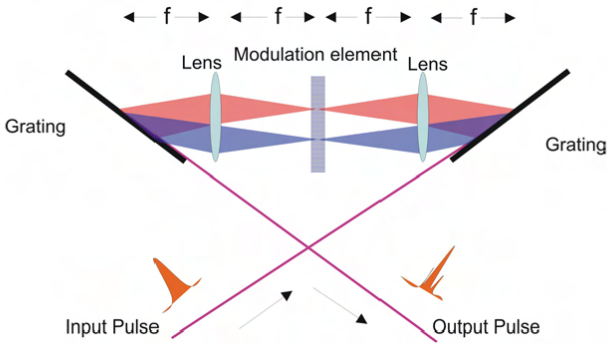

Figure 2.15: 4-f pulse shaper set-up [21].

the total length of the pulse shaper set up is four times the focal length (4-f) of the lens. The 4-f shaper is used because it is symmetric since without the SLM in the focal plane, the output beam is an exact replica of the input beam. A laser beam incident on the first grating is first dispersed angularly according to it's wavelength. The first lens transforms (Fourier transform) this angular dispersed beam, to a spatial position in the focal plane of the lens. Our SLM in the femtosecond laboratory, consists of two back to back arrays of liquid crystal. It is this arrangement that allows for complete control over the phase and the amplitude of a pulse. A spatial light modulator is placed along the focal plane of each lens. The set up of the pulse shaper is symmetric, hence, the second lens in the second half of the set up performs the inverse process (Inverse Fourier transform).

2.6.2.1 Components of the pulse shaper

Diffraction grating

The diffraction grating disperses angularly, the wavelength components of the laser pulse or beam. The angular dispersion is defined as $\frac{\triangle\theta}{\triangle\lambda}$. The diffraction is governed by [22],

$$m\lambda = d(\sin\theta_i + \sin\theta_d) \tag{2.6.23}$$

where

m=order of diffraction

d=groove period

λ=wavelength of the beam

θ_i=angle of incidence to the diffraction grating

θ_d=angle of diffraction from the diffraction grating.

Equation (2.6.23) measures the difference $\triangle\theta$ between the angles of the principal maxima of a given order due to two nearly equal wavelengths which differ by $\triangle\lambda$. To be able to differentiate between two lines, it is desirable that $\frac{\triangle\theta}{\triangle\lambda}$ is sufficiently large [23]. Consider two almost similar wavelengths λ and $\lambda + \triangle\lambda$ with maxima θ and $\theta + \triangle\theta$ respectively, and $\theta_i = 0$ we get [23]

$$d\sin\theta_d = m\lambda \tag{2.6.24}$$

and we can calculate the difference between the angular position of their maxima [23]

$$\sin(\theta_d + \triangle\theta_d) - \sin\theta_d = \frac{m}{d}\Big[(\lambda + \triangle\lambda - \lambda\Big] \tag{2.6.25}$$

$$= m\frac{\triangle\lambda}{d}. \tag{2.6.26}$$

If $\triangle\lambda$ is small, so is $\triangle\theta$,

$$\sin(\theta_d + \triangle\theta_d) = \sin\theta_d \cos\triangle\theta_d + \sin\triangle\theta_d \cos\theta_d \tag{2.6.27}$$

$$\sim \sin\theta_d + \triangle\theta_d \cos\theta_d, \tag{2.6.28}$$

and equation (2.6.28) holds since $\triangle\theta_d$ is small. Substituting equation (2.6.28) into equation (2.6.25) we have [23]

$$\sin\theta_d + \triangle\theta_d \cos\theta_d - \sin\theta_d = m\frac{\triangle\lambda}{d} \tag{2.6.29}$$

$$\frac{\triangle\theta_d}{\triangle\lambda} = \frac{m}{d\cos\theta_d}. \tag{2.6.30}$$

Equation (2.6.30) shows that angular dispersion increases with increasing m, and decreases as d increases. The angular spread is not linear since it depends on a cosine function [24].

Lens

The lens in the shaper ensures that the individual wavelengths diffracted from the grating are focused onto the Fourier plane (where the modulator already discussed in section 2.6.2 is positioned). The spot-size should be less than the width of the SLM pixel. If this condition is not met, the modulation will be poor, thus reducing the range of temporal shapes produced [25]. The spot-size associated with each component of a lens of focal length f is given by [26]

$$w_0 \approx \frac{f\lambda}{\pi w(f)} \tag{2.6.31}$$

where

λ=wavelength of laser beam

w_0=spot-size of that wavelength component at the focus of the lens

$w(f)$=spot-size at the lens.

Thus, a pulse leaving the set-up has an altered temporal profile due to the change of its spectral phase which is possible because of the ability of the SLM to alter the polarization of the pulse incident on it's surface. The overall importance of polarization in ultrafast optics cannot be underestimated. The SLM, quarter and half wave plates are just a few of it's many applications.

Chapter 3

Dispersion in optics

3.1 Definition

Dispersion corresponds to the phenomenon whereby the index of refraction of a medium is frequency dependent [3]. All material media are dispersive; only vacuum is non-dispersive. In equation (2.1.23) in section 2.1.1, n was assumed independent of frequency but in general this is not true because for example, as a laser pulse travels through say glass, it experiences dispersion, and hence is stretched in time.

3.1.1 Mathematical description

Mathematically, dispersion can be treated by considering the frequency dependence of the propagation constant β. Since the index of refraction is frequency dependent we have [12]

$$\beta(\omega) = k_0 n(\omega) \tag{3.1.1}$$

$$= \frac{\omega n(\omega)}{c} \tag{3.1.2}$$

and

$$\frac{\partial \beta(\omega)}{\partial \omega} = \frac{1}{c}\Big[n + \omega \frac{dn}{d\omega}\Big]. \tag{3.1.3}$$

Inverting equation 3.1.3, we have [12]

$$\frac{\partial \omega}{\partial \beta(\omega)} = \frac{c}{n + \omega(dn/d\omega)} \tag{3.1.4}$$

$$= \frac{c/n}{1 + (\omega/n)dn/d\omega}. \tag{3.1.5}$$

Using,

$$\lambda = \frac{2\pi c}{\omega} \tag{3.1.6}$$

$$\frac{d\lambda}{d\omega} = \frac{-2\pi c}{\omega^2} = \frac{-\lambda^2}{2\pi c} \tag{3.1.7}$$

and applying the chain rule,

$$\frac{dn}{d\omega} = \frac{dn}{d\lambda}\frac{d\lambda}{d\omega} = \frac{dn}{d\lambda} \cdot \frac{-\lambda^2}{2\pi c}. \tag{3.1.8}$$

To write equation (3.1.5) in terms of wavelength, we substitute equations (3.1.7) and (3.1.8) into equation (3.1.5) and have [12]

$$\frac{\partial\omega}{\partial\beta(\omega)} = \frac{c/n}{1-\Big[(2\pi c/n\lambda)\cdot(dn/d\lambda)\cdot(\lambda^2/2\pi c)\Big]} \tag{3.1.9}$$

$$= \frac{c}{n}\Big/\Big[1-\frac{\lambda}{n}\frac{dn}{d\lambda}\Big] \tag{3.1.10}$$

$$= \frac{c}{n}\Big/\Big[\frac{n-\lambda dn/d\lambda}{n}\Big] \tag{3.1.11}$$

$$= \frac{c}{n}\cdot\frac{n}{n-\lambda\frac{dn}{d\lambda}}. \tag{3.1.12}$$

Simplifying equation (3.1.12) we have [12]

$$\frac{\partial\omega}{\partial\beta(\omega)} = \frac{c}{n-\lambda dn/d\lambda}. \tag{3.1.13}$$

Equation (3.1.13) is the group velocity v_g. Thus, equation (3.1.13) simply becomes [12],

$$v_g = \frac{c}{n-\lambda dn/d\lambda}. \tag{3.1.14}$$

If the refractive index doesn't depend on wavelength then,

$$\frac{dn}{d\lambda} = 0 \tag{3.1.15}$$

and equation (3.1.13) becomes, [12]

$$v_g = v_p = \frac{c}{n} \tag{3.1.16}$$

where v_p is called the phase velocity. It is the rate at which the phase of the wave propagates in space. Clearly we see that, phase and group velocity are equal if equation (3.1.15) holds. Substituting equation (3.1.16) into equation (3.1.5), we have

$$\frac{\partial\omega}{\partial\beta(\omega)} = \frac{v_p}{1+\left(\frac{\omega}{n}\frac{dn}{d\omega}\right)}. \tag{3.1.17}$$

We have shown in equation (3.1.13), that the left hand side of equation (3.1.17) is the group velocity v_g, thus we can write equation (3.1.17) as

$$v_g = \frac{v_p}{1+\left(\frac{\omega}{n}\frac{dn}{d\omega}\right)}. \tag{3.1.18}$$

A simplified sketch of the variation of refractive index with frequency ω is shown in figure 3.1.

In the UV region, that is the region between ω_{02} and ω_{03} in figure 3.1, $n > 0$ and $\frac{dn}{d\omega} > 0$. This means from equation (3.1.18), that the group velocity v_g is less than the phase velocity v_p. This behaviour, termed normal dispersion is shown in figure 3.1 [12]. Within each absorption resonance which is depicted by the shaded bands in figure 3.1, the refractive index n decreases with frequency, that is $\frac{dn}{d\omega} < 0$. This behaviour, which is opposite to the normal dispersion, is termed

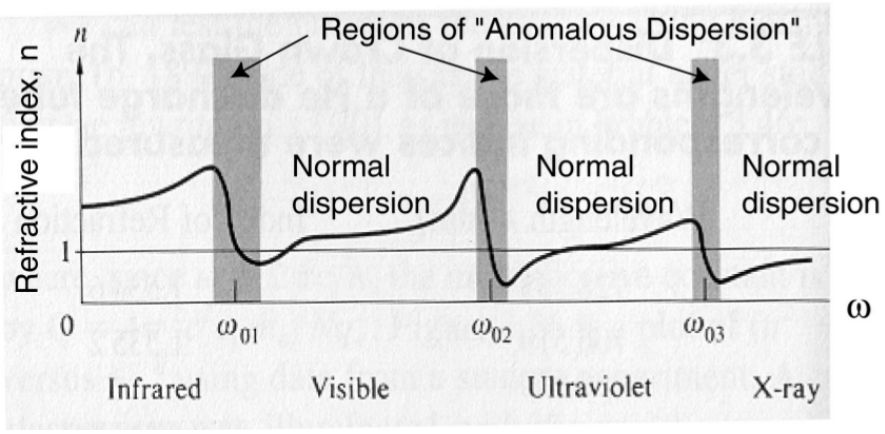

Figure 3.1: Typical refractive index variation for transparent optical materials [12].

anomalous dispersion. Again from equation (3.1.18), this means that the group velocity v_g is greater than the phase velocity v_p. Anomalous dispersion is shown by the rectangular bars in figure 3.1. In time, when an ultrafast laser pulse is normally dispersed, the red light components of the pulse will arrive before blue light component. This is because in normal dispersive media, longer wavelengths, that is lower frequencies travel faster than shorter wavelengths (higher frequencies). But, if it is anomalously dispersed in an anomalous dispersive media, in time, the blue light components will arrive before the red light components.

3.1.2 Group velocity dispersion

Dispersion could be described as a phenomenon in which the group velocity is frequency dependent as seen in equation (3.1.5). To emphasize the dependency of the group velocity on dispersion, dispersion is referred to as group velocity dispersion GVD. GVD is defined as the derivative with respect to angular frequency of the inverse of the group velocity [27]. Mathematically this definition is given as,

$$GVD = \frac{d}{d\omega}\left(\frac{1}{v_g}\right). \tag{3.1.19}$$

In equation (3.1.19), v_g is the group velocity already discussed in section 3.1.1. Equation (3.1.19) is a mathematical statement of the definition of GVD given at the beginning of this section.

Let $e_{in}(t)$ be an input pulse with spectrum $E_{in}(\omega)$. After propagating through a dispersive medium that adds a spectral phase $\psi(\omega)$, the output pulse is given by [12]

$$e_{out}(t) = \frac{1}{2\pi}\int_{-\infty}^{+\infty} d\omega E_{in}(\omega)e^{i\omega t}e^{i\psi(\omega)}. \tag{3.1.20}$$

If the spectral phase was due to propagation through a dispersion medium of length L then, [12]

$$\psi(\omega) = -\beta(\omega)L \tag{3.1.21}$$

where $\beta(\omega)$ is the propagation constant in the medium. β and ψ as a Taylor series expansion about a central frequency ω_0 gives [12]

$$\psi(\omega) = \psi(\omega_0) + \frac{\partial\psi}{\partial\omega}(\omega-\omega_0) + \frac{1}{2}\frac{\partial^2\psi}{\partial\omega^2}(\omega-\omega_0)^2 + \frac{1}{6}\frac{\partial^3\psi}{\partial\omega^3}(\omega-\omega_0)^3 + \cdots \tag{3.1.22}$$

$$= \psi_0 + \psi_1(\omega-\omega_0) + \frac{\psi_2}{2}(\omega-\omega_0)^2 + \frac{\psi_3}{6}(\omega-\omega_0)^3\cdots \tag{3.1.23}$$

$$\beta(\omega) = \beta(\omega_0) + \frac{\partial\beta}{\partial\omega}(\omega-\omega_0) + \frac{1}{2}\frac{\partial^2\beta}{\partial\omega^2}(\omega-\omega_0)^2 + \frac{1}{6}\frac{\partial^3\beta}{\partial\omega^3}(\omega-\omega_0)^3 + \cdots \tag{3.1.24}$$

$$= \beta_0 + \beta_1(\omega-\omega_0) + \frac{\beta_2}{2}(\omega-\omega_0)^2 + \frac{\beta_3}{6}(\omega-\omega_0)^3\cdots. \tag{3.1.25}$$

Let the positive frequency part, $E_{in}(\omega)$ be replaced by $A(\tilde{\omega})$ and $\tilde{\omega} = \omega - \omega_0$, then equation (3.1.20) can be written as [12]

$$e_{out}(t) = Re\{e^{\omega_0 t-\beta_0 L}a_{out}(t)\} \tag{3.1.26}$$

$$\tag{3.1.27}$$

where

$$a_{out} = \frac{1}{2\pi}\int_{-\infty}^{+\infty} d\tilde{\omega}A(\tilde{\omega})e^{(\omega t-(\beta_1\tilde{\omega}+\frac{\beta_2}{2}\tilde{\omega}^2+\frac{\beta_3}{6}\tilde{\omega}^3)L)}. \tag{3.1.28}$$

Hence, $e_{out}(t)$ is the product of a carrier term $e^{i(\omega t-\beta_0 z)}$ and the envelope function $a_{out}(t)$. The carrier term propagates at a phase velocity given by [12]

$$\nu_p = \frac{\omega_0}{\beta_0}. \tag{3.1.29}$$

Equation (3.1.29) is unaffected by variations of β and ψ with ω. The envelope function $a_{out}(t)$ is clearly affected by the form of $\beta(\omega)$. A unique case occurs when $\beta(\omega)$ is a linear function of ω given by [12]

$$\beta(\omega) = \beta_0 + \beta_1(\tilde{\omega}) \tag{3.1.30}$$

with equation (3.1.30), equation (3.1.28) becomes [12]

$$a_{out}(t) = a_{in}(t-\beta_1 L). \tag{3.1.31}$$

Hence, the output pulse is an undistorted replica of the input pulse travelling with velocity β_1^{-1}, called the group velocity (already discussed in section 3.1.1).

When a pulse $f(t)$, propagates in a material of refractive index $n(\omega)$, it broadens because there is a delay say, τ of it's spectral components. The shifting property of a Fourier transform can also be used to understand the group velocity in terms of the delay τ. The Fourier transform of a pulse $f(t)$ shifted by τ is given by [12]

$$\mathcal{F}\{(t-\tau)\} = F(\omega)e^{-i\omega\tau}. \tag{3.1.32}$$

Thus, the Fourier transform of a shifted function is simply the transform of the unshifted function multiplied by an exponential factor having linear phase. Hence, the Fourier transform of a delayed pulse $a(t-\tau)$ is $A(\omega)e^{-i\omega\tau}$. The electric field of a delayed pulse is given by [12]

$$e_{out}(t-\tau) = \frac{1}{2\pi}\int_{-\infty}^{+\infty} d\omega E_{in}(\omega)e^{i\omega t}e^{i\tau(\omega)}. \tag{3.1.33}$$

As was done for $\psi(\omega)$ in equation (3.1.21), we write $\tau(\omega)$ as

$$\tau(\omega) = -\beta(\omega)L \tag{3.1.34}$$

with $\beta(\omega)$ having same definition given in equation (3.1.21). Similarly, Taylor expanding $\tau(\omega)$ as was done for $\psi(\omega)$ in equation (3.1.22) we get,

$$\tau(\omega) = \tau(\omega_0) + \frac{\partial\tau}{\partial\omega}(\omega-\omega_0) + \frac{1}{2}\frac{\partial^2\tau}{\partial\omega^2}(\omega-\omega_0)^2 + \frac{1}{6}\frac{\partial^3\tau}{\partial\omega^3}(\omega-\omega_0)^3 + \cdots \tag{3.1.35}$$

$$= \tau_0 + \tau_1(\omega-\omega_0) + \frac{\tau_2}{2}(\omega-\omega_0)^2 + \frac{\tau_3}{6}(\omega-\omega_0)^3\cdots. \tag{3.1.36}$$

Using equation (3.1.21) in equation (3.1.30), we get

$$-\beta(\omega) = -\beta_0 - \beta_1\tilde{\omega} \tag{3.1.37}$$

and differentiating equation with respect to ω (3.1.34) with respect to ω we get,

$$\frac{\partial\tau}{\partial\omega} = -\frac{\partial\beta(\omega)}{\partial\omega}L. \tag{3.1.38}$$

Differentiating equation (3.1.37) and substituting into equation (3.1.38) we have

$$\frac{\partial\tau}{\partial\omega} = -\big(\frac{\partial}{\partial\omega}(-\beta_1(\omega))\big)L \tag{3.1.39}$$

Substituting equation (3.1.21) into equation (3.1.39) we have,

$$\frac{\partial\tau}{\partial\omega} = -\frac{\partial\big(\psi(\omega)\big)}{\partial\omega}. \tag{3.1.40}$$

Also, substituting equation (3.1.39) into equation (3.1.38) we have,

$$\frac{\partial\tau}{\partial\omega} = -\frac{\partial}{\partial\omega}(-\beta_0-\beta_1\omega)L = \frac{\partial\beta_1(\omega)}{\partial\omega}L. \tag{3.1.41}$$

Differentiating equation (3.1.21) with respect to ω we get,

$$\frac{\partial\psi(\omega)}{\partial\omega} = -L\frac{\partial\beta(\omega)}{\partial\omega}. \tag{3.1.42}$$

Group delay dispersion, GDD is given by [12],

$$GDD = \frac{\partial^2\psi(\omega)}{\partial\omega^2} = \frac{d}{d\omega}\big(-L\frac{\partial\beta(\omega)}{\partial\omega}\big). \tag{3.1.43}$$

Since equation (3.1.13) in section 3.1.1 is the group velocity v_g, we can write

$$\frac{\partial\omega}{\partial\beta} = v_g. \tag{3.1.44}$$

Equation (3.1.44) can be written as [12]

$$\frac{\partial\beta}{\partial\omega} = \frac{1}{v_g}. \tag{3.1.45}$$

Substituting equation (3.1.45) into equation (3.1.43) we have, [12]

$$\frac{\partial^2\psi(\omega)}{\partial\omega^2} = \frac{d}{d\omega}\Big(-\frac{L}{v_g}\Big). \tag{3.1.46}$$

Equation (3.1.46) can be written as [12]

$$\frac{\partial^2\psi(\omega)}{\partial\omega^2} = -L\frac{d}{d\omega}\Big(\frac{1}{v_g}\Big). \tag{3.1.47}$$

Now, we recall the definition of GVD already given by equation (3.1.19) in section 3.1.2, that is,

$$GVD = \frac{d}{d\omega}\Big(\frac{1}{v_g}\Big). \tag{3.1.48}$$

Substituting equation (3.1.48) into equation (3.1.47) we have [12]

$$GDD = \frac{\partial^2\psi(\omega)}{\partial\omega^2} = -GVD \cdot L. \tag{3.1.49}$$

Equation (3.1.49) simply tells us that group delay dispersion, GDD is the product of GVD and L, were L is the length of dispersion medium which the pulse has travelled.

Substituting equation (3.1.4) into equation (3.1.45) we have,

$$\frac{\partial\beta}{\partial\omega} = \Big(\frac{n+\omega(dn/d\omega)}{c}\Big), \tag{3.1.50}$$

and substituting equation (3.1.50) into equation (3.1.43) we have,

$$\frac{\partial^2\psi(\omega)}{\partial\omega^2} = -\frac{d}{d\omega}\Big(\frac{1}{c}(n+\omega(dn/d\omega)\Big)L. \tag{3.1.51}$$

Using equations (3.1.6), (3.1.7) and (3.1.8), equation (3.1.51) can be written as,

$$\frac{\partial^2\psi(\omega)}{\partial\omega^2} = -\frac{1}{c}\cdot-\frac{2\pi c}{\omega^2}\frac{d}{d\lambda}\Big(n+\frac{2\pi c}{\lambda}(\frac{dn}{d\omega})\Big)L \tag{3.1.52}$$

$$= \frac{2\pi}{\omega^2}\frac{d}{d\lambda}\Big(n+\frac{2\pi c}{\lambda}\frac{dn}{d\lambda}\cdot-\frac{\lambda^2}{2\pi c}\Big)L \tag{3.1.53}$$

$$= \frac{2\pi}{\omega^2}\frac{d}{d\lambda}\Big(n-\lambda\frac{dn}{d\lambda}\Big)L \tag{3.1.54}$$

$$= -\frac{2\pi}{\omega^2}\lambda\frac{d^2n}{d\lambda^2}L \tag{3.1.55}$$

but,

$$\frac{1}{\omega^2} = \frac{\lambda^2}{4\pi^2c^2}. \tag{3.1.56}$$

Substituting equation (3.1.56) into equation (3.1.55) we get,

$$\frac{\partial^2\psi(\omega)}{\partial\omega^2} = -\frac{\lambda^3}{2\pi c^2}\frac{d^2n}{d\lambda^2}L \tag{3.1.57}$$

but, $P = nL$ where P is the optical path length, thus substituting for P, equation (3.1.57) becomes

$$\frac{\partial^2\psi(\omega)}{\partial\omega^2} = -\frac{\lambda^3}{2\pi c^2}\frac{d^2P}{d\lambda^2}. \tag{3.1.58}$$

Equation (3.1.57) in equation (3.1.40) gives,

$$\frac{\partial\tau}{\partial\omega} = \frac{\lambda^3}{2\pi c^2}\frac{d^2P}{d\lambda^2}. \tag{3.1.59}$$

Equations (3.1.57) and (3.1.59) gives the group delay dispersion in terms of the optical path length. This is of importance as it helps determine how much an ultrafast pulse has been stretched when it propagated in a dispersive medium. It's unit is fs^2.

3.1.3 The effect of dispersion on a Gaussian pulse.

In the time domain, the electric field for a Gaussian pulse with a carrier frequency ω_0, pulse duration, Δt and phase $\theta(t)$ can be described by [28]

$$E(t) = \sqrt{A_t e^{-ln2(\frac{2t}{\Delta t})^2}} e^{-i(\omega_0 t+\theta(t))} + c.c. \tag{3.1.60}$$

where c.c. denoantes the complex conjugate.

A_t = amplitude of the pulse

ω_0 = center frequency

Δt = determines the minimum pulse duration and consequently the bandwidth

$\theta(t)$ = determines the temporal relationship among the frequency components contained within the bandwidth of the pulse.

$\theta(t)$ is important in changing the pulse duration. It is responsible for pulse broadening when the pulse is propagated through dispersive media. It can be thought of as adding a complex width to the Gaussian envelope [28].

It is fairly straightforward to visualize a pulse given by equation (3.1.60) when working in the time domain. However, when dealing with pulses travelling through dispersive media, it is not easy working with equation (3.1.60) in the time domain. For example, to determine the pulse duration of a pulse after travelling through some dispersive media, it is necessary to solve a convolution integral [29] which in general is solved numerically. Because these convolutions become products upon a Fourier transformation, [30] it is convenient to solve this type of problem in the frequency domain.

Time and frequency along with position and momentum represent a class of variables known as Fourier pairs [30]. Fourier pairs are quantities that are interconnected through the Fourier transform [28]. Fourier transform of equation (3.1.60) yields [28]

$$E(\omega) = \sqrt{A_0 e^{-ln2(\frac{2(\omega-\omega_0)}{\Delta\omega})^2}} e^{-i\psi_{pulse}(\omega-\omega_0)}. \tag{3.1.61}$$

As expected equation (3.1.61) is also a Gaussian. The electric field in equation (3.1.60) is now expressed as a function of frequency as given by equation (3.1.61). $\Delta\omega$ and Δt are related through the uncertainty relation [29]

$$\Delta\omega\Delta t = 4ln(2). \tag{3.1.62}$$

$\psi(\omega)$ describes the relationship between the frequency components of the pulse. In equation (3.1.61), ω as well as $\Delta\omega$ represent angular frequencies which can be converted to linear frequency ν by the relation [28]

$$\nu = \frac{\omega}{2\pi}. \tag{3.1.63}$$

In terms of linear frequency, equation (3.1.62) becomes,

$$C_B = \Delta\nu\Delta t \tag{3.1.64}$$

$$= \frac{2ln(2)}{\pi}. \tag{3.1.65}$$

C_B is a numerical constant which depends on the pulse shape. For a Gaussian, $C_B = 0.441$. When an input pulse, $E_{in}(\omega)$ propagates through a dispersive medium, the phase added by the material is given by the product of the input field with the transfer function of the material. The output pulse $E_{out}(\omega)$ is given by [28]

$$E_{out}(\omega) = E_{in}(\omega)R(\omega)e^{-i\psi_{mat}(\omega-\omega_0)} \tag{3.1.66}$$

where $\psi_{mat}(\omega - \omega_0)$ = Spectral phase added by the material.

$R(\omega)$ is an amplitude scaling factor for which a linear transparent medium can be approximated by $R(\omega) \approx 1$ [29]. The spectral phase $\psi(\omega - \omega_0)$ is expanded in a Taylor's expansion as done in a similar way as in equation (3.1.22) [28]

$$\psi(\omega - \omega_0) = \psi_0 + \psi_1(\omega - \omega_0) + \psi_2\frac{(\omega - \omega_0)^2}{2} + \psi_3\frac{(\omega - \omega_0)^3}{6} + \cdots. \tag{3.1.67}$$

Equation (3.1.67) allows for an in depth understanding of the effect of material dispersion on the properties of the pulse. Also, [28]

$$\psi(\omega) = \beta(\omega)L. \tag{3.1.68}$$

Truncating equation (3.1.67) on the second term and using it to re-write equation (3.1.61) as [28]

$$E_{out}(\omega) = \sqrt{A_\omega e^{-ln2\left(\frac{2(\omega-\omega_0)}{\Delta\omega}\right)^2}}\, e^{-i(\psi_{2,pulse}+\psi_{2mat})\frac{(\omega-\omega_0)^2}{2}}. \tag{3.1.69}$$

Equation (3.1.69) shows that phases in the frequency domain are simply additive and it shows the power of simplicity in working in the frequency domain. To calculate the new pulse duration, equation (3.1.69) is inverse Fourier transformed, taking it back to the time domain. The inverse Fourier transform of equation (3.1.69) gives [28]

$$E_{out}(t) = \sqrt{A'_t}\exp\left[\frac{4(ln2)t^2}{2\left[\Delta t^2 + i4(ln2)\psi_2\right]}\right] \tag{3.1.70}$$

In equation (3.1.70), ψ_2 is the sum of the group delay dispersion of the material and the group delay of the pulse [28].

Square equation (3.1.70) and relating it to the general form of a Gaussian pulse. This gives [28]

$$\exp\left[-ln2(\frac{2t}{\Delta t_{out}})^2\right] = \exp\left[\frac{4(ln2)t^2\Delta t^2}{\Delta t^4 + 16(ln2)^2\psi_2^2}\right]. \tag{3.1.71}$$

Solving equation (3.1.71) for the pulse duration Δt_{out} gives [28]

$$\Delta t_{out} = \frac{\sqrt{\Delta t^4 + 16(ln2)^2\psi_2^2}}{\Delta t}. \tag{3.1.72}$$

Equation (3.1.72) is an equation for the pulse duration. To get the group delay dispersion, ψ is made subject of the formula in equation (3.1.72).

In order to estimate the amount of GDD given to a pulse on propagating in a material of length L, equation (3.1.57) is used. The wavelength dependence of the refractive index $n(\lambda)$ usually in the form of a Sellmeier type equation must be determined, then a second derivative at the wavelength of interest is taken.

By measuring the spectrum and autocorrelation for a Gaussian pulse, equation (3.1.57) can be used to determine the amount of GDD on the pulse. Figures 3.2 and 3.3 shows results of a numerical simulation developed in this work of the electric field for two pulses. Both pulses in figures 3.2 and 3.3 are centred around 800nm. The first pulse, see figure 3.2 corresponds to a pulse with $GDD = 0$. The second pulse, see figure 3.3 corresponds to a pulse with GDD =300fs^2.

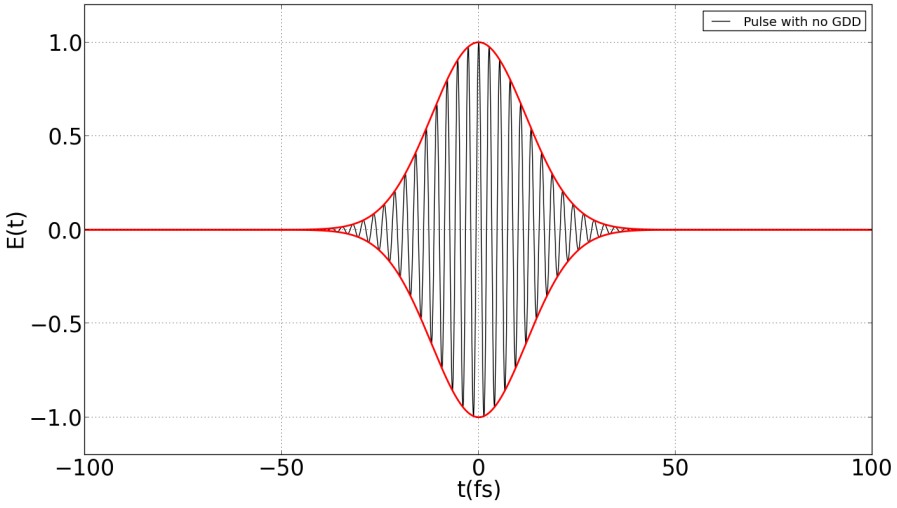

Figure 3.2: Simulation showing pulse with $GDD = 0$.

Clearly from figure 3.4 we see that GDD affects the intensity of a pulse, hence the need for a prism pulse compressor which is discussed in detail in section 4.2 to compensate for the GDD, thus increasing the intensity which consequently decreases pulse duration.

3.1.4 Self-phase modulation

The concept of self phase modulation is very similar to dispersion introduced in section 3.1. Self phase modulation is a nonlinear optical effect of light matter interaction. An ultrashort pulse of light, when travelling in a medium, will induce a varying refractive index in the medium due to the Kerr effect. The Kerr effect is a change in the refractive index of a material in response to an applied electric field. This variation in refractive index will produce a phase shift in the

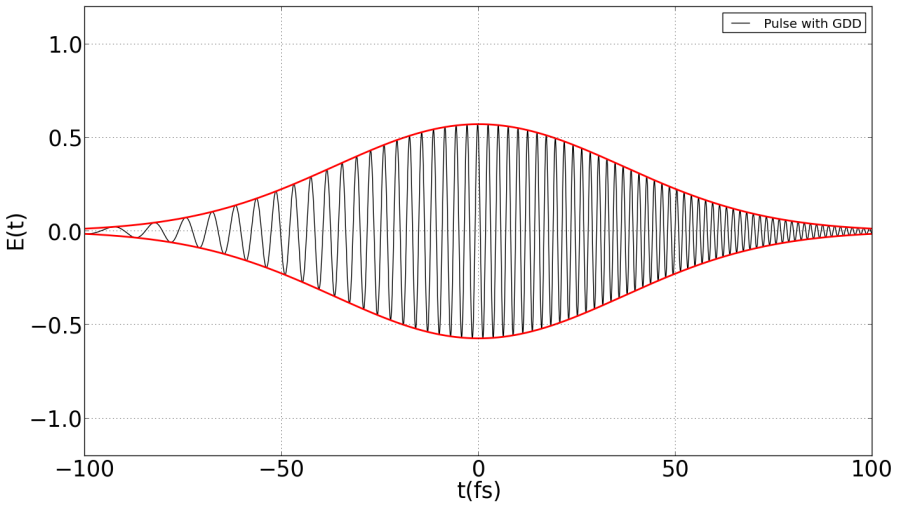

Figure 3.3: Simulation showing pulse with $GDD = 400\text{fs}^2$.

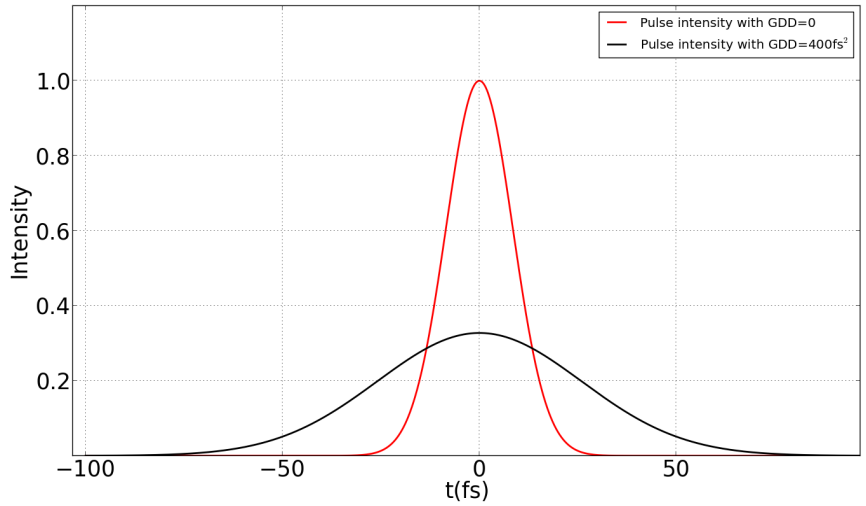

Figure 3.4: Simulation comparing intensities of both pulses. Pluse with $GDD = 0$ has a pulse duration of 20fs while pulse with $GDD = 400\text{fs}^2$ has a pulse duration of 60fs.

pulse, leading to a change in the pulse's frequency spectrum [31]. A Gaussian ultrashort pulse with an intensity profile given by [31]

$$I(t) = I_0 \exp(-\frac{t^2}{\tau^2}) \tag{3.1.73}$$

where I_0 is the peak intensity, and τ is half of the pulse duration. If the pulse is travelling in a medium, the Kerr effect produces a refractive index change with intensity given by [31]

$$n(I) = n_0 + n_2.I \tag{3.1.74}$$

where n_0 is the linear refractive index, and n_2 is the second order refractive index of the medium. As the pulse propagates, the intensity at any one point in the medium rises and falls as the pulse

goes past. This will produce a time-varying refractive index given by [31]

$$\frac{dn(I)}{dt} = n_2 \frac{dI}{dt} \tag{3.1.75}$$

$$= n_2 I_0 \frac{-2t}{\tau^2} \exp\left(\frac{-t^2}{\tau^2}\right). \tag{3.1.76}$$

This variation in refractive index produces a shift in the instantaneous phase of the pulse given by [31]

$$\phi(t) = \omega_0 t - kx \tag{3.1.77}$$

$$= \omega_0 t - \frac{2\pi}{\lambda_0} n(I) L \tag{3.1.78}$$

where ω_0 and λ_0 are the center and frequency and wavelength respectively. L is the distance the pulse has propagated. The phase shift results in a frequency shift of the pulse. The instantaneous frequency $\omega(t)$ is given by [31]

$$\omega(t) = \frac{d\phi(t)}{dt} \tag{3.1.79}$$

$$= \omega_0 - \frac{2\pi L}{\lambda_0} \frac{dn(I)}{dt}. \tag{3.1.80}$$

Equation (3.1.75) in equation (3.1.80) yields, [31]

$$\omega(t) = \omega_0 + \frac{4\pi L n_2 I_0}{\lambda_0 \tau^2} \exp\left(\frac{-t^2}{\tau^2}\right). \tag{3.1.81}$$

A plot of equations (3.1.73) and (3.1.81) is shown in figure 3.5. The blue pulse is a plot of equation (3.1.73) while the red pulse is a plot of equation (3.1.81). As can be seen in figure 3.5, the variation in refractive index produces a phase shift in the pulse, leading to a change in the pulse's frequency spectrum [31].

3.1.5 Chirped pulses

Suppose a monochromatic signal is given as [32]

$$E(t) = T(t) e^{i\phi t} e^{i\omega_0 t} \tag{3.1.82}$$

where $T(t)$ is the temporal amplitude. Taylor expanding $\phi(t)$ about $t_0 = 0$ in equation (3.1.82) we get [32]

$$\phi(t) = \phi_0 + \frac{d\phi}{dt} t + \frac{1}{2} \frac{d^2\phi}{dt^2} t^2 + \cdots \tag{3.1.83}$$

$$= a_0 + a_1 t + \frac{1}{2} a_2 t^2 \tag{3.1.84}$$

where

$$a_0 = \phi_0 \tag{3.1.85}$$

called the zeroth-order phase [33] is the constant phase of the electric field. The second term $\frac{d\phi}{dt}$ is called the first-order phase [33]. It describes the linear variation of the phase with time $\phi(t)$

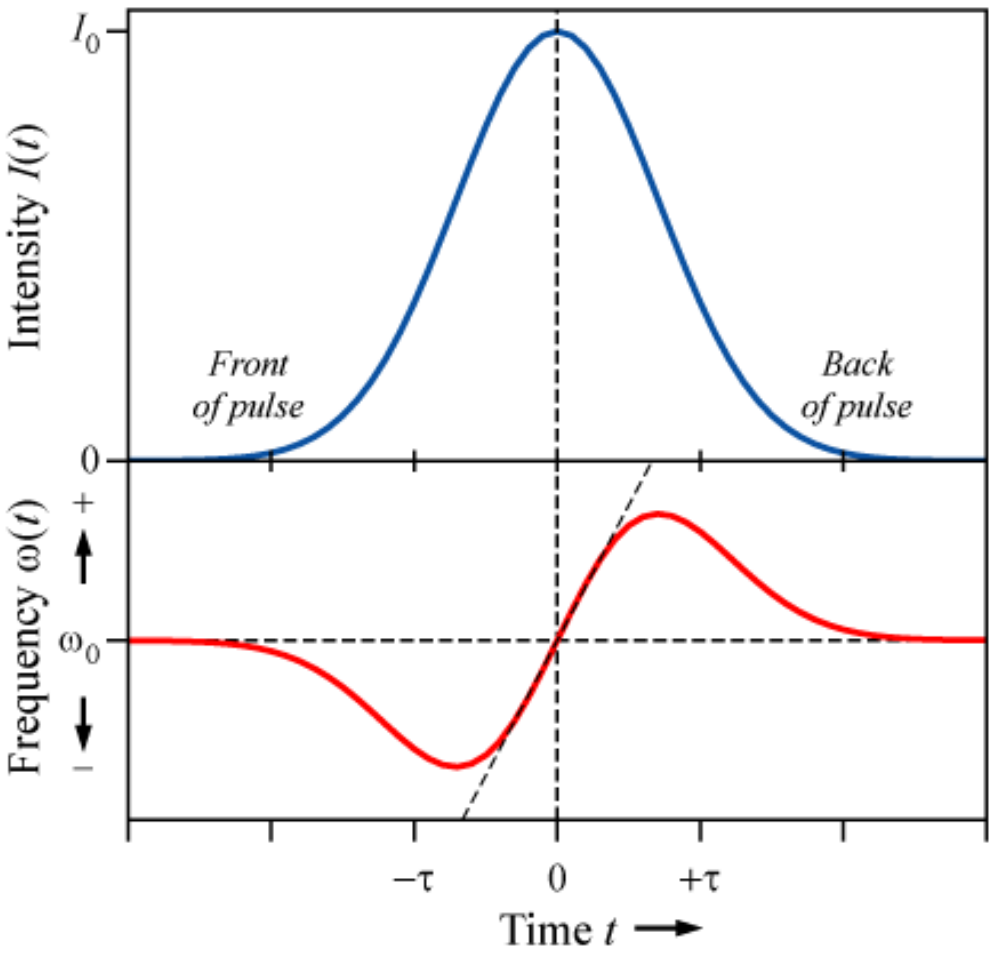

Figure 3.5: The blue pulse represents $I(t)$ while the red pulse represents $\omega(t)$. The front of the plot is shifted to lower frequencies, and the back to higher frequencies. In the center, the frequency shift is approximately linear [31].

which gives the shift of the carrier frequency [32]. The third term a_2 is called the second-order phase and is responsible for the stretching of the pulse in time [33]. It is given by [32]

$$a_2 = \frac{d^2\phi}{dt^2}. \tag{3.1.86}$$

Suppose the monochromatic signal given in equation (3.1.82) is centred at zero, then $a_0 = 0$. In addition, if the phase $\phi(t)$ in equation (3.1.82) is a second order phase and all higher order phase are not considered in equation (3.1.84), and there is no linear variation of phase with time ($a_1 = 0$), then we can write equation (3.1.82) as [32]

$$E(t) = T(t)e^{ia_2t^2}e^{i\omega_0 t} \tag{3.1.87}$$

$$= T(t)e^{i(\omega_0 t + a_2 t^2)}. \tag{3.1.88}$$

We can write the phase $\theta(t)$, of the pulse given by equation (3.1.88) as [32]

$$\theta(t) = \omega_0 t + a_2 t^2. \tag{3.1.89}$$

Substituting equation (3.1.89) into equation (3.1.88) we have,

$$E(t) = T(t)e^{i\theta(t)}. \tag{3.1.90}$$

Instantaneous frequency ω_{inst} of equation (3.1.90), is given by [5]

$$\omega_{inst}(t) = \frac{d\theta(t)}{dt} = \omega_0 + 2a_2 t. \tag{3.1.91}$$

We see from equation (3.1.91) that a quadratic phase modulation in time corresponds to a linear frequency modulation. The pulse is said to be linearly chirped, figure 3.3 in section 3.1.3 is an example of a linearly chirped pulse. For $a_2 > 0$, $\omega(t)$ increases with time, this is referred to as positive chirp. For $a_2 < 0$, the frequency decreases with time and is called negative chirp.

Let us consider a pulse with a quadratic phase (qp), $\tilde{E_{qp}}(\omega)$ given by [5]

$$\tilde{E_{qp}}(\omega) = E_0 \exp\big[-i\beta(\omega+\omega_0)^2\big]\sqrt{\frac{\pi}{\alpha}}\exp\Big[\frac{(\omega+\omega_0)^2}{4\alpha}\Big] \tag{3.1.92}$$

α measures the spectral width of the pulse. β which is similar to $\psi(\omega)$ in equation (3.1.25) already discussed in section 3.1.2, is the spectral phase due to propagation through a dispersive medium. From equation (3.1.92), we see that β is a quadratic spectral phase factor, which again is similar to ψ_2, the second term in the Taylor expansion of the spectral phase $\psi(\omega)$ in equation (3.1.23) already discussed in section 3.1.2. Equation (3.1.92) can be written as [5]

$$\tilde{E_{qp}}(\omega) = E_0\sqrt{\frac{\pi}{\alpha}}\exp\Big[-\big(\frac{1}{4\alpha}+i\beta\big)\big(\omega+\omega_0\big)^2\Big] \tag{3.1.93}$$

equation (3.1.93) can further be written as [5]

$$\tilde{E_{qp}}(\omega) = E_0\sqrt{\frac{\pi}{\alpha}}\exp\Big[-\big(\frac{\omega+\omega_0}{4\Gamma}\big)^2\Big] \tag{3.1.94}$$

where Γ is given as

$$\Gamma = \frac{\alpha}{1+i4\alpha\beta} \tag{3.1.95}$$

Equation (3.1.93) can be written as [5]

$$\tilde{E_{qp}}(\nu) = E_0\sqrt{\frac{\pi}{\alpha}}\delta(\nu+\nu_0)\times\exp\Big(-\frac{-\pi^2}{\Gamma}\nu^2\Big) \tag{3.1.96}$$

where

$$\nu_0 = \frac{\omega_0}{2\pi} \tag{3.1.97}$$

Inverse Fourier transform of (3.1.96) yields, [5]

$$\mathcal{F}^{-1}\big[\tilde{E_{qp}}(\nu)\big](t) = E_0\sqrt{\frac{\pi}{\alpha}}\mathcal{F}^{-1}\big[\delta(\nu+\nu_0)\big](t)\mathcal{F}^{-1}\Big[\exp\big(\frac{-\pi^2}{\Gamma}\nu^2\big)\Big] \tag{3.1.98}$$

$$= E_0\sqrt{\frac{\pi}{\alpha}}\sqrt{\frac{\Gamma}{\alpha}}\exp(-i2\pi\nu_0 t)\sqrt{\frac{\Gamma}{\pi}}\exp(-\Gamma t^2) \tag{3.1.99}$$

$$E_{qp}(t) = E_0\sqrt{\frac{\Gamma}{\alpha}}\exp(-i\omega_0 t)\exp(-\Gamma t^2) \tag{3.1.100}$$

Γ can be written as [5]

$$\Gamma = a + ib \tag{3.1.101}$$

Rationalizing equation (3.1.95) we have [5],

$$a = \mathrm{Re}\{\Gamma\} = \frac{\alpha}{1 + 16\alpha^2\beta^2} \tag{3.1.102}$$

$$b = \mathrm{Im}\{\Gamma\} = -\frac{4\alpha^2\beta}{1 + 16\alpha^2\beta^2} \tag{3.1.103}$$

The amplitude of equation (3.1.100) is, [5]

$$E_0' = E_0\sqrt{\frac{\Gamma}{\alpha}}. \tag{3.1.104}$$

Re-writing equation (3.1.100) in a similar manner to equation (3.1.92), we get [5]

$$E(t) = E_0' \exp\big(-i\omega_0 t\big) \exp\big(-\Gamma t^2\big). \tag{3.1.105}$$

Substituting equation (3.1.102) and equation (3.1.103) into equation (3.1.105) we get, [5]

$$= E_0'\big[-i(\omega_0 t \ + bt^2)\big] \exp\big(-at^2\big). \tag{3.1.106}$$

Equation (3.1.106) describes the temporal pulse shape belonging to figure 3.7, having a Gaussian envelope and quadratic phase variation. From equations (3.1.102) and (3.1.103) we have [5],

$$\frac{b}{a} = -4\alpha\beta \tag{3.1.107}$$

$$a^2 + b^2 = \frac{\alpha^2}{1 + 16\alpha^2\beta^2} = \alpha a. \tag{3.1.108}$$

If the temporal parameter a and chirp parameter b, of the temporal pulse described by equation (3.1.106) are given, its corresponding spectral parameters α and β can be determined using equations (3.1.107) and (3.1.108) as [5],

$$\alpha = \frac{a^2 + b^2}{a} \tag{3.1.109}$$

$$\beta = -\frac{b}{4(a^2 + b^2)}. \tag{3.1.110}$$

From equation (3.1.110), we see that the chirp parameter b in the time domain, is related to β which is responsible for the stretching of the pulse in the frequency domain. It is worthy to note that the chirp parameter b, is the same as a_2, the second order phase term in the Taylor expansion of $\phi(t)$ in equation (3.1.84). The pulse in figure 3.7 was simulated using equation (3.1.106). The envelope of the pulse is a Gaussian function whose width $\Delta t_G'$, is larger than the width Δt_G, of the unchirped pulse. The pulse width of the unchirped pulse is given by [5]

$$\Delta t_G = 2\tau_G = \sqrt{\frac{2\ln 2}{a}} \tag{3.1.111}$$

where Δt_G is the full width at half maximum (FHWM) of the unchirped Gaussian pulse. The full width at half maximum is defined as twice the time τ_G, at which the intensity $I(t) = |E_0|^2 \exp(-2at^2)$ attains half of it's maximum value. The width $\Delta t_G'$ of the chirped pulse is given as [5]

$$\Delta t_G' = \Delta t_G\sqrt{\frac{\alpha}{a}}. \tag{3.1.112}$$

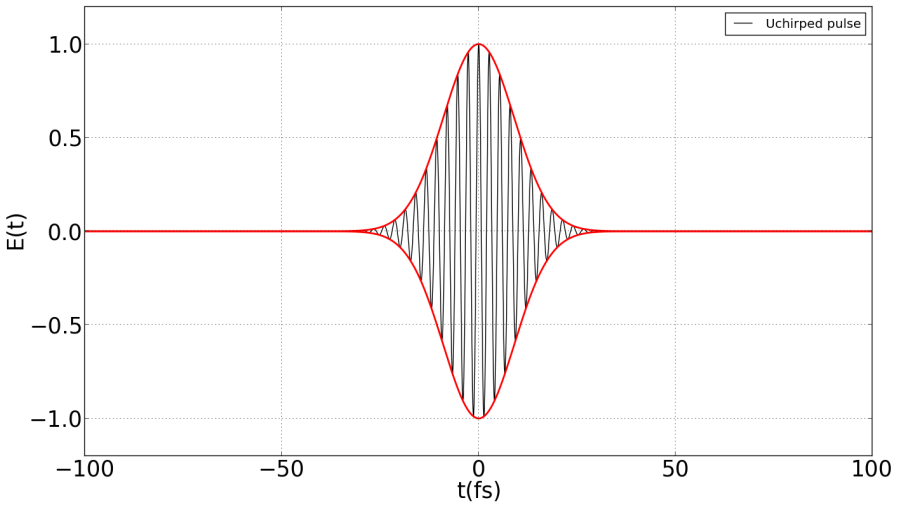

Figure 3.6: Simulated result of a temporal profile of a Gaussian pulse with chirp parameter $b = 0$

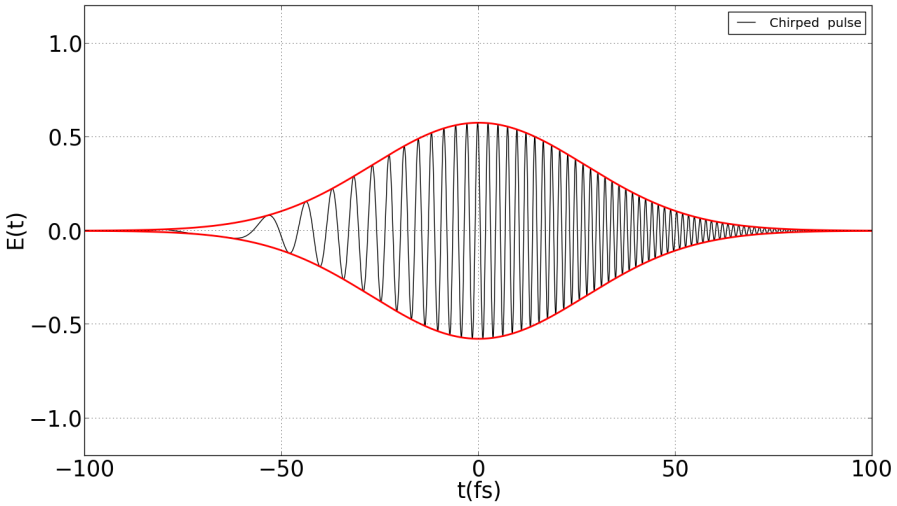

Figure 3.7: Simulated result of a temporal profile of a Gaussian pulse with chirp parameter $b = 0.0175$ fs^{-2}.

Clearly from equation (3.1.112), $\Delta t'_G$ depends on α which in turn depends on the chirp parameter as shown in equation (3.1.109). Further, making α subject in equation (3.1.108) and substituting into equation (3.1.112) we have [5]

$$\Delta t'_G = \Delta t_G \sqrt{1 + 16\alpha^2\beta^2}. \tag{3.1.113}$$

Equation (3.1.113) is the FWHM of the chirped pulse. Figure 3.8 is a simulation comparing the intensities of the chirped and unchirped pulses in figures 3.6 and 3.7. As a result of the chirp, the FWHM of the chirped pulse is 45fs and the FWHM of unchirped pulse is 15fs (see figure 3.8).

From this analysis, some important results are worthy of note. The first is given by equation (3.1.112). It tells us that the new pulse duration $\Delta t'_G$ of a pulse, after propagating through a dispersive medium which adds a chirp b to it, is dependent on α which also depends on the chirp

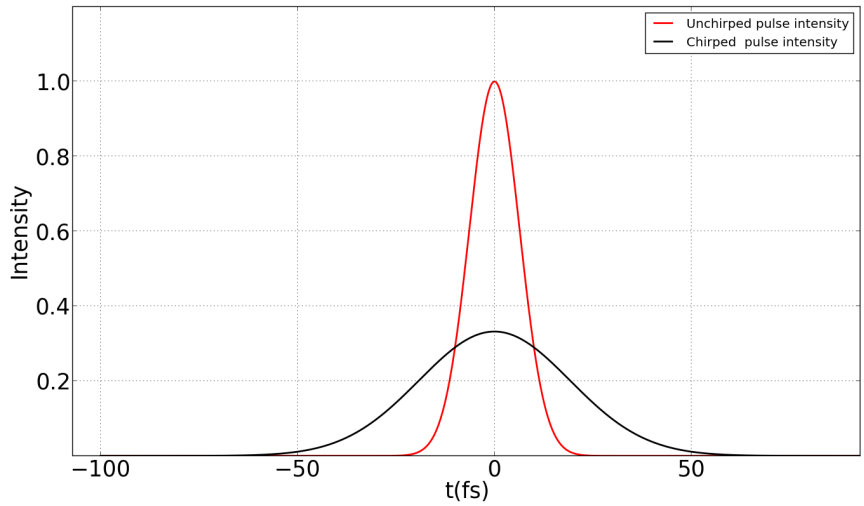

Figure 3.8: Simulated result comparing intensities of chirped and unchirped pulses.

parameter b, as given by equation (3.1.109). Secondly, the amplitude given by equation (3.1.104) of the chirped pulse is also dependent on α which depends on the chirp parameter b as given by (3.1.109). These are important because after a pulse is chirped, the total area under the intensity graph, must be the same as the total area under the intensity graph of the pulse before it was chirped. This is a consequence of the conservation of energy.

Stretching of a pulse can be observed in time or frequency domain. In the time domain, it is called a chirp and in the frequency domain it is called dispersion. They both describe the same concept (stretching of pulse). Therefore, the third term a_2, in the Taylor expansion of $\phi(t)$ in equation (3.1.84) and the ψ_2 term in the Taylor expansion in equation (3.1.23) both determine how much a pulse is stretched. Whilst a_2 describes the stretching of a pulse in the time domain, ψ_2 describes it in the frequency domain. Because the prism pulse compressor is studied in the frequency space, all calculations were done in the frequency space. Moreover, analytical calculations in the frequency space are easier to perform than in the time domain.

Chapter 4

Prism pulse compressor

4.1 Pulse re-compression

In section 1.4.1 the all normal dispersion photonic crystal fibre, ANDi-PCF was introduced. A pulse from a femtosecond laser with pulse duration of 80fs and a bandwidth at full width and half maximum of 15nm is allowed to propagate through an ANDi-PCF. Self phase modulation discussed in section 3.1.4 is the major non-linear process that occurs inside the ANDi-PCF, which is responsible for the increased bandwidth of the pulse emerging at the output of the ANDi- PCF. The pulse now has a larger bandwidth than the original femtosecond laser pulse at it's input. Also, this output pulse has a chirp as discussed in section 5.10 due to dispersion in the fibre. The larger the bandwidth of the pulse from the ANDi-PCF, the shorter the pulse can be recompressed. This is true since the Fourier limit Δt of a pulse is given by [28]

$$\Delta t = \frac{C_B \lambda^2}{c \Delta \lambda} \tag{4.1.1}$$

where $\Delta\lambda$ is the bandwidth of the pulse, c the speed of light and C_B for a Gaussian pulse is 0.441. Clearly, from equation (4.1.1), as $\Delta\lambda$ increases Δt decreases, hence the broader the pulse the shorter it can be compressed. The job of any pulse compressor such as the prism pulse compressor is to re-compress the broadened pulse and get to as close as possible to it's Fourier limit. Such a re-compressed pulse has a higher intensity and also a shorter pulse duration. Prisms, often used in the separation of white light into it's various components, can be used as a device for compensating for dispersion of light after travelling through optical elements. The prism can be used thus because it generates a negative GDD. To clearly see this, consider figure 4.1.

White light incident on the prism is dispersed into it's components. The angular spread of the red light component measured from the optic axis is denoted $\theta(\omega)$, and θ is a function of ω since different frequencies will be spread by different amounts. The phase delay $\psi(\omega)$, a given frequency ω experiences is given as [34]

$$\psi(\omega) = \vec{k}(\omega).\vec{r}_{\text{optic axis}} \tag{4.1.2}$$

$$= k(\omega) z \cos[\theta(\omega)] \tag{4.1.3}$$

$$= (\frac{\omega}{c}) z \cos[\theta(\omega)]. \tag{4.1.4}$$

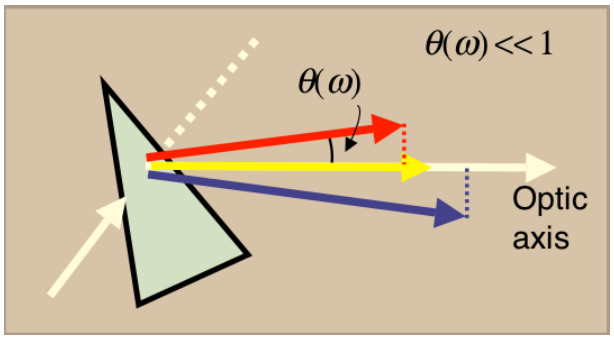

Figure 4.1: *GDD* from a dispersing prism [34].

The first and second partial derivatives of equation (4.1.4) with respect to ω gives [34]

$$\frac{\partial\psi}{\partial\omega} = \frac{z}{c}\cos(\theta) - \frac{\omega}{c}z\sin(\theta)\frac{\partial\theta}{\partial\omega} \tag{4.1.5}$$

and

$$\frac{\partial^2\psi}{\partial\omega^2} = -\frac{z}{c}\sin(\theta) - \frac{z}{c}\sin(\theta)\frac{\partial\theta}{\partial\omega} - \omega\frac{z}{c}\cos(\theta)\left(\frac{\partial\theta}{\partial\omega}\right)^2 - \omega\frac{z}{c}\sin(\theta)\frac{\partial^2\theta}{\partial\omega^2}. \tag{4.1.6}$$

But $\theta << 1$, so the sine terms can be neglected, and $\cos\theta \approx 1$. With these approximations, equation (4.1.6) becomes [34]

$$\frac{\partial^2\psi}{\partial\omega^2} \approx -\frac{\omega z}{c}\left(\frac{\partial\theta}{\partial\omega}\right)^2. \tag{4.1.7}$$

Note that equation (4.1.7) is always negative, thus a prism can be used to correct for *GDD*

4.2 Geometry of a prism used in a pulse compressor

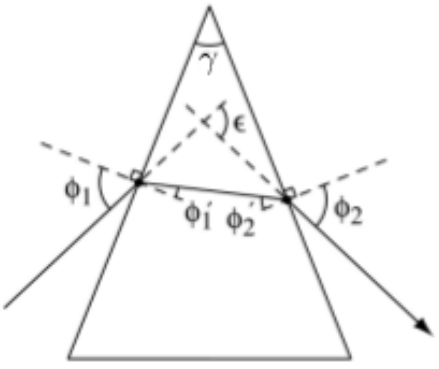

Figure 4.2: Ray diagram of light passing through a prism [12].

Consider figure 4.2, γ is the prism's apex angle, ϕ_1 and ϕ_2 are the incident and output angles respectively. The corresponding interior angles are ϕ_1' and ϕ_2' respectively [12]. The angle

between the emergent and incident rays ε, is the angle of deviation. From the geometry of figure 4.2 we have [12]

$$\phi_1 + \phi_2 = \varepsilon + \gamma \tag{4.2.1}$$

$$\phi_1' + \phi_2' = \gamma. \tag{4.2.2}$$

Also, from Snell's law we have,

$$\sin\phi_k = n\sin\phi_k'. \tag{4.2.3}$$

The angle of deviation ε has a minimum value when $\phi_1 = \phi_2$. This happens when the rays propagate symmetrically through the prism [12]. In the laboratory, minimum deviation is observed by rotating the prism about an axis perpendicular to the plane of the paper, the deviation angle first decreases to a minimum ε_{min} and then increases again as the prism is further rotated. For the purpose of dispersion-compensation using the prisms at minimum deviation ensures no astigmatism since input and output pulses have the same diameters. Also, when $\phi_1 = \phi_2$, the prism apex angle can be chosen to satisfy Brewster's angle for both input and output beams simultaneously, which is important to realize low loss. Brewster's angle condition is given as [12]

$$\tan\phi_1 = \tan\phi_2 = n. \tag{4.2.4}$$

The derivative of the output angle ϕ_2 with respect to wavelength is [12]

$$\frac{\partial\phi_2}{\partial\lambda} = \frac{\partial\phi_2}{\partial n}\frac{\partial n}{\partial\lambda} \tag{4.2.5}$$

and

$$\frac{\partial^2\phi_2}{\partial\lambda^2} = \frac{\partial^2\phi_2}{\partial n^2}\left(\frac{\partial n}{\partial\lambda}\right)^2 + \frac{\partial\phi_2}{\partial n}\frac{\partial^2 n}{\partial\lambda^2}. \tag{4.2.6}$$

Differentiating equation (4.2.2), we get

$$\frac{\partial\phi_1'}{\partial n} = -\frac{\partial\phi_2'}{\partial n}. \tag{4.2.7}$$

For each interface, equation (4.2.3) can be written as

$$\sin\phi_1 = n\sin\phi_1' \tag{4.2.8}$$

$$n\sin\phi_2' = \sin\phi_2. \tag{4.2.9}$$

Differentiating equations (4.2.8) and (4.2.9) respectively yields

$$0 = n\cos\phi_1'\frac{\partial\phi_1'}{\partial n} + \sin\phi_1' \tag{4.2.10}$$

$$n\cos\phi_2'\frac{\partial\phi_2'}{\partial n} + \sin\phi_2' = \cos\phi_2\frac{\partial\phi_2}{\partial n}. \tag{4.2.11}$$

From equation (4.2.11),

$$\frac{\partial\phi_2}{\partial n} = \frac{n\cos_1'}{\cos\phi_2}\frac{\partial\phi_2'}{\partial n} + \frac{\sin\phi_2'}{\cos\phi_2}. \tag{4.2.12}$$

Equation (4.2.7) in equation (4.2.12) gives

$$\frac{\partial\phi_2}{\partial n} = -n\frac{\cos\phi_2'}{\cos\phi_2}\frac{\partial\phi_1}{\partial n} + \frac{\sin\phi_2'}{\cos\phi_2}. \tag{4.2.13}$$

From equation (4.2.10)

$$\frac{\partial\phi_1'}{\partial n} = -\frac{\sin\phi_1'}{n\cos\phi_1'} \tag{4.2.14}$$

$$= -\frac{1}{n}\tan\phi_1'. \tag{4.2.15}$$

Put equation (4.2.15) in equation (4.2.13) and get

$$\frac{\partial\phi_2}{\partial n} = (\cos\phi_2)^{-1}\big[\cos\phi_2'\tan\phi_1' + \sin\phi_2'\big]. \tag{4.2.16}$$

Differentiating equation (4.2.16) taking note of equations (4.2.7) and (4.2.16) we have,

$$\frac{\partial^2\phi_2}{\partial n^2} = \tan\phi_2\Big(\frac{\partial\phi_2}{\partial n}\Big)^2 + (\cos\phi_2)^{-1}\frac{\partial\phi_2'}{\partial n}\Big[-\sin\phi_2'\tan\phi_1' - \cos\phi_2'\sec^2\phi_1' + \cos\phi_2'\Big]. \tag{4.2.17}$$

Applying equation (4.2.7) and using the identity $\sec^2\phi_1' - 1 = \tan^2\phi_1'$, equation (4.2.17) becomes

$$\frac{\partial^2\phi_2}{\partial n^2} = \tan\phi_2 + (\cos\phi_2)^{-1}\frac{\partial\phi_1'}{\partial n}\Big[\sin\phi_2'\tan_1' + \tan^2\phi_1'\cos\phi_2'\Big]. \tag{4.2.18}$$

From equation (4.2.11), we have,

$$\frac{\partial\phi_1'}{\partial n} = -\frac{\tan\phi_1'}{n}. \tag{4.2.19}$$

Using equation (4.2.19), equation (4.2.18) becomes

$$\frac{\partial^2\phi_2}{\partial n^2} = \tan\phi_2\Big(\frac{\partial\phi_2}{\partial n}\Big)^2 - \frac{\tan^2\phi_1'}{n}\Big(\frac{\partial\phi_2}{\partial n}\Big). \tag{4.2.20}$$

From equation (4.2.4), we get,

$$\cos\phi_2 = \cos\phi_1 = \frac{1}{\sqrt{1+n^2}}. \tag{4.2.21}$$

Applying Snell's law on each interface of figure 4.2 yields,

$$\sin\phi_1 = n\sin\phi_1' \tag{4.2.22}$$

$$\sin\phi_2 = n\sin\phi_2'. \tag{4.2.23}$$

Equations (4.2.22) and (4.2.23) can be written as

$$\tan\phi_1\cos\phi_1 = n\sin\phi_1' \tag{4.2.24}$$

$$\tan\phi_2\cos\phi_2 = n\sin\phi_1'. \tag{4.2.25}$$

From equation (4.2.25),

$$\sin\phi_2' = \frac{\tan\phi_2\cos\phi_2}{n} \tag{4.2.26}$$

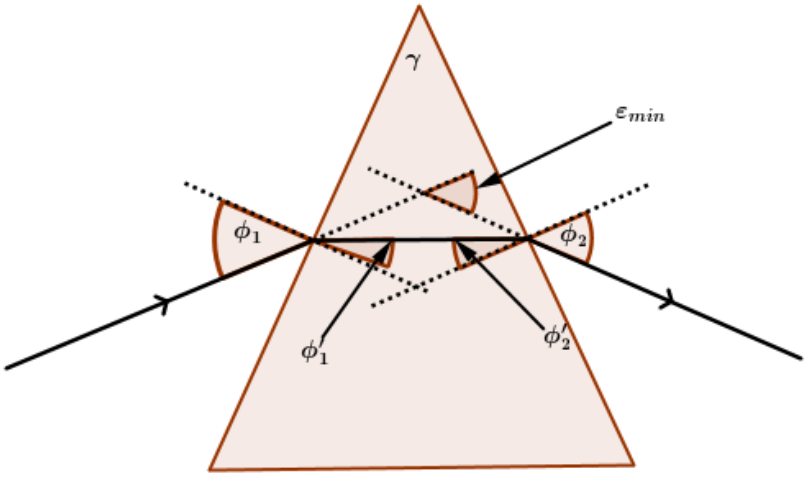

Figure 4.3: Ray diagram of light passing through a prism at Brewster's angle, $\phi_1 = \phi_2$ and angle of minimum deviation $\phi' = \phi_2'$. ε_{min} = angle of minimum deviation [12].

but from trigonometry,

$$\sin\phi_2' = \tan\phi_2' \cos\phi_2'. \tag{4.2.27}$$

By substituting equation (4.2.27) into equation (4.2.26) we get,

$$\tan\phi_2 \cos\phi_2 = n \tan\phi_2' \cos\phi_2', \tag{4.2.28}$$

$$\cos\phi_2' = \frac{\tan\phi_2 \cos\phi_2}{n \tan\phi_2'} \tag{4.2.29}$$

and by substituting equations (4.2.29), (4.2.26) and (4.2.21) into equation (4.2.16) we get,

$$\frac{\partial\phi_2}{\partial n} = \sqrt{1+n^2}\Big[\frac{\tan\phi_2 \cos\phi_2}{n} + \frac{\tan\phi_2 \cos\phi_2}{n \tan\phi_2'} \tan\phi_1'\Big]. \tag{4.2.30}$$

Since the prism is used at minimum deviation, $\phi_1' = \phi_2'$, hence, $\tan\phi_1' = \tan\phi_2'$ therefore, they cancel out in the second term in equation (4.2.30)

Putting equation (4.2.4) in equation (4.2.30) one gets,

$$\frac{\partial\phi_2}{\partial n} = \sqrt{1+n^2}\Big[\frac{n}{n\sqrt{1+n^2}} + \frac{n}{n\sqrt{1+n^2}}.1\Big] \tag{4.2.31}$$

$$= 2 \tag{4.2.32}$$

Using, equation (4.2.27), equation (4.2.24) can be written as

$$\tan\phi_1 \cos\phi_1 = n \tan\phi_1' \cos\phi_1' \tag{4.2.33}$$

dividing equation (4.2.33) by equation (4.2.25) one gets,

$$1 = \frac{n \tan\phi_1' \cos\phi'}{n \sin\phi_2'} \tag{4.2.34}$$

$$n \sin\phi_2' = n \tan\phi_1' \cos\phi_1'. \tag{4.2.35}$$

From Brewster's angle theory,

$$\theta_t + \theta_p = 90 \tag{4.2.36}$$

$$\text{and} \quad \theta_p = 90 - \theta_t \tag{4.2.37}$$

where θ_t= angle of transmitted light
and θ_p= polarizing angle or Brewster's angle.
Equation (4.2.37) can be written as,

$$\sin\theta_p = \sin(90 - \theta_t) = \cos\theta_t \tag{4.2.38}$$

and similarly,

$$\sin\phi_1 = \sin(90 - \phi_1') = \cos\phi_1'. \tag{4.2.39}$$

Substituting equation (4.2.21) or equation (4.2.4) into equation (4.2.39) we have

$$\cos\phi_1' = \frac{n}{\sqrt{n^2+1}}. \tag{4.2.40}$$

From equation (4.2.40),

$$\tan\phi_1' = \frac{1}{n} \tag{4.2.41}$$

$$\tan^2\phi_1' = \frac{1}{n^2}. \tag{4.2.42}$$

Equations (4.2.32), (4.2.4) and (4.2.42) in equation (4.2.20), yields,

$$\frac{\partial^2\phi_2}{\partial n^2} = 4n - \frac{2}{n^3}. \tag{4.2.43}$$

Two models of the prism pulse compressor are proposed. The first model discussed in section 4.2.1, is most commonly encountered in literature. It is accurate if the bandwidth of light to be compressed is small, but becomes less accurate as bandwidth increases. Also, it does not account for all three optical paths that the light travels in the prism pulse compressor, but the second model, a more accurate one, does take into account all optical paths that the light travels.

4.2.1 Model considering one optical path by Fork et al [35]

In this model, only one optical path, path DEK denoted by P_{DEK} is considered, see figure 4.4. Both prisms are positioned such that the exit face of prism I is parallel to the input face of prism II. Optical path P_{DEK} is found by inspection if we note that both AD and CK are possible wavefronts, where point A is chosen such that AC is parallel to DE and AD is perpendicular to DE [12].

Path P_{DEK} is approximated as [12]

$$P_{DEK} = P = n_2 L\cos\theta(\omega) \tag{4.2.44}$$

were L is the separation from the apex of both prisms, $\theta(\omega)$ the angular spread of the light dispersed and n_2 is the refractive index of air. The first and second derivatives of equation

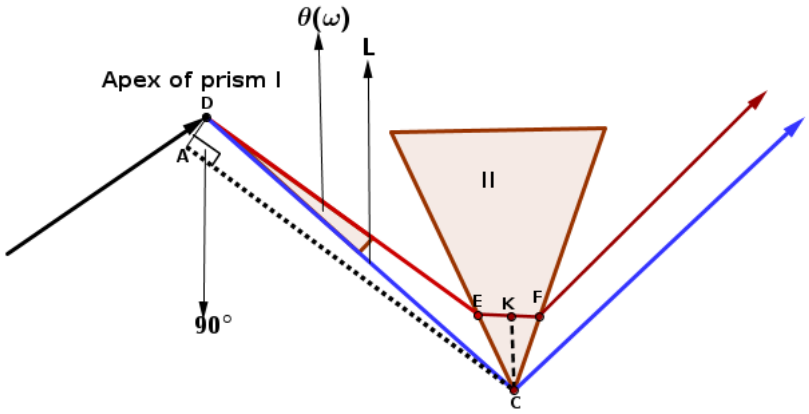

Figure 4.4: Model of prism pulse compressor by Fork et al [35].

(4.2.44) are [12]

$$\frac{\partial P}{\partial \lambda} = L\Big[\frac{dn_2}{d\lambda}\cos\theta - n_2\sin\theta\Big(\frac{d\theta}{d\lambda}\Big)\Big] \text{and} \tag{4.2.45}$$

$$\frac{\partial^2 P}{\partial \lambda^2} = L\Big[\frac{d^2 n_2}{d\lambda^2}\cos\theta - 2\frac{dn_2}{d\lambda}\sin\theta\Big(\frac{d\theta}{d\lambda}\Big) - n_2\cos\theta\Big(\frac{d\theta}{d\lambda}\Big)^2 - n_2\sin\theta\Big(\frac{d^2\theta}{d\lambda^2}\Big)\Big] \tag{4.2.46}$$

but n_2 is the refractive index of air. Substituting $n_2 = 1$ in equation (4.2.46) yields [12]

$$\frac{\partial^2 P}{\partial \lambda^2} = -L\Big[\cos\theta\Big(\frac{d\theta}{d\lambda}\Big) + \sin\theta\Big(\frac{d^2\theta}{d\lambda^2}\Big)\Big]. \tag{4.2.47}$$

Recall, dispersion in terms of wavelength derived earlier in section 3.1.2 is given by

$$\frac{\partial^2 \psi}{\partial \omega^2} = -\frac{\lambda^3}{2\pi c^2}\frac{\partial^2 P}{\partial \lambda^2} \tag{4.2.48}$$

where ψ is a frequency-dependent phase difference between different spectral components. Note that θ is defined in the opposite sense compared to ϕ_2, so that [12]

$$\frac{\partial \theta}{\partial \lambda} = -\frac{\partial \phi_2}{\partial \lambda}. \tag{4.2.49}$$

Substituting equations (4.2.49) and (4.2.5) into equation (4.2.47) one gets,

$$\frac{\partial^2 P}{\partial \lambda^2} = -L\left\{\cos\theta\Big(-\frac{\partial \phi_2}{\partial n}\frac{\partial n}{\partial \lambda}\Big)^2 + \sin\theta\Big[\Big(-\frac{\partial^2 \phi_2}{\partial n^2}\Big(\frac{\partial n}{\partial \lambda}\Big)^2 - \frac{\partial \phi_2}{\partial n}\frac{\partial^2 n}{\partial \lambda^2}\Big)\Big]\right\}. \tag{4.2.50}$$

In the special case of minimum deviation and Brewster's angle, we substitute equations (4.2.32) and (4.2.43) into equation (4.2.50) and get

$$\frac{\partial^2 P}{\partial \lambda^2} = -L\left\{4\cos\theta\Big(\frac{\partial n}{\partial \lambda}\Big)^2 + 2\sin\theta\Big[\Big(\Big(2n - \frac{1}{n^3}\Big)\Big(\frac{\partial n}{\partial \lambda}\Big)^2\Big) - \frac{\partial^2 n}{\partial \lambda^2}\Big)\Big]\right\}. \tag{4.2.51}$$

Substituting equation (4.2.51) into equation (4.2.48) yields [12],

$$\frac{\partial^2 \psi}{\partial \omega^2} = \frac{\lambda^3}{2\pi c^2}\Big[4L\cos\theta\Big(\frac{dn}{d\lambda}\Big)^2 - 2L\sin\theta\Big[\frac{d^2 n}{d\lambda^2} + (2n - \frac{1}{n^3})\Big(\frac{dn}{d\lambda}\Big)^2\Big]\Big]. \tag{4.2.52}$$

In the model by Fork et al, the dispersion $\frac{\partial^2 P}{\partial \lambda^2}$ and group delay dispersion $\frac{\partial^2 \psi}{\partial \omega^2}$ are respectively given by [12]

$$\frac{\partial^2 P}{\partial \lambda^2} = -L\left\{4\cos\theta\left(\frac{\partial n}{\partial \lambda}\right)^2 + 2\sin\theta\left[\left(\left(2n - \frac{1}{n^3}\right)\left(\frac{\partial n}{\partial \lambda}\right)^2\right) - \frac{\partial^2 n}{\partial \lambda^2}\right]\right\} \tag{4.2.53}$$

and

$$\frac{\partial^2 \psi}{\partial \omega^2} = \frac{\lambda^3}{2\pi c^2}\left[4L\cos\theta\left(\frac{dn}{d\lambda}\right)^2 - 2L\sin\theta\left[\frac{d^2 n}{d\lambda^2} + (2n - \frac{1}{n^3})\left(\frac{dn}{d\lambda}\right)^2\right]\right]. \tag{4.2.54}$$

When θ is small, $L\cos\theta \approx L$. The first term in equation (4.2.54) represents normal temporal dispersion due to angular dispersion of the first prism. The magnitude of the temporal dispersion can be increased by increasing L, the apex-to apex prism spacing.

Assuming a Brewster prism at minimum deviation, the distance which the reference ray travels, satisfies [12]

$$EF = 2L\sin\theta \tag{4.2.55}$$

$-2L\sin\theta\left(\frac{d^2 n}{d\lambda^2}\right)$ which is usually the dominant part in the second term in equation (4.2.54) is simply the material dispersion arising due to a length $2L\sin\theta$ of prism II. Hence, suppose the material dispersion of prism II is $\Psi = 2L\sin\theta$ then, varying L will also vary Ψ. In, this way the GDD offered by the prism pulse compressor can be optimized such that the compressed pulse is as short as possible. This will again be discussed in section 5.1.2. The merit of this model is it's simplicity. It provides a rough estimate of the apex to apex prism spacing L necessary to compress a pulse with a GDD. This is true because in equation 4.2.54, all there is to do is to solve for L since other parameters in equation 4.2.54 are constants.

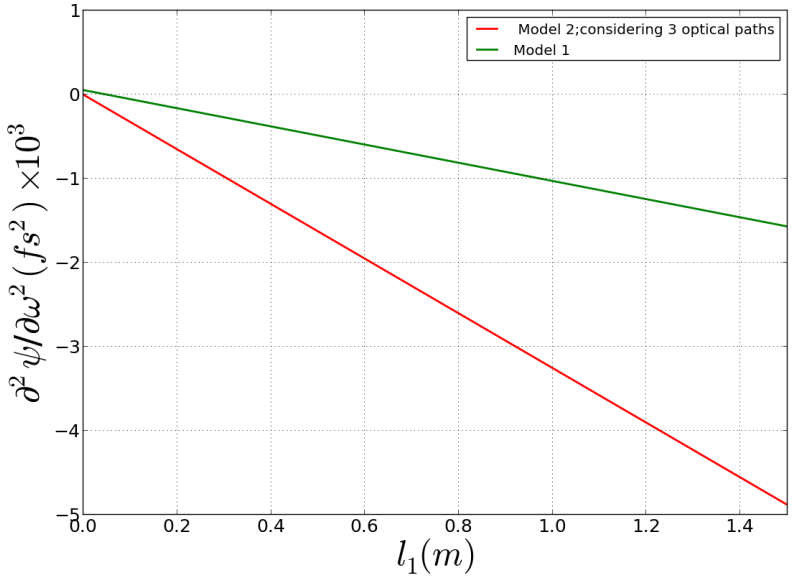

Figure 4.5: Simulation comparing GDD of both models.

4.2.2 Model considering all optical paths

The prism pulse compressor consist of two prisms I and II. The prisms are set up such that the exit face of prism I is parallel to the entrance face of prism II and the entrance face of prism I is parallel to the exist face of prism II. Both prisms are cut such that the angle of minimum deviation also equals the Brewster's angle which also equals α, the incident angle. This ensures that the losses due to reflection will be minimal [36]. This configuration also ensures that a ray travels symmetrically through both prisms. Each prism has an apex angle $2A$. l_1 is the slant height between the apexes of both prisms, l_2 is the distance from the apex of prism II to the symmetry mirror. β is the angle between the red light component of the beam and a reference ray l_1. β also determines the angular spread of the beam.

The total optical path in a prism pair consist of three components; P_1, P_2 and P_3. P_1 is the optical length between prisms I and II, P_2 is the optical path length in prism II and P_3 is the optical path length from prism II to the symmetry mirror. Since the refractive index $n = 1$ in air, the total optical path length can be written as [36]

$$P = P_1 + P_2 + P_3 \tag{4.2.56}$$

$$= L_1 + nL_2 + L_3 \tag{4.2.57}$$

where n is the refractive index of prism material and L_1, L_2 and L_3 are the corresponding geometrical lengths respectively (Consider fig 4.6).

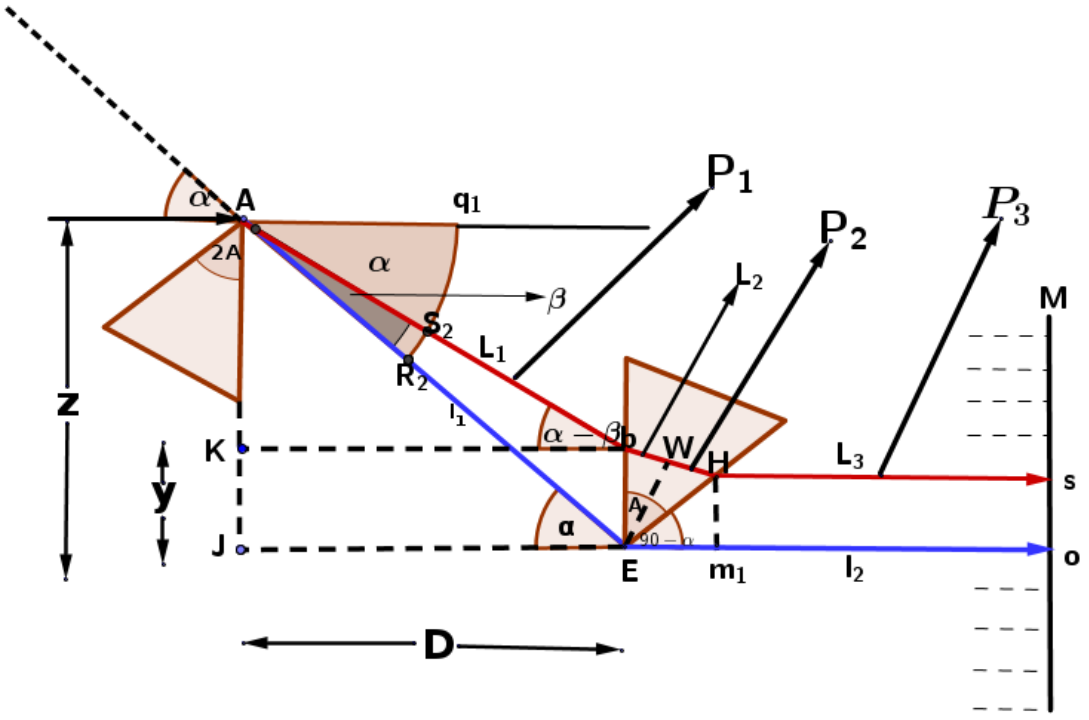

Figure 4.6: Light path in a pair of dispersing prisms [36].

From the geometry in figure 4.6,

$$\cos\alpha = \frac{JE}{l_1} \tag{4.2.58}$$

$$= \frac{D}{l_1}. \tag{4.2.59}$$

Hence,

$$l_1 = \frac{JE}{\cos\alpha} \tag{4.2.60}$$

$$= \frac{D}{\cos\alpha}. \tag{4.2.61}$$

Also,

$$\cos(\alpha - \beta) = \frac{JE}{L_1}. \tag{4.2.62}$$

From equation (4.2.60),

$$JE = l_1 \cos\alpha \tag{4.2.63}$$

Equation (4.2.63) in equation (4.2.62) yields [36],

$$= \frac{l_1 \cos\alpha}{\cos(\alpha - \beta)}. \tag{4.2.64}$$

A perpendicular drawn from the midpoint W of L_2 will divide $\hat{E}$ into two equal angles. Hence, from ΔbEW we get,

$$\sin A = \frac{bW}{bE} \tag{4.2.65}$$

$$\tag{4.2.66}$$

and hence,

$$bW = bE \sin A. \tag{4.2.67}$$

Since bW is the midpoint of L_2, $bH = 2 \times bW$. Hence,

$$bH = 2bE \sin A. \tag{4.2.68}$$

Let $AJ = Z$ and $KJ = y$, thus $AK = z - y$. From ΔAKb,

$$\sin(\alpha - \beta) = \frac{z - y}{L_1} \tag{4.2.69}$$

and

$$\sin\alpha = \frac{z}{l_1}. \tag{4.2.70}$$

eliminating y from equations (4.2.69) and (4.2.70) we have,

$$y = l_1 \sin\alpha - L_1 \sin(\alpha - \beta). \tag{4.2.71}$$

Substituting equation (4.2.64) into equation (4.2.71) we get,

$$y = l_1 \sin\alpha - \frac{l_1 \cos\alpha \sin(\alpha - \beta)}{\cos(\alpha - \beta)} \tag{4.2.72}$$

$$= l_1 \frac{\sin\alpha \cos\alpha}{\cos\alpha} - l_1 \cos\alpha \tan(\alpha - \beta). \tag{4.2.73}$$

Equation (4.2.73) simplifies to

$$y = l_1 \cos\alpha \big[\tan\alpha - \tan(\alpha - \beta)\big]. \tag{4.2.74}$$

Note that equation (4.2.74) is the beam size on the prism and will be referred to in chapter 6. From ΔbEW,

$$\sin A = \frac{bW}{bE} = \frac{bW}{y}. \tag{4.2.75}$$

but since EW is a perpendicular to bH, $bW = \frac{L_2}{2}$, equation (4.2.75) becomes

$$\sin A = \frac{L_2}{2y} \tag{4.2.76}$$

$$\tag{4.2.77}$$

or

$$L_2 = 2y \sin A. \tag{4.2.78}$$

Substituting equation (4.2.74) into equation (4.2.78) yields [36],

$$L_2 = 2l_1 \sin A \cos\alpha \big[\tan\alpha - \tan(\alpha - \beta)\big]. \tag{4.2.79}$$

At minimum deviation, the beam traverses the prism symmetrically hence,

$$y = KJ = bE = HM. \tag{4.2.80}$$

From ΔGHM,

$$\sin\alpha = \cos(90 - \alpha) = \frac{EM}{y} \text{and} \tag{4.2.81}$$

from equation (4.2.81),

$$EM = y\cos(90-\alpha) = y\sin\alpha. \tag{4.2.82}$$

. From figure 4.6,

$$L_3 = l_2 - EM \tag{4.2.83}$$

Substituting equation (4.2.74) in equation (4.2.82) and substituting the result in equation (4.2.83), we have [36]

$$L_3 = l_2 - l_1\sin\alpha\cos\alpha[\tan\alpha - \tan(\alpha-\beta)]. \tag{4.2.84}$$

From equation (4.2.64), the first, second and third derivative yields, [36]

$$\frac{dL_1}{d\beta} = -\frac{l_1\cos\alpha\sin(\alpha-\beta)}{\cos^2(\alpha-\beta)} \tag{4.2.85}$$

and

$$\frac{d^2L_1}{d\beta^2} = \frac{l_1\cos\alpha[\sin^2(\alpha-\beta)+1]}{\cos^3(\alpha-\beta)} \tag{4.2.86}$$

Similarly from equations (4.2.79) and (4.2.84), we get,

$$\frac{dL_2}{d\beta} = \frac{2l_1\cos\alpha\sin A}{\cos^2(\alpha-\beta)} \tag{4.2.87}$$

$$\frac{d^2L_2}{d\beta^2} = -\frac{4l_1\cos\alpha\sin A\sin(\alpha-\beta)}{\cos^3(\alpha-\beta)} \tag{4.2.88}$$

$$\frac{dL_3}{d\beta} = -\frac{l_1\cos\alpha\sin\alpha}{\cos^2(\alpha-\beta)} \tag{4.2.89}$$

$$\frac{d^2L_3}{d^2\beta} = \frac{2l_1\cos\alpha\sin\alpha\sin(\alpha-\beta)}{\cos^3(\alpha-\beta)}. \tag{4.2.90}$$

As expected, observing equations (4.2.89) and (4.2.90), the derivatives of P with respect to β is independent of l_2 since

$$\frac{dP_3}{d\beta} = \frac{dL_3}{d\beta}.$$

Clearly, the geometric lengths L_i change with wavelength because for longer wavelengths, L_1 will be shorter and for shorter wavelengths, L_i will be longer. Hence we can write [36]

$$\frac{dL_i}{d\lambda} = \frac{dL_i}{d\beta}\frac{d\beta}{dn}\frac{dn}{d\lambda} \tag{4.2.91}$$

where $i = 1, 2, 3$ for different paths. Equation (4.2.91) is justified since β varies with n, L_i varies with β and n with λ

$$\frac{d^2L_i}{d\lambda^2} = \frac{d^2L_i}{d\beta^2}\left(\frac{d\beta}{dn}\frac{dn}{d\lambda}\right)^2 + \frac{dL_i}{d\beta}\left[\frac{d^2\beta}{dn^2}\left(\frac{dn}{d\lambda}\right)^2 + \frac{d\beta}{dn}\frac{d^2n}{d\lambda^2}\right]. \tag{4.2.92}$$

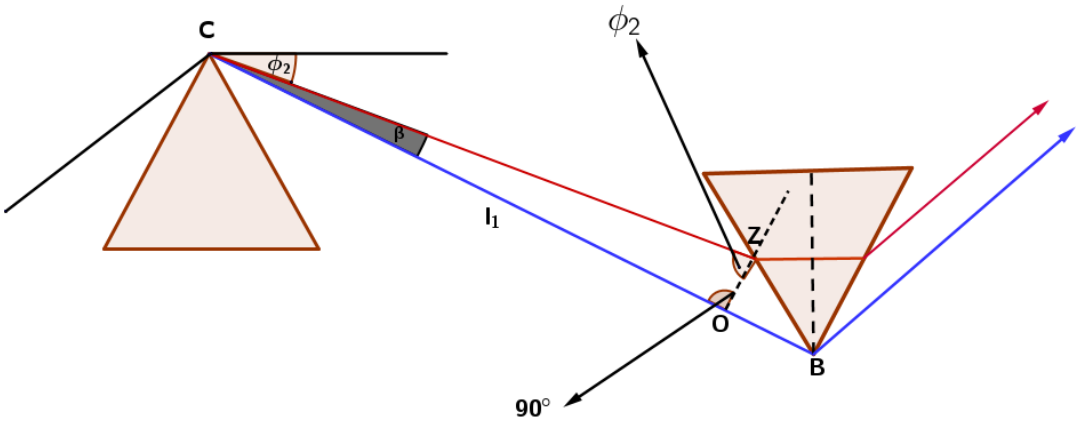

Figure 4.7: Light path in a pair of prisms [37].

Considering figure 4.7, we see from $\triangle COZ$, OZ is a perpendicular to CB at point Z. Hence,

$$\beta + \phi_2 = 90^\circ \tag{4.2.93}$$

$$\frac{d\beta}{d\lambda} + \frac{d\phi_2}{d\lambda} = 0 \tag{4.2.94}$$

$$\frac{d\beta}{d\lambda} = -\frac{d\phi_2}{d\lambda} \tag{4.2.95}$$

Using equation (4.2.5), equation (4.2.95) becomes,

$$-\frac{d\beta}{d\lambda} = \frac{d\phi_2}{dn}\frac{dn}{d\lambda} \tag{4.2.96}$$

and inserting equation (4.2.32) in equation (4.2.96) yields,

$$\frac{d\beta}{d\lambda} = -2\frac{dn}{d\lambda}. \tag{4.2.97}$$

Integrating equation (4.2.97) from λ_1 to λ_2, we get,

$$\beta = -2\frac{dn}{d\lambda}\Delta\lambda. \tag{4.2.98}$$

Differentiating equation (4.2.93) with respect to n yields,

$$\frac{d\beta}{dn} = -\frac{d\phi_2}{dn} \tag{4.2.99}$$

$$\frac{d^2\beta}{dn^2} = -\frac{d^2\phi_2}{dn^2} \tag{4.2.100}$$

and inserting equations (4.2.32) and (4.2.43) in equation (4.2.100) yields,[35]

$$\frac{d\beta}{dn} = -2 \tag{4.2.101}$$

$$\frac{d^2\beta}{dn^2} = -4n + \frac{2}{n^3}\ . \tag{4.2.102}$$

Differentiating equation (4.2.57) with respect to λ, we get the total dispersion as [36]

$$\frac{dP}{d\lambda} = \frac{dL_i}{d\lambda} + L_2\frac{dn}{d\lambda} + n\frac{dL_2}{d\lambda} + \frac{dL_3}{d\lambda} \tag{4.2.103}$$

$$\frac{d^2P}{d\lambda^2} = \frac{d^2L_1}{d\lambda^2} + L_2\frac{d^2n}{d\lambda^2} + 2\frac{dn}{d\lambda}\frac{dL_2}{d\lambda} + n\frac{d^2L_2}{d\lambda} + \frac{d^2L_3}{d\lambda^2} \tag{4.2.104}$$

Recall, equation (4.2.105) in section 3.1.2 [12]

$$\frac{\partial^2\psi(\omega)}{\partial\omega^2} = -\frac{\lambda^3}{2\pi c^2}\frac{d^2P}{d\lambda^2}. \tag{4.2.105}$$

Hence, substituting equation (4.2.104) into equation (4.2.105), we get the GDD as [36]

$$\frac{\partial^2\psi(\omega)}{\partial\omega^2} = -\frac{\lambda^3}{2\pi c^2}\Big(\frac{d^2L_1}{d\lambda^2} + L_2\frac{d^2n}{d\lambda^2} + 2\frac{dn}{d\lambda}\frac{dL_2}{d\lambda} + n\frac{d^2L_2}{d\lambda} + \frac{d^2L_3}{d\lambda^2}\Big). \tag{4.2.106}$$

In equation (4.2.106), the first and second derivatives with respect to λ of L_1 and L_2 and L_3 is calculated using equation (4.2.91) and equation (4.2.92) respectively.

A simulated result for the GDD of both models given by equations (4.2.105) and (4.2.52) is shown in figure 4.5. Clearly, as expected the GDD increases with increase in prism separation l_1. This enables the determination of the distance between the prisms required to compensate for a given GDD.

Comparing equation (4.2.53), the dispersion of the model by Fork et al which did not consider all optical paths and equation (4.2.106) which considered all optical paths, we see that the former is less accurate and consequently, the GDD from the two models will differ. But, both models will give similar results if the bandwidth of light to be compressed is small.

4.2.3 Spatial light modulator (SLM) as a pulse compressor

In section 1.5, the SLM was introduced and in section 2.6.2, the SLM as a pulse shaper was discussed. The SLM can also be used as a pulse compressor. The pulse shaping technique using the spatial light modulator (SLM) for pulse compression has the advantage over the prism pulse compressor because of it's ability to compensate for higher order chirp which the prism pulse compressor cannot compensate for. If the bandwidth of light to be compressed by a prism pulse compressor is large, some of the light will be clipped, this means that not all bandwidth of the light is captured by the prism which in turn, plays a role in the duration of the compressed pulse. For the compressed pulse to be as short as possible, all the bandwidth of the light must be captured. This is important if the compressed pulse is to be as short as possible that is, theoretically close to the Fourier limit. To avoid clipping and capture more bandwidth, bigger prisms must be used. Further explanation will be given in chapter 6. An SLM has been employed by Karasawa et al to compress broadband(500-1500nm) pulses from an argon-filled capillary fibre [11]. An SLM consists of a single row of 640 independent pixels with one large calibration pixel at the end of the row. This large calibration pixel is used to ascertain the response of the liquid crystal with different drive voltages. A pixel in the SLM has a width of 97μm, 2mm height and a dead region between pixels of 3μm [25]. The SLM comprises of a thin layer of zero-twist liquid crystals placed in between glass covers [25]. These glass covers have microscopically etched parallel valleys on the inside. They are also coated with transparent electrodes. The liquid crystals inside the SLM are not like crystal balls as one might expect but instead, are long rod like molecules. The crystals align themselves parallel to the surface of the etched glass covers when no electric field is present i.e. no applied voltage across the electrodes. But when a voltage is applied, the molecules, as expected, align themselves to the electric field. Therefore, polarised light parallel to the liquid crystals experiences a change in refractive index [25]. The pixel is

what houses these liquid crystals. Light of wavelength λ passing through an SLM of thickness l, experiences a retardation given by [25],

$$\triangle\phi = \frac{2\pi\triangle n(V)l}{\lambda} \tag{4.2.107}$$

where $\triangle n(V)$=change in the refractive index of the material with voltage.

Now, in a dispersive medium as discussed in section 3.1, dispersion corresponds to the phenomenon whereby the index of refraction of a medium is frequency dependent [3]. Since dispersion is frequency dependent, it is also wavelength dependent since

$$c = f\lambda \tag{4.2.108}$$

where c is the speed of light. From equation (4.2.107), different wavelengths experience different amounts of retardation $\triangle\phi$. For the SLM to be effectively used as a pulse compressor, appropriate voltages must be applied to different wavelengths in order to reverse the effect of a dispersive medium on $\triangle\phi$ of a pulse incident on it's pixels.

4-f shaper

The SLM which is the most important component of the 4-f set up was described in section 2.6.1. By combining two gratings and two lenses with the SLM in the Fourier plane, one can obtain a set up which can compress or stretch a pulse see figure 4.8. The first grating spectrally disperses the pulse. This implies that each spectral component now has a unique spatial frequency. The first lens performs a Fourier transform on the beam, mapping each of the unique spatial frequencies to a unique spatial position, at the plane of the SLM. All the frequency components are therefore spatially separated at the SLM plane. The second lens then performs an inverse Fourier transform, mapping all the different spatial positions, corresponding to different frequencies, to different spatial frequencies. All the frequencies, with their unique spatial frequencies, will be recombined by the second grating. In the set up in figure 4.8, if all the optical elements are symmetrically separated by the focal length of the lenses f, then without any modulation from the SLM, the pulse leaving the setup is same as the one entering the setup.

To obtain a good compression of a stretched pulse using the SLM, it is important that the phase Ψ of the masking function $H(\omega)$ given by equation (4.2.113), be such that it reverses the effect any dispersive medium has on a pulse. In this way, the original form of the pulse is obtained. The SLM is used as a pulse compressor in the frequency domain in a 4-f set up already discussed in section 2.6.2. In this section, a theoretical background of the 4-f shaper will be given.

Any electric field can be separated into it's envelope $S(\omega)$ and phase $\varphi(\omega)$ as [32]

$$\tilde{E_{in}^{+}}(\omega) = S(\omega)e^{i\varphi(\omega)} \tag{4.2.109}$$

where the envelope $S(\omega)$ calculated from the measured spectrum $I(\omega)$ is given by [32]

$$S(\omega) = \frac{1}{\sqrt{2\varepsilon_0}}\sqrt{I(\omega)}. \tag{4.2.110}$$

The masking function $H(\omega)$ is written on a computer and sent to the SLM. It is described by the complex function [32]

$$H(\omega) = R(\omega)e^{-i\Psi(\omega)} \tag{4.2.111}$$

where $R(\omega)$ represents the amplitude filter. Equation (4.2.111) is usually written on a computer via a Labview program and sent to the SLM. Carefully choosing $H(\omega)$, a pulse can be manipulated arbitrarily in time. In equation (4.2.111), Ψ is responsible for the phase delay of every frequency. A Taylor expansion of Ψ gives [32]

$$\Psi(\omega) = \Psi(\omega_0) + \frac{d\Psi(\omega)}{d\omega}\Big|_{\omega_0}(\omega-\omega_0) + \frac{1}{2}\frac{d^2\Psi(\omega)}{d\omega^2}\Big|_{\omega_0}(\omega-\omega_0) + \cdots \tag{4.2.112}$$

$$= b_0 + b_1(\omega-\omega_0) + \frac{1}{2}b_2(\omega-\omega_0)^2. \tag{4.2.113}$$

Similar to equations (3.1.83) and (3.1.84) in section 5.10, b_0 determines the absolute phase of the pulse, $b_1 = \frac{d\Psi(\omega)}{d\omega}\Big|_{\omega_0}$ is the group delay and the coefficient b_2 gives the GDD already discussed in section 3.1.2. After the pulse passes through the SLM, the output electric field is [32]

$$\tilde{E^+_{out}}(\omega) = H(\omega)\tilde{E^+_{in}}(\omega) = R(\omega)e^{-i\Psi(\omega)}\tilde{E^+_{in}}(\omega). \tag{4.2.114}$$

Substituting equation (4.2.113) into (4.2.114) and doing an inverse Fourier transform, we obtain the shape of the electric field after passing through the SLM as [32]

$$\tilde{E^+_{out}}(t) = \frac{1}{2\pi}R_0e^{-ib_0}e^{i\omega t}\int_{-\infty}^{+\infty}\tilde{E^+_{in}}(\omega)e^{-i\sum_{n=2}^{\infty}\frac{1}{n!}b_n(\omega-\omega_0)^n}e^{i(\omega-\omega)(t-b_1)}d\omega. \tag{4.2.115}$$

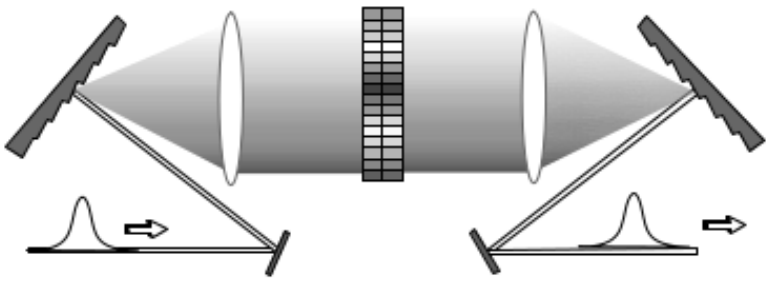

Figure 4.8: 4-f set up. The spectrum can be modulated if in the Fourier plane, an SLM is placed. As shown if the modulator isn't modulating, the outing pulse is same as the incoming pulse [32].

Chapter 5

Experimental set up and results

5.1 Characterization of PCF output

The shortest pulses generated via supercontinuum (SC) generation with a duration of 2.6fs have been generated in a gas-filled hollow core fibre and subsequent temporal recompression with an active phase shaping device [38]. Unfortunately, this technique requires very high pulse energies of several hundreds of microjoules. In contrast, optical fibres with a solid core can produce sufficient spectral broadening for few-cycle pulse generation even at nanojoule pulse energies [39]. Using a short piece of single mode fibre and a chirped mirror-compressor, it has been possible to achieve pulse durations of 4fs (1.7 optical cycles) [40]. Especially, photonic crystal fibres (PCF) are well suited for generation of ultrafast broadband SC spectra due to the possibility to tailor their dispersion properties [39].

In all experiments performed, we used an all-normal dispersion PCF (ANDi-PCF) for supercontiuum (SC) generation. This fibre is used because it possesses only normal dispersion in the region of interest (500nm to 1500nm) and therefore does not suffer from noise sensitive soliton dynamics [39]. The process is governed by self-phase modulation (SPM) and optical wave breaking only [41] which results in very smooth and highly coherent ultra-broad SC spectra. Such spectra are well suited for temporal recompression and it has already been shown that the sub-two cycle regime (5.0fs, 1.9 optical cycles) is achieved by compensating for linear chirp [10]. The SC or white light generated is of interest because it has a broad bandwidth thus, potentially can be compressed to shorter pulses. This is further discussed in chapter 6. The PCF used was manufactured by NKT photonics and is made of pure silica. It has a cladding diameter is $127\pm5\mu$m, with a coating diameter of $245\pm10\mu$m and a core diameter of $2.3\pm0.3\mu$m. In addition, it has a dispersion of -2ps/nm/km and a numerical aperture of approximately 0.37 at 1064nm [42]. The numerical aperture at 800nm will be very similar to that at 1064nm because numerical aperture varies slowly with wavelength.

A femtosecond laser at a center wavelength of 800nm, with a spectral width of (12.4 ± 0.5)nm, an average power of 840mW, a maximum pulse power of 130kW, a maximum pulse energy of 10nJ, and a minimum pulse duration of (75 ± 5)fs is allowed to propagate through an optical isolator, and reflected off mirror M1 (see figure 5.3). A lens located just before the photonic crystal fibre with a very short focal length of 10mm is mounted on the translation stage on which the photonic crystal fibre is mounted. This lens focuses light into the fibre. With three

knobs on the translation stage, each independently able to translate the stage and thus the fibre in the x,y and z directions, the fibre is aligned such that the maximum coupling efficiency is achieved. Figures 5.1 and 5.2 show the measured spectrum from the fibre for different input powers.

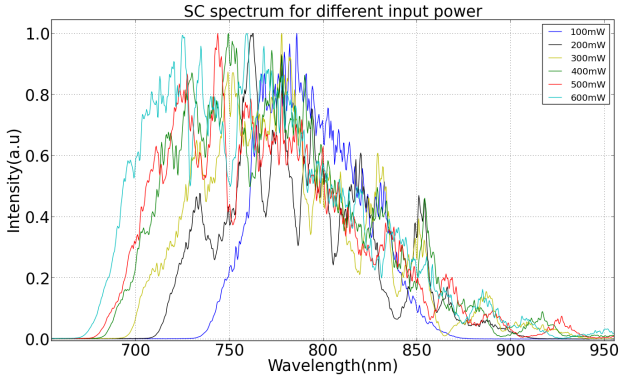

Figure 5.1: Normalized measured super continuum(SC) of PCF for various input power.

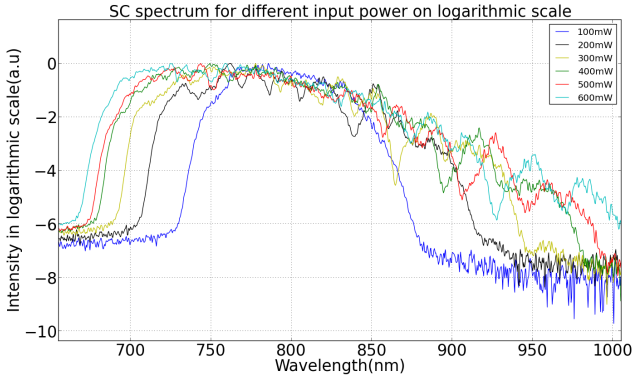

Figure 5.2: Measured super continuum(SC) of PCF for various input power on logarithmic scale.

From figure 5.2, we clearly see that as the input power is increased, the broader the super continuum gets. Pulse compression is very important because few-cycle laser pulses are indispensable for a wide range of applications such as time-resolved spectroscopy in chemistry, biology, physics and material science. In particular, few-cycle laser pulses can be used for probing the ultrafast vibrational dynamics of chemical bonds [43].

5.1.1 Prism pulse compressor set up

The prisms used are manufactured by Newport Corporation. Both prisms are ultrafast laser dispersion prisms made of LaKL21 glass grade AA with a Newport part number of 10LK10 [28]. The pick off mirror assembly with Newport part number 10D20ER.2 is a broadband mirror (480nm-2000nm) and has a protected silver coating [28].

Light exiting the photonic crystal is collimated with a collimating lens CL (see figure 5.3). To ensure that light from CL was properly collimated, it was allowed to travel about 2m. By

positioning CL appropriately, the size of the beam at this distance was same as that just at the output of CL. M2 and M3 are used to alter beam height from about 13cm to 14.5cm, this was to allow the beam to hit the prisms at the right height. The beam from the photonic crystal fibre has a beam size of about 3mm hence, L1 and L2 are used to reduce the beam size from 3mm to 1.5mm. A polariser P ensures that horizontally polarized light is sent to the prisms. M4 reflects light to the tip of the first prism at an angle of 58°, the Brewster's angle for LAkL21 glass(See figure 5.3).

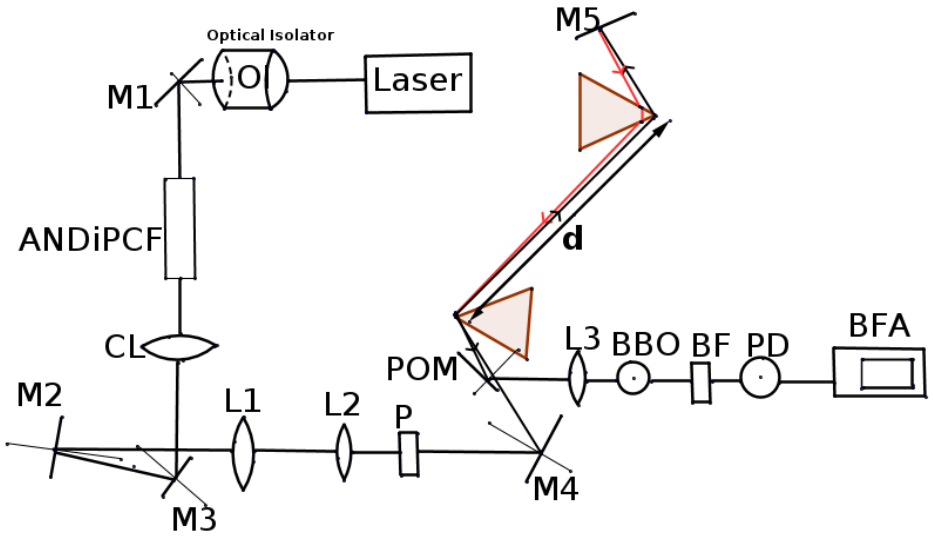

Figure 5.3: Experimental set up. CL: Collimating lens, L1,L2,L3: Lenses, P: Polarizer, BBO: 2nd harmonic crystal, BF: Blue filter, Z: Background free autocorrelator(BFA) setup.

Both prisms in the set up are cut such that the angle of minimum deviation and Brewster's angle conditions are satisfied. Each prism is supported by a post, with a circular base on which the prism rests. The circular base has a prism holder at it's top to hold the prism in place. See figure 5.4.

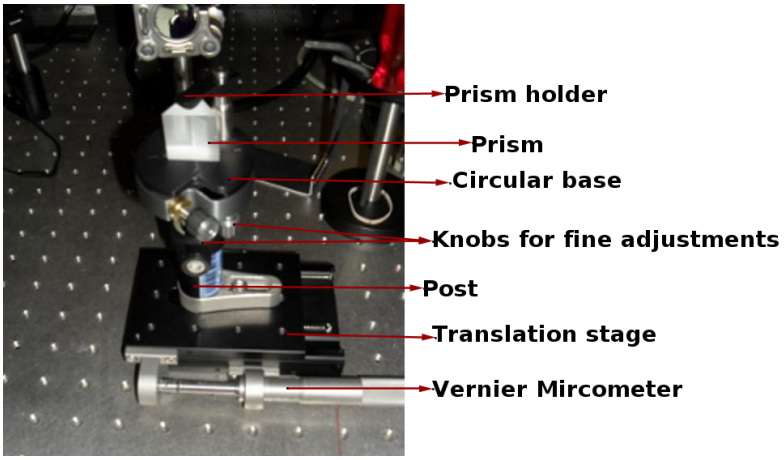

Figure 5.4: Prism support.

The circular base on which each prism is mounted has three knobs which are used to tilt the prisms angularly in the x, y and z directions for fine adjustments to prism orientation. The prism post is screwed onto a translation stage. The translation stage allows the prism to be moved in and out of the beam, thus allowing for finer adjustments to the beam path inside the prism. The translation stage is in turn screwed onto the optical table. See figures 5.5 and 5.6

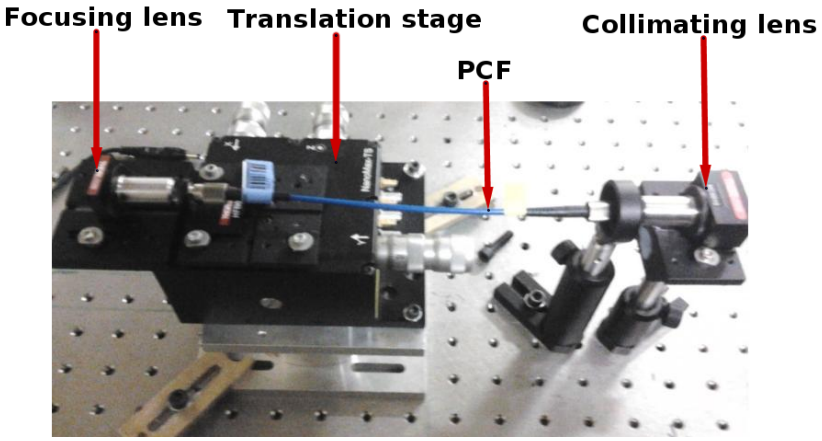

Figure 5.5: Some components of experimental set up

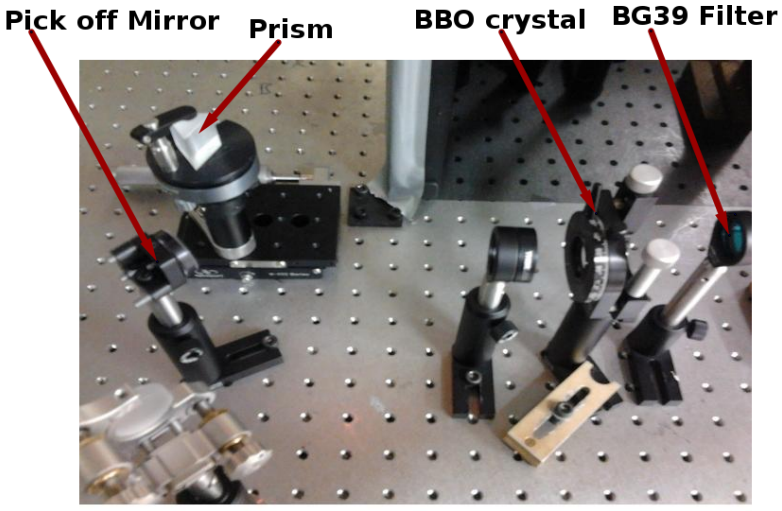

Figure 5.6: Some components of experimental set up

Light from the first prism travels to the second prism and M5 is positioned such that the reflected light travels just below the in-coming light. Pick off mirror POM reflects the compressed light into a lens L3 of 35mm focal length which in turn focuses the light onto a BBO crystal. BF is a BG39 glass filter that transmits light between 380nm to 580nm see figure 5.7. In figure 5.7, the shaded region, which denotes the spectral range for which the transmission is $> 50\%$ of the maximum transmission, represents the range for which the manufacturer (thorlabs) recommends when using this filter [18]. It is used to filter the second harmonic light generated by the BBO crystal. A BBO crystal is a non-linear crystal made of Barium borate. A photo-diode PD, is

used to measure the intensity of the generated second harmonic and to optimize the set-up such that the intensity of the second harmonic is maximized. Once optimized, the filter and BBO crystal are removed and the light is then sent to the background free autocorrelator set up.

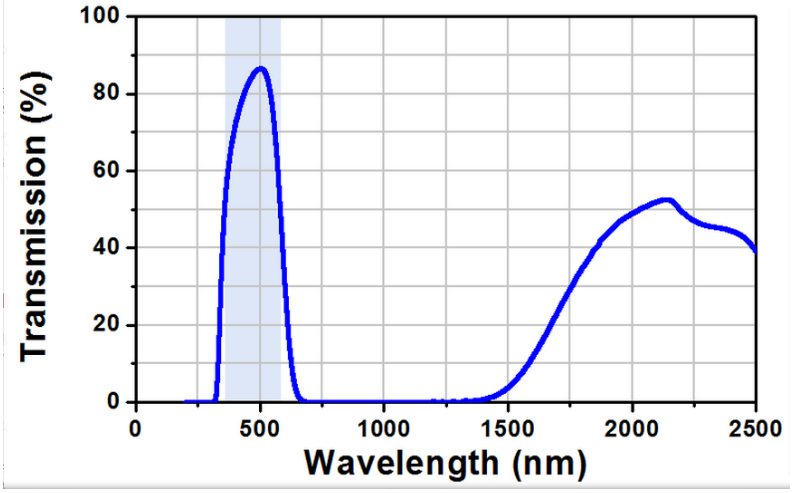

Figure 5.7: Spectral range of BG39 filter [18].

5.1.2 Optimizing prism compressor set up

Figure 5.8 is the result of the optimization of the prism pulse compressor set up. The translation stage of the second prism was moved until a position is found where maximum blue light was obtained after the BG39 glass filter. Moving the translation stage of the second prism changes the amount of glass the beam travels inside the prism. And in turn, this helps in optimizing the GDD introduced by the prism pulse compressor. The theory behind this was discussed using equation (4.2.55) in section 4.2.1. When a pulse is compressed, it's intensity increases but it's total energy remains constant. Also, since the second harmonic signal increases with the square of the incident intensity, a high second harmonic signal is expected as the pulse gets more compressed.

5.2 Pulse duration measurement using background free autocorrelation technique

Background-free autocorrelation (BFA) is an intensity autocorrelation pulse characterization technique only capable of determining the pulse width $\Delta\tau$. BFA, is merely the normal second-order intensity autocorrelation described by [44]

$$C_0(\tau) = \int_{-\infty}^{\infty} dt\{I^2(t-\tau) + I^2(t) + 4I(t-\tau)I(t)\} \tag{5.2.1}$$

The third term in equation (5.2.1) is the second order intensity while the first and second terms are the background terms. Since the BFA is just a second-order intensity autocorrelation, there are no background terms hence, the BFA signal can be expressed as [44]

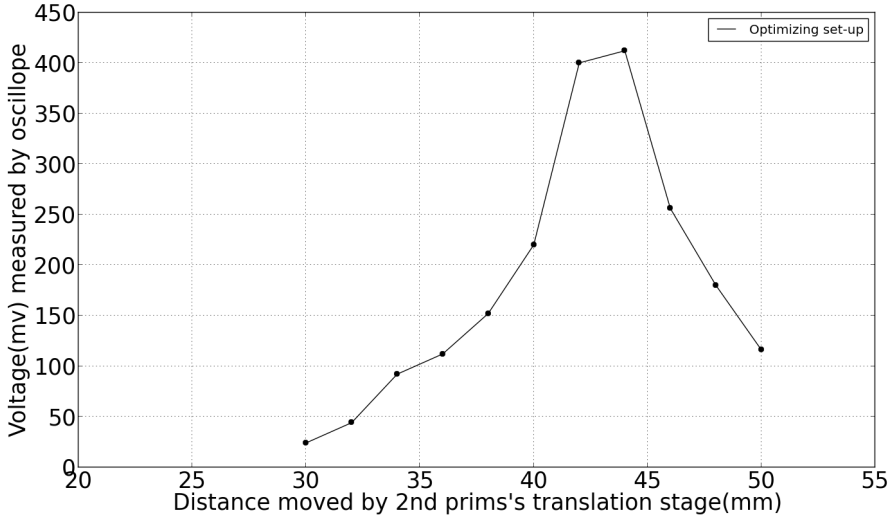

Figure 5.8: Optimization graph of prism pulse compressor set up

$$G^{(2)}_{BFA} = \int_{-\infty}^{\infty} I(t-\tau)I(t)dt \tag{5.2.2}$$

It is impossible to extract any phase information from equation (5.2.2) since phase information is lost when considering intensities only. The power of the BFA in the determination of pulse durations becomes obvious if equation (5.2.2) is re-written for a Gaussian pulse described by [44]

$$E(t) = A_0 \exp\left\{-2\log(2)\left[1 + ib_0\right]\left(\frac{t}{\Delta\tau}\right)^2\right\} \tag{5.2.3}$$

where A_0 is the amplitude, $\Delta\tau$ and pulse width b_0 the linear chirp parameter. Using equation (5.2.3), equation (5.2.2) becomes,

$$G^{(2)}_{BFA} = A_0^4 \exp\left\{-2\log(2)\left(\frac{t}{\Delta\tau}\right)^2\right\} \tag{5.2.4}$$

where $\Delta\tau$ is the pulse duration. The full width at half maximum FWHM of the BFA signal in equation (5.2.4) is given by [44]

$$\Delta\tau_{BFA} = \sqrt{2}\Delta\tau. \tag{5.2.5}$$

Equation (5.2.5) simply gives the relation between the FWHM of the pulse and that of the BFA signal.

5.2.1 Background free autocorrelation set up

As shown in figure 5.9 [44], the input pulse is divided by a 50/50 dielectric beam splitter (BS) mounted at an angle of 45° into paths A and B. The pulse in path B is reflected onto itself from

mirror M1 which is mounted on a linear translation stage (TS). TS creates a temporal delay between τ between the pulse copies $I(t)$ and $I(t-\tau)$ [44]. In path A, the pulse $I(t)$ is sent to a set of perpendicularly arranged mirrors M2 and M3 which ensures that the reflected pulse is horizontally displaced. A portion of the reflected pulse from path B then moves through BS and is focused together with a portion of the reflected pulse from path A into a thin β-Barium Borate(BBO)crystal [44]. Note that due to the horizontal displacement of the pulse copy in path A, focusing into the BBO crystal is non-collinear [44]. If aligned properly, this non-collinear arrangement of the input pulse on a non-linear optical crystal such as the BBO, results in second harmonic light generated in the forward direction. Because of this non-collinear setup, the input pulse copies can be filtered after they interact inside the BBO crystal using an iris(A) [44]. This suggests that the generated second harmonic light in the forward direction, is free of any contributions from $I(t)$ or $I(t-\tau)$, that is, it is background free [44]. The generated second harmonic signal then travels through a BG39 filter whose transmission curve is shown in figure 5.7 [44].

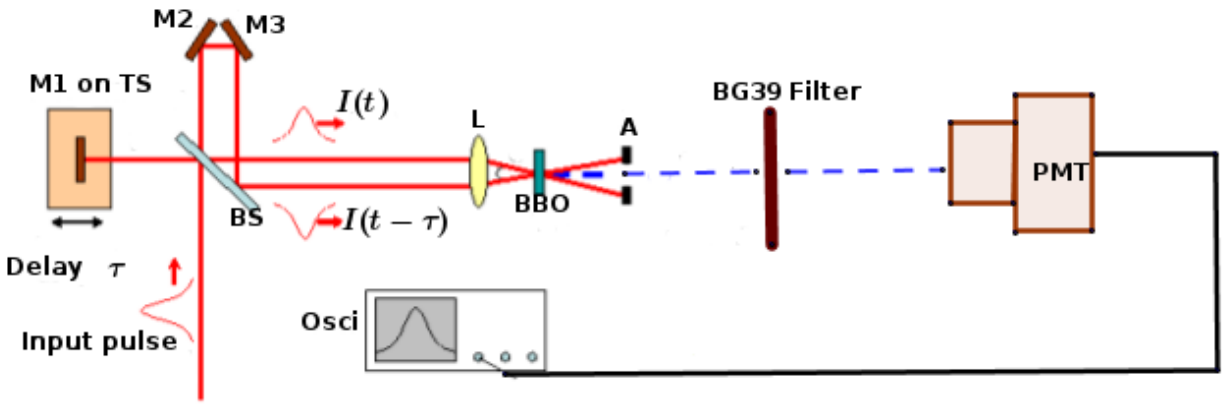

Figure 5.9: BFA set up. BS: 50/50 Beam splitter, M1,M2,M3: Au coated mirrors, TS: Linear translation stage, τ: Temporal delay, L: Lens, α: Angle between input pulse, BBO: β-Barium Borate crystal, A: Iris as variable aperture, PMT: Photo-multiplier tube, Osci: Oscilloscope.

Measured pulse duration from BFA

The linear translation stage (TS) in figure 5.9 was moved at a speed of 0.01mm/s for 20s. This translates to a distance of 0.2mm and an optical path length (OPL) of 0.4mm. The delay is given by

$$t_{delay} = OPL/c \tag{5.2.6}$$

$$= \frac{0.4 \times 10^{-3}\text{m}}{3 \times 10^{8}\text{m/s}} \tag{5.2.7}$$

$$= 1.3 \times 10^{-12}\text{s}, \tag{5.2.8}$$

equation (5.2.8) is delay between pulses in real time. To convert from oscilloscope time to real time, we note from the simple calculation in equation (5.2.7) and equation (5.2.8) that, 20s of oscilloscope time correspond to 1.3×10^{-12}s in real time. Hence, 1s of oscilloscope time corresponds to 6.5×10^{-14} or 65fs real time. Therefore, all data points on the x-axis in figure 5.10 were multiplied by a factor of 65fs to get figure 5.11.

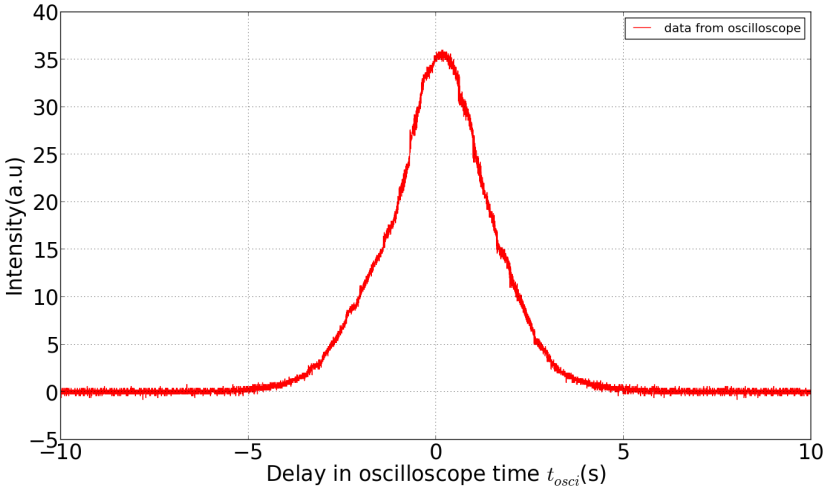

Figure 5.10: Pulse as seen on oscilloscope

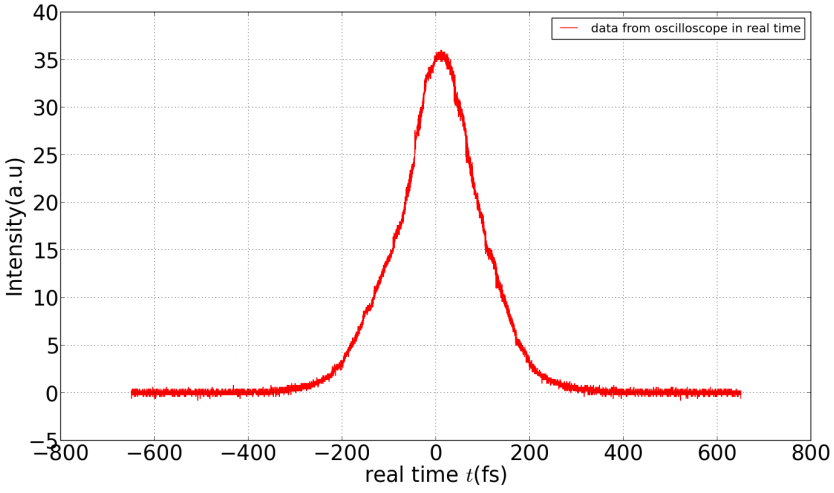

Figure 5.11: Compressed pulse in real time

Using equation (5.2.5), the pulse duration of uncompressed and compressed pulse was determined to be 2ps and 140fs, respectively. Figure 5.12 shows uncompressed and compressed pulse.

Figure 5.13 is the spectrum of the pulse that was compressed and was obtained with an input power of 212mW into the fibre and an output power of 111mW from the fibre. A fit of the compressed pulse using equation (5.2.4) is shown in figure 5.14.

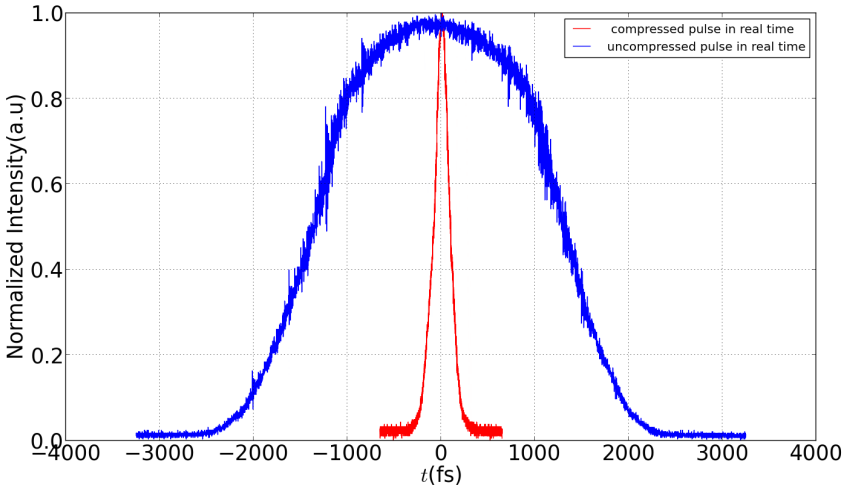

Figure 5.12: Compressed and uncompressed pulse in real time

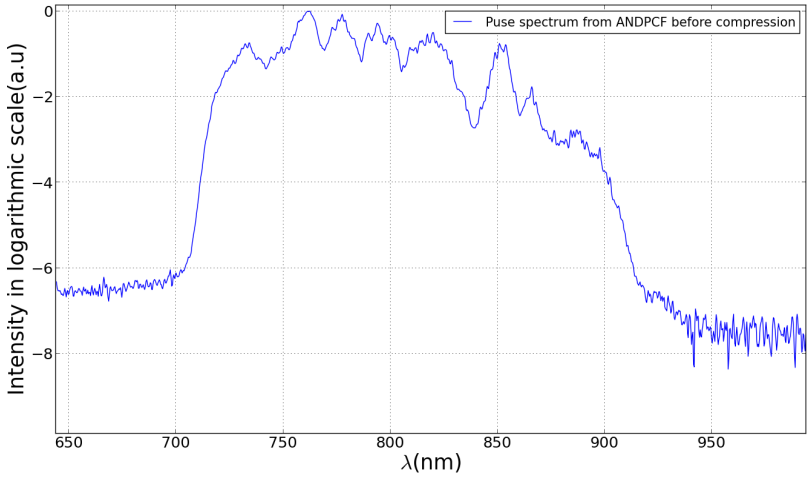

Figure 5.13: Pulse spectrum from ANDi-PCF before compression at 212mW input power

In figure 5.14, a pulse duration of 140fs was extracted. This is a remarkable achievement since the experimentally measured original pulse, has a pulse duration of about 2ps.

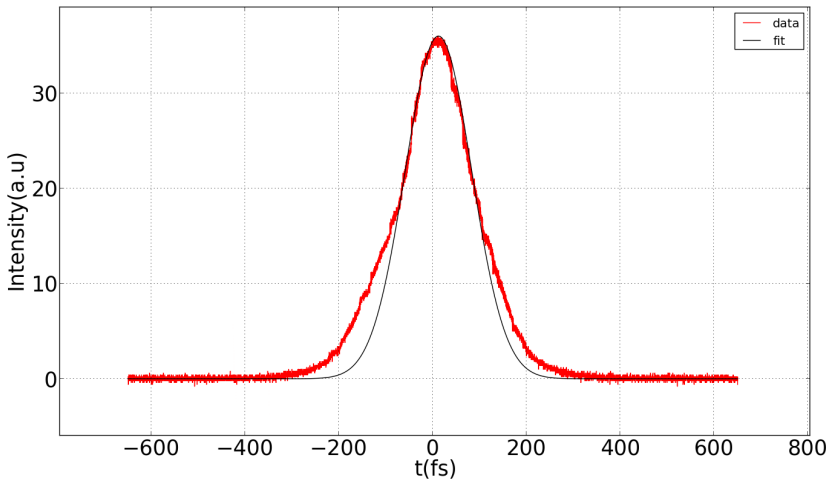

Figure 5.14: Fit of compressed pulse

Chapter 6

Discussions

In this section, the results obtained in chapter 5 are discussed. Two main factors played a huge role in the measured pulse duration of the compressed pulse. These factors were the prism size and the higher order chirp present in the pulse. These effects, the role they play and how they can be eliminated will be discussed.

Not all the light incident on the second prism in figure 6.2 is intercepted on it's face. Some of the light is clipped and lost in air. This happens because, the prisms are 25mm long on each side. Hence, the amount of light it can intercept without clipping is limited. This means that not all the bandwidth in the broadband white light from the ANDi-PCF is compressed and this has an effect on the pulse duration of the compressed pulse as will be discussed shortly.

As can be seen from figure 6.1, as the bandwidth of light from the ANDi-PCF increases, the size of the prism required to intercept all the light increases. In figure 6.1, the graph shows that

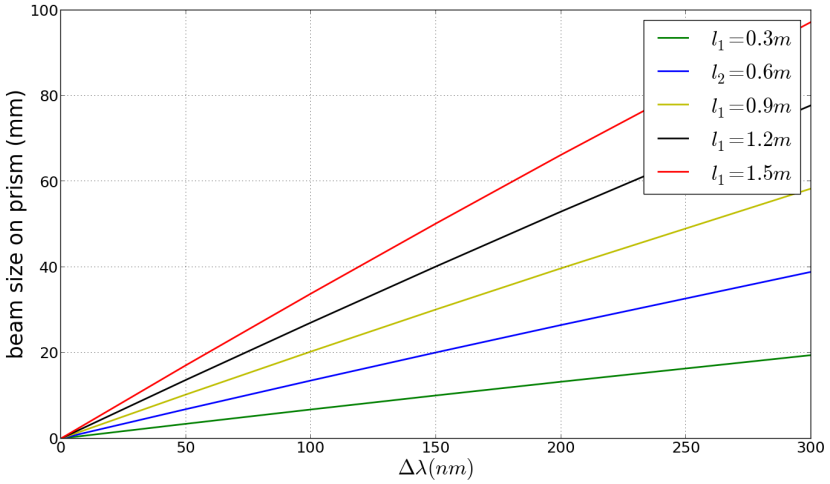

Figure 6.1: Dependence of beam size on prism with bandwidth for LAkL21 Glass $\frac{dn}{d\lambda} = -0.02623 \times 10^6 \mathrm{m}^{-1}$

for a particular prism separation l_1, the beam size on the prism increases with bandwidth $\Delta\lambda$. Consider below figure 6.2 discussed earlier in section 4.2.2.

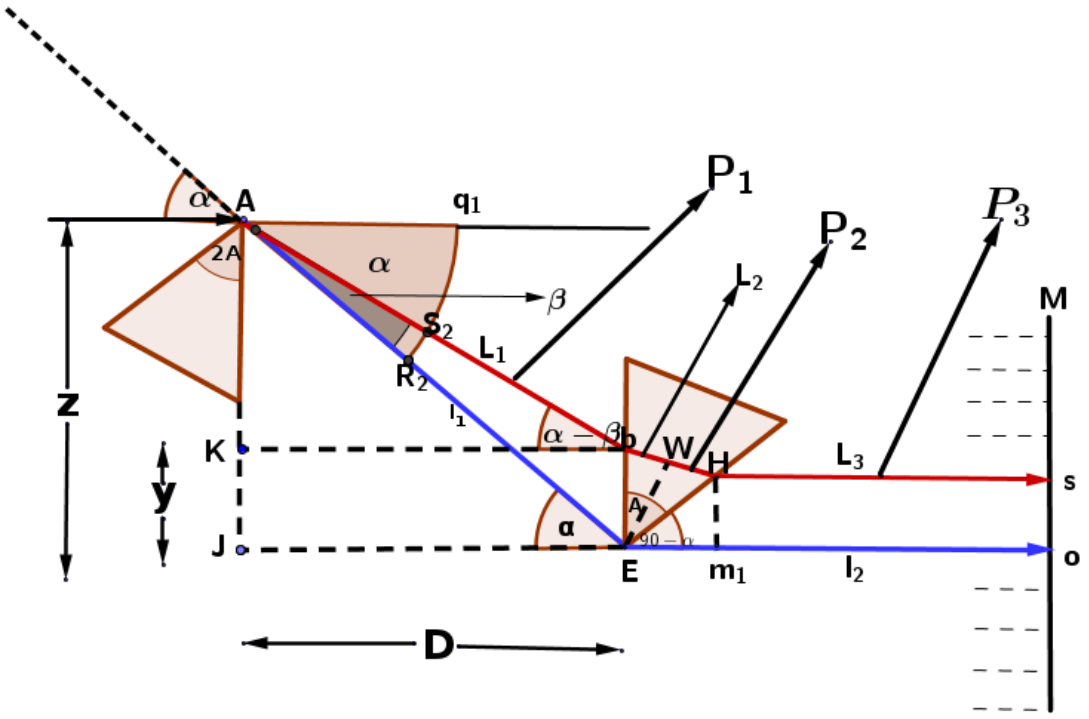

Figure 6.2: Light course in a pair of dispersing prisms [36].

Recall equation (6.0.1) in section 4.2.2 given by

$$y = l_1 \cos\alpha\big[\tan\alpha - \tan(\alpha - \beta)\big] \tag{6.0.1}$$

where α is the Brewster's angle of incidence and β as explained in equation (4.2.98) in section 4.2.2, is the angular spread of the beam. Equation (6.0.1) gives an estimate of the beam size on the prism. If the second prism in figure 6.2 is moved closer to the first prism, distance bE or y which is the beam size on the second prism will be reduced accordingly. Indeed this is the case because from equation (6.0.1), y is directly proportional to l_1. This result is clearly shown in figure 6.1, as l_1 increases the beams size on prism increases.

Consider equation (6.0.2) already encountered in section 4.2.52 given by [28]

$$\Delta t = \frac{c_B \lambda^2}{c\Delta\lambda} \tag{6.0.2}$$

where Δt is the Fourier limit of the pulse which simply is the shortest pulse duration any pulse can potentially be compressed to and $\Delta\lambda$ is the bandwidth of the pulse. From equation (6.0.2), as $\Delta\lambda$ increases, Δt gets smaller. Since the size of the prism pulse compressor is limited, not all bandwidth is accommodated, this means in equation (6.0.2), $\Delta\lambda$ is not as large as possible. Thus not all the light is compressed, and from equation (6.0.2) it is clear that the limit to which our pulse can be compressed is also limited.

Theoretically, if all chirps (both linear and higher order chirps) in the entire bandwidth of the pulse are compensated then, the pulse duration Δt calculated using equation (6.0.2) using $\Delta\lambda_{\text{ALL}} = 200\text{nm}$ gives $\Delta t = 4.7\text{fs}$. In figure 6.3, the black arrow depicts the point where a

pulse duration of $\Delta t = 4.7$fs would be obtainable. As can be seen on this point, if the all the bandwidth $\Delta\lambda_{\text{ALL}}$ is compressed, a prism size of 52mm will be required.

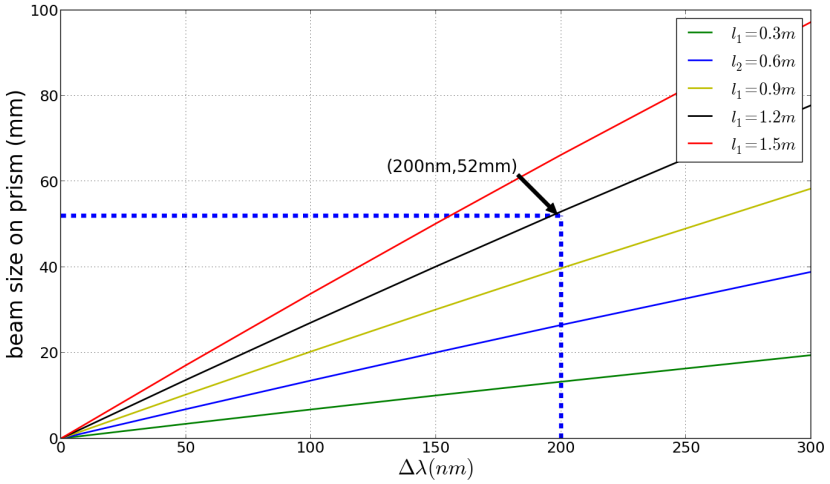

Figure 6.3: Dependence of beam size on prism with bandwidth for LAkL21 Glass. It indicates limit of prism size to pulse duration of compressed pulse.

In our experiment, we assumed the pulse shape of the supercontinuum to be a Gaussian and considered a FWHM bandwidth $\Delta\lambda_{\text{FWHM}}$ of about 100nm. Calculating Δt using $\Delta\lambda_{\text{FWHM}}$ in equation 6.0.2, we get a pulse duration of $\Delta t = 9.4$fs. But from experiment a pulse duration of 140fs was measured.

The difference between the calculated pulse duration of $\Delta t = 9.4$fs and the experimentally measured pulse duration of 140fs arises for a couple of reasons. Firstly, not all the 200nm bandwidth is accommodated by the prism. Secondly, since the second harmonic crystal used in the BFA setup (see figure 5.9) is only 100μm thin, the shortest possible pulse duration that can be measured from such a crystal is 20fs [45] because of the phase matching condition [46]. Also, the apex-apex prism separation d (see figure 5.3) may be more than 1.2m as estimated from calculation because the GDD varied by 6.6% for a 0.2m change in d. Also, d couldn't be increased further due to limited space on the optical table. However, if all the linear chirp present in the pulse is compensated and the pulse duration is not still close to the Fourier limit, then the SLM can be used to compensate for higher order chirp present in the pulse.

Conclusions

The purpose of the presented work was to develop the prism pulse compressor to compress a spectrally broadened pulse from an all normal dispersion photonic crystal fibre. Two models of the prism pulse compressor were studied. The first model discussed, proposed by Fork et al is accurate for small bandwidths but doesn't give accurate results when the bandwidth of light to be compressed is large. The second model which took into account all the optical path length of the beam through the prisms proved to be more accurate at large bandwidth. Calculations from this model were used to calculate the apex to apex prism distance necessary to compress the pulse from the all normal dispersion photonic crystal fibre.

With a prism size of 25mm, a 100μm second harmonic crystal and an apex to apex prism separation distance of 1.2m, the shortest pulse duration we measured was 140fs. Future work to further compress the pulse will include, use of bigger prisms, recalculating the apex to apex prism separation distance and also using a thinner (50μm) second harmonic crystal. Also, the SLM will be employed to further compress the pulse if higher order chirp is present.

Bibliography

[1] Jack Gaskill. *Linear Systems, Fourier Transforms and optics*. John Wiley and sons, 1973.

[2] Raphael Okoye. Assignment 2a, biomedical signal processing, african institute for mathematical sciences. Transform of a Gaussian.

[3] Eugene Hecht. *Optics*. Addison Wesley, 2001.

[4] Numerical apeture of optical fibre. `http://amrita.vlab.co.in/?sub=1&brch=189&sim=343&cnt=1`, Accessed November 2012.

[5] W.Lauterborn and T.Kurz. *Coherent Optics, Fundamentals and Applications*. Springer, 2002.

[6] Single mode optical fiber. `http://en.wikipedia.org/wiki/Single-mode_optical_fiber`, Accessed November 2012.

[7] Super continuum generation in photonic crystal fibres. `http://www.nktphotonics.com/files/files/Application_note_-_Supercontinuum%20-%20General.pdf`, Accessed November 2012.

[8] Coherence. `http://www.rp-photonics.com/coherence.html`, Accessed November 2012.

[9] E.Hooper et al. Coherent supercontinuum generation in photonic crystal fibre with all-normal group velocity dispersion. *Optical Society of America*, 19(6), 2011.

[10] A.M. Heidt et al. High quality sub-two cycle pulses from compression of supercontiuum generated in all-normal dispersion photonic crystal fibre. *Optical Society of America.*, 2011.

[11] Akira S Karasawa N, Liming L. Optical pulse compression to 5fs using only the spatial light modulator. *IEEE.*, 9:234–235, 2001.

[12] Andrew. M. Wiener. *Ultrafast Optics*. John Wiley and Sons Inc, 2009.

[13] Logitudinal waves. `http://montalk.net/notes/longitudinal-waves`, Accessed November 2012.

[14] Jones vector. `http://www.lunatechnologies.com/files/23jonesintro.pdf`, Accessed July 2012.

[15] B.E.A.Saleh and M.C.Teich. *Fundamentals of Photonics*. Wiley and Sons Inc, 2007.

[16] Polarization of light. `http://www.yorku.ca/marko/PHYS2212/Lab8.pdf`, Accessed November 2012.

[17] Polarization of light. `http://www.sjsu.edu/faculty/beyersdorf/Archive/Phys158F06/11-9%20polarization%20of%20light.pdf`, Accessed November 2012.

[18] Optical isolator tutorial. `http://www.thorlabs.com/2996Isolator%20Tutorial`, Accessed July 2012.

[19] J.S Patel A.M Weiner, D.E Leaird and Wullert. Quantum electron. *IEEE*, 28:908, 1992.

[20] A.M Weiner. Femtosecond pulse shaping using spatial light modulators. *Review of scientific instruments*, 2000.

[21] *Mathematical Methods for Physics and Engineering*. Cambridge University press, 2006.

[22] *Diffraction Grating Handbook*. Newport Corporation, London, 2005.

[23] *Physics for Scientists and Engineers*. Pearson, Prrentice Hall, 2005.

[24] *Fundamentals of physics*. JOHN WILEY and SONS INC, 1993.

[25] Investigation into mid-infra-red pulse shaping using an optical parametric oscillator. `http://www.orc.soton.ac.uk/publications/theses/4074_nan/4074_nan.pdf`, Accessed November 2012.

[26] *Principles of lasers*. Plenum Press, New york, 1998.

[27] Group delay dispersion. `http://en.wikipedia.org/wiki/Group_delay_dispersion`, Accessed November 2012.

[28] Application note. prism compressor for ultrashort laser pulses. `http://assets.newport.com/webDocuments-EN/images/12243.pdf`, Accessed November 2012.

[29] J.Diels and W.Rudolf. *Ultrashort Laser Phenomena*. Massachusetts, Academic Press, 2006.

[30] E.Oran Brigham. *The Fast Fourier Transform: An Introduction to its theory and Application*. New Jersey, Prentice Hall, 1973, 1973.

[31] Self phase modulation. `http://en.wikipedia.org/wiki/Self-phase_modulation`, Accessed November 2012.

[32] Femtosecond pulse shaping with liquid crystal modulators. `http://www.diss.fu-berlin.de/diss/servlets/MCRFileNodeServlet/FUDISS_derivate_000000001304/03_kap3.pdf?hosts=`, Accessed November 2012.

[33] Rick Trebino. Ultrafast short pulses. Technical report, Georgia Institute of Technology, 2010.

[34] Dispersion and ultrashort pulses. `http://ticc.mines.edu/csm/wiki/images/f/f0/UFO05-Dispersion.pdf`, Accessed November 2012.

[35] J.P.Gordon R.Fork, O.E.Martinez. Negative dispersion using pairs of prisms. *Optical Society of America.*, 1987.

[36] Xu et al Yang, Lee. An accurate method to calculate the negative dispersion generated by prism pairs. *Optics and Laser Engineering*, 36(381), 2001.

[37] Ultrafast laser physics. `http://www.ulp.ethz.ch/education/ultrafastlaserphysics/3_Dispersion_compensation.pdf`, Accessed November 2012.

[38] S.Hadrich et al. Visible pulse compression to 4fs by optical parametric amplification and programmable dispersion control. *Optical Society of America.*, 2002.

[39] S.Demmler et al. Generation of high quality, 1.3 cycle pulses by active phase control of an octave spanning supercontnuum. *Optical Society of America.*, 2011.

[40] V.S. Yakovlev et al. Phase-stabilized 4fs pulses at the full oscillator repetition rate for a photoemission experiment. *Applied physics Journal.*, 2003.

[41] A.M. Heidt. Pulse preserving flat-top supercontiuum generation in all-normal dispersion photonic crystal fibres. *Optical Society of America.*, 2011.

[42] Super continuum generation in photonic crystal fibres. `http://www.nktphotonics.com/files/files/NL-1050-NEG-1.pdf`, Accessed November 2012.

[43] Phd project : Femtosecond few-cycle mid-infrared laser pulses. `http://www.fotonik.dtu.dk/upload/institutter/com/phdopslag_march2012/femtosecond%20few-cycle%20mid-infrared%20laser%20pulses.pdf`, Accessed November 2012.

[44] Gurthwin Wendell Bosman. Ultrashort optical pulse characterization. Master's thesis, University of Stellenbosch, 2008.

[45] Femtosolutions. bbo crystals for shg of ti:sapphire lasers-documents and drawings. `http://www.femtosolutions.eu/bbo-crystals-for-shg-of-ti-sapphire-lasers.html`, Accessed November 2012.

[46] Phase matching. `http://www.rp-photonics.com/phase_matching.html`, Accessed November 2012.